Scattering at Ultracold Temperature: from Statistics to Dimensionality

by

Chen Zhang

B.S., Peking University, 2008

M.S., University of Colorado at Boulder, 2011

A thesis submitted to the

Faculty of the Graduate School of the

University of Colorado in partial fulfillment

of the requirements for the degree of

Doctor of Philosophy

Department of Physics

2014

This thesis entitled:
Scattering at Ultracold Temperature: from Statistics to Dimensionality
written by Chen Zhang
has been approved for the Department of Physics

Chris H. Greene

John L. Bohn

Date

The final copy of this thesis has been examined by the signatories, and we find that both the content and the form meet acceptable presentation standards of scholarly work in the above mentioned discipline.

Zhang, Chen (Ph.D., Physics)

Scattering at Ultracold Temperature: from Statistics to Dimensionality

Thesis directed by Prof. Chris H. Greene

In this dissertation, we study the few-body ultracold Bose-Fermi mixture and quasi-1D scattering at ultracold temperature. Degenerate quantum gases have attracted enormous attentions during the past two decades. They have opened new platforms of quantum simulation, precision measurement and quantum chemistry. The scattering properties of degenerate quantum gases are the first things to study in order to gain insight into various novel phenomena at ultracold temperatures.

To address the role of quantum statistics at ultracold temperature, we study the spectrum and dynamics of a few-body Bose-Fermi mixtures. In particular, we focus the dynamical evolution of a few-body Bose-Fermi mixture and concentrate on its universal behavior at large inter-particle scattering length. We predict the molecule formation efficiency in many-body Bose-Fermi mixtures by mapping this critical observable in few-body calculations. We also propose that a the quantum beat experiment could be used to measure the energy of the lowest Efimov trimer at unitarity.

To address the role of dimensionality, we study confinement induced resonances and similar phenomena in general transverse confining potentials. Well-separated energy scales in different dimensions allow the creation of reduced dimensional systems at ultracold temperatures. We develop a general framework to regularize the low-energy quasi-1D scattering phase shift associated with a zero range interaction.

Lastly, we discuss future prospects for the study of an ultracold Bose-Fermi mixture, and scattering in reduced dimensional systems of a more general topology.

Dedication

I would like to dedicate my thesis to my beloved parents.

Acknowledgements

First, I want to thank my advisor Chris Greene, for his guidance through my Ph.D study. Chris's dedication and enthusiasm for AMO physics have motivated me in these explorations into the rich yet sometimes intriguing world of AMO physics. Chris's immense knowledge and uniquely sharp physics intuitions have always inspired me at the critical points of my research. I wish I could learn more from Chris. During my Ph.D study, Chris offered me the opportunity to do research in two completely different institutions, namely JILA and Purdue. I will benefit in my future career from this unique experience that I gained during my Ph.D study.

I also would like to thank Professor Ana Maria Rey for her vast support and help after I moved to Indiana. As my academical advisor, Professor Rey has helped me through many academic issues in an unbelievably efficient manner.

I want to thank all the Greene group members that I have worked with. I feel lucky and honored that I have overlapped with our group members in two different generations, one from JILA and the other in Purdue. I spent the first three years in Chris's group in JILA. Within that time, I learned so much from the senior members in the group, including Jose D'Incao, Javier von Stecher, Jia Wang, Yujun Wang, Michal Tarana. Javier von Stecher is always resourceful and patient in sharing his valuable knowledge and experience in research. Javier's unique insights in both few-body and many-body physics have inspired many aspects of my Ph.D work. Jose D'Incao has also been generous in sharing his unique numerical and analytical techniques and offering me career path advice. I would also like to thank Jia Wang for countless insightful discussions. Yujun Wang's broad knowledge, work ethics and his unbelievably nice balance between academics and

life are a role model of a young scientist for me. Although working on completely different topics, Michal Tarana offered me many valuable suggestions about numerical techniques as well. I also want to thank Michal Tarana particularly for driving during the long road trip from Colorado to Indiana. I spend the last two years of my Ph. D study in the Purdue Physics Department. The strong academic background and work ethic of the Purdue team members constitute an active research environment. Discussions with Kevin Daily have been nice and stimulating. Though from a completely different background, Jesus Perez-Rios has been always patient in explaining novel methods from the chemical physics point of view. I want to thank Panos Giannakeas for sharing his vast knowledge in reduced dimensional systems. And I want to thank both Panos and Jesus for proof reading this thesis.

I would like to to thank Professor Deborah Jin and the KRb group members: Tyler Cumby, Ruth Shewmon Bloom and Mingguang Hu for their patience in explaining to me the experimental subtleties and for discussing with me my theoretical predictions. I want to thank Professor Shinichi Watanabe and Mr. Tomotake Yamakoshi, for collaborating with me during my Ph.D study.

I thank Professor Ana Maria Rey, Professor Deborah Jin, Professor Michael Hermele, Professor John Bohn and Professor Joel Eaves for being my thesis committee members.

Finally, I would like to thank the National Science Foundation and the JILA Physics Frontier Center for funding my research in the past few years.

Contents

Chapter

Tables

Table

Figures

Figure

Chapter 1

Introduction

1.1 Brief History of Modern Atomic, Molecular and Optical (AMO) Physics

Emergent phenomena from ensembles of interacting particles are intriguing. Knowledge of individual particle's structure and dynamics is not enough to predict the behavior of many-particle systems. The pursuit of unraveling how particles interact with each other and how they form matter with diversified structures and dynamics have pushed forward the development of new branches of physics. As probing techniques have developed, the structures and dynamics of matter can be directly observed and controlled on a larger range of space-time and a broader range of energy scales. In the scope of atomic, molecular and optical physics, ultracold quantum gases are the cornucopia to explore emergent phenomena.

From the perspective of modern atomic molecular and optical physics, advances in laser technology have allowed for the precise manipulation of matter at the single atom and molecule levels. Although the idea of using light to manipulate the motion of atoms started since the era of Maxwell [MAJ88, Leb01, NH01] in the early 1900s, the light sources back to that time delayed active explorations in this direction due to the lack of monochromaticity and coherence. Einstein foresaw stimulated emission as early as 1917 [Ein17]. However, the invention of laser was in the 1960s [Maint], several decades after the original work of Einstein. Lasers subsequently became important probing tools to understand the structure of individual particles. In the meantime, the variety of lasers have paved the way for realizing manipulation of the mechanical motions of particles with light. One of the research directions is to reduce the average kinetic energies of atoms

and molecules using laser fields. The techniques of laser cooling of atoms to the quantum regime have developed rapidly since then.

In addition to the light pressure exerted on particles, the gradient of the electromagnetic (EM) field also exerts significant forces on charged or neutral particles moving inside an EM field. The gradient forces of the laser field can capture atoms in the valleys or nodes of a standing EM wave or at least change the paths of an atomic beams [Ash70]. Hansch *et al.* proposed laser cooling of trapped neutral atoms [HS75] in the 1970s. At nearly the same time, Wineland *et al.* proposed laser cooling of ions in ion traps [WDW78]. Achievements in laser cooling a large variety of atomic species followed these seminal experiments [WDW78, NHTD78, BFAP78]. These two classes of experiments (ion trap and neutral atom trap) became the basis of candidate systems for realizing quantum computing in from the perspective of atomic molecular and optical physics [CZ95]. (Of course there are candidate systems that are based on low temperature materials such as quantum dots [LD98] and topological quantum computing devices [NSS$^+$08]. Even hybrid systems combining all those elements have been proposed.)

Cooling beyond the Doppler limit was realized by Chu *et al.* [CHB$^+$85] and Philips *et al.* [LWW$^+$88] independently in the late 1980s. Microkelvin optical molasses with cold atomic gases were created in both their sets of experiments. Later, the velocity-selective coherent population trapping method enabled the experimentalist to cool the atomic ensemble below the temperature corresponding to the recoil photons from a laser, allowing experiments to reach the nK and pK regimes [AAK$^+$88]. Atom trapping techniques were also revolutionized by the discovery of the magneto-optical trap by Wiemann [MSRW90]. These experimental breakthroughs in the cooling and trapping of neutral atoms eventually led to the Bose-Einstein condensation (BEC) of atoms [BSTH95, PAEC95, DMA$^+$95]. BEC is a new phase of matter in which a macroscopic number of atoms are in the same quantum mechanical ground orbital. This happened over 70 years after the first prediction of the BEC by Bose and Einstein in the 1920s. In fact, there are a considerable number of qualitative differences in the experimental realizations of those first few BECs from the non-interacting BEC predicted by Bose and Einstein.

Soon after the realization of quantum degenerate Bose gases, efforts were put into the experimental realization of the quantum-degenerate Fermi gas [DJ99, TSM$^+$01]. Next, the BCS-BEC crossover was realized in two-component Fermi gases [ZSS$^+$04, BAR$^+$04, RGJ04]. (BCS in the context of two-component Fermi gas refers to the Bardeen-Cooper-Schrieffer type momentum pairing mechamism for two fermions with opposite spins). Strongly interacting Bose-Fermi mixtures were created during the same period [RRMI02a]. The boom in explorations of interacting quantum degenerate gases of different statistics resulted from the development of atom-atom Fano-Feshbach resonance [CGJT10]. The development of techniques to control strong and stable magnetic fields played a pivotal tole in the precise control of the interparticle interaction strength at ultracold temperatures by scanning across the magnetic Feshbach resonances. The physical reason is that the interactions are, in general, short-range potentials possessing a van der Waals tail [PS04]. The van der Waals tails converge the fine and hyperfine split of internal atomic energy levels, which in turn can be controlled by an external the magnetic field.

The tunability of the interaction strength between ultracold atoms opened the door towards performing quantum simulation in degenerate quantum gases. For example, the BCS-BEC crossover in two-component fermions is the first quantum simulation experiment to explore the long-standing question (since 1950s) [Fey57] of the interrelation between superconductivity and superfluidity. This discovery made ultracold atoms gases a popular playground for exploring novel phases of matter. Studies of the quantum phases in ultracold atomic ensembles have not only been limited to simulating phenomena in electron gases in materials, but also have been extended to the atomic nucleus, *e.g.* simulating dynamics of the QGP(quark-gluon plasma) in Bose-Fermi mixtures.

Exploring and simulating exotic many-body phases and phase transitions has become a major subfield of ultracold quantum gases. A second direction towards the exploration of non-trivial single particle behaviors also became feasible as the magneto and optical control over atoms in quantum gases developed. Although research is still in the embryonic stage of simulating gauge fields that follow nontrivial gauge transformations, developments in this direction have been exciting during the past few years [DGJbuO11, LCJG$^+$nt].

A gauge regards simply to a convention for getting rid of redundant degrees of freedom in the electromagnetic potential $(\mathbf{A}, \psi)$ in classical EM theory [Jac02]. Gauge theories were later discovered to be fundamentally important in high-energy [Gro92] and condensed matter physics [Kle89]. Generally speaking, the word "gauge" simply refers the redundant degrees of freedom in the system. As a consequence, the Lagrangian of the system is invariant under a continuous group of local transformations, referred as gauge transformations. The invariance under such transformations is referred as gauge symmetry. The transformation operations form a Lie group, and the generators of the group together with the commutation relations form the Lie algebra. Each group generator corresponds to a vector field, namely, the gauge field. The quantization of such fields gives rise to quanta, namely, the gauge bosons.

How are these concepts from elementary particles related to ultracold atoms and why are they important? In an intuitive manner, the universality of physics laws across a wide range of energy scales is the beauty of theoretical physics. Physicists realized this fact even from Newton's era, after finding that the motion of objects moving on earth and planets moving in space follow the same Newtonian law of motion. Nowadays, explorations into much wider space-time and energy regimes are confirming this universality. By looking at the energy scales and length scales of electron gases in solid state materials and elementary particles in the LHC (the large hadron collider), it is hard to imagine that the effective theories that describe their behaviors could share any similarity. However, some of emergent the phenomena in exotic condensed matter systems resemble what happens in the high energy world. (Nonabelian gauge theory for spin-orbit interaction *e.g.* [BM13].)

What is special about gauge fields in the context of ultracold quantum gases? The interparticle interactions (coupling of fields) in neither high energy physics nor condensed matter physics share the high controllability that is possible in AMO physics. This unique aspect gives ultracold quantum gases the potential to be engineered to exhibit and simulate non-trivial gauges that are proposed but not directly measured in other physical systems. From a theoretical viewpoint, to understand and design the quantum simulation in ultracold quantum gases, *ab initio* calculations starting from the elementary particle level and phenomenological theory are complementary to each

other. The state-of-the-art in manipulating dilute ultracold atoms offers the opportunity to bridge theories from different perspectives, and therefore shed more light on creating new states of matter that are beyond the scope of previous theories.

1.2 Research Frontiers of Few-Body Physics in AMO

Between many-body physics and single-particle physics is the so-called few-body physics. The definition of a few-body system varies. Strictly speaking, the definition of a few-body system is relative. For example, as the number of particles increases, the thermal dynamical limit is reached. However, as the control of coherence properties of particles have developed, macroscopic systems have been seen to exhibit coherence and fluctuations as well. This is the beauty of emergent phenomena, in which we can see how it builds up from fundamental blocks and clusters, namely the few-body systems.

Few-body systems exhibit novel phenomena in many branches of physics, *e.g.* nuclear physics, high energy physics as well as atomic and molecular physics. One example is the Efimov states discovered in three-body systems. Efimov states, an exotic class of three-body bound states, were first proposed by Efimov in the context of three identical non-relativistic bosons in nuclei [Efi70b]. In this particular set up, each interparticle interaction does not support two-body bound states. Although the prediction of Efimov states was originally raised in the context of solving the three-body nonrelativistic Schroedinger equation in the 1970s, the impact of Efimov states goes far beyond that, both theoretically and experimentally.

The first detailed connection between Efimov physics and three-body recombination at ultracold temperatures was a theoretical study [ELG96] that showed Efimov resonances and interference minima, which were later observed in ultracold ^{133}Cs [KMW^{+}06, KFM^{+}nt]. Although none of the experimental observations of Efimov resonances have been directly in a nucleus, it sheds light on our understanding of the nature of three-body bound states in the nuclei level. From a theoretical point of view, Efimov states are one of the few scenarios that build connections between different theoretical methods. For example, the scattering theory describes Efimov states as a series of

bound states whose energies scale geometrically in hyperspherical picture. The hyperangular wave functions are the same for the whole series of bound states, whose energies scaled by a factor of $\exp(-2\pi/s_0)$ in size. The number of hyper radial nodes increase by one in the sequence of Efimov series. Hyperradial wave function for Efimov states formed in three identical boson system is plotted in Fig. 1.1.

However, scattering theory in the hyperspherical picture is not the only theoretical approach that can be used to understand Efimov states. One other approach is the renormalization group (RG) theory [Wil83]. In the RG nomenclature, the geometrically-scaled bound state originates from poles of the differential equation of RG flow of the effective three-momentum coupling constant in a quadratic boson Lagrangian. The existence of poles in RG flow equation indicates that the continuous-scaling symmetry of a unitary gas (when the two-body scattering length diverges) has to be broken. The consequence of breaking the continuous scaling symmetry in an Efimov scenario is a discrete-scaling symmetry in a three-body system.

The discrete scaling symmetric bound states in a stable three-body system imply that a new length scale must emerge, which corresponds to the cutoff in energy. This length scale is set by the so-called three-body parameter, which sets the binding energy for the lowest Efimov state that avoids Thomas collapse. What was discussed above is not the end of the story in the world of Efimov states. Active studies are heading into larger clusters and in clusters systems where spin-orbit couplings take place. Although the prediction of Efimov states occurred earlier than the theoretical conceptualization of renormalization group in critical phenomena by Wilson [Wil83], the renormalization group approach shows a non-trivial interpretation from the point of view of modern field theory, which is complementary to the hyperspherical approach, and vice versa.

The research into Efimov states is not limited to identical bosons, but also extends to heteronuclear systems [WWDG12]. One reason is that for heteronuclear systems, the scaling parameter s_0 depends on both the mass of each particle and the quantum statistics of the particles. In nuclei, elementary particles that interact strongly could also be either bosons or fermions, and their masses could be strongly dependent on energy. Thus, the studies of few-body heteronuclear systems could

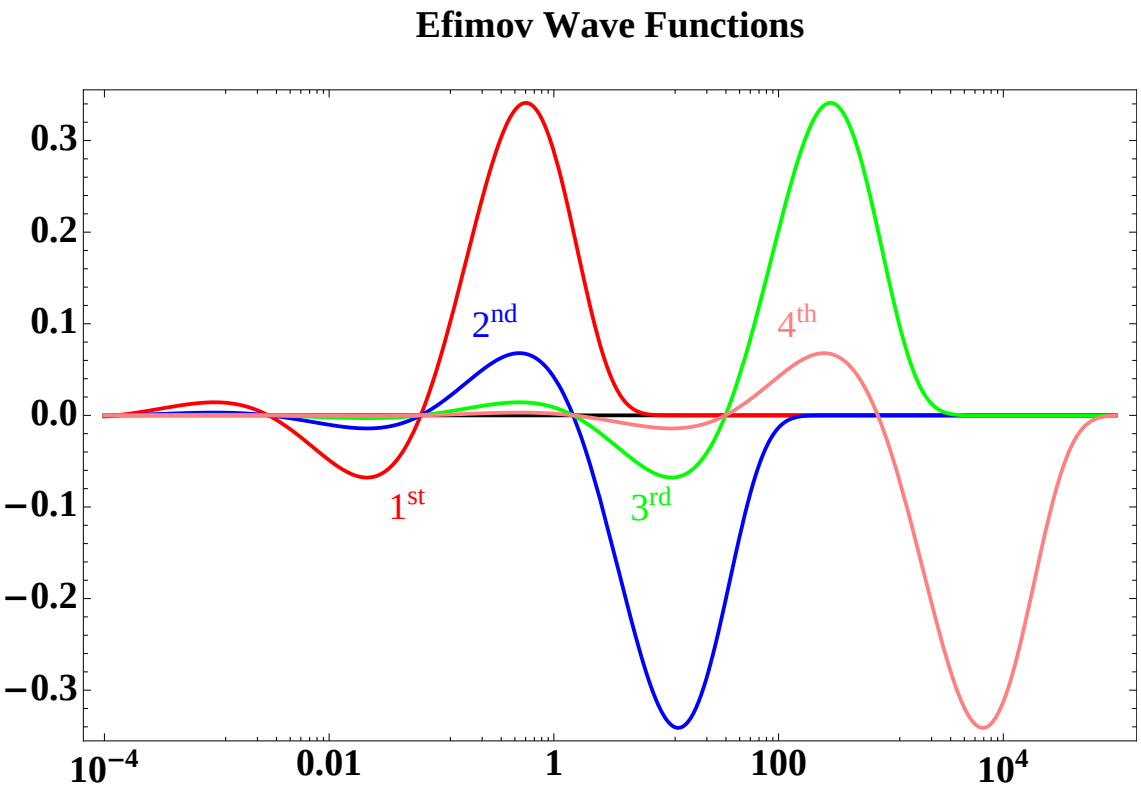

Figure 1.1: Hyperradial wave functions for Efimov states formed in a three identical boson system.

result in a systematic understanding of bound states and resonances in a wide range of interacting systems. Experimentally, adiabatic approaches to unitarity in ultracold quantum gases always suffer from three-body losses.

Thus to study the formation and decay of Efimov states, the current experiments are limited to observing the three-body resonance position and the atom-dimer resonance position. However, neither of these points directly indicates the bound state energy of the Efimov trimer, nor do they directly test the discrete scaling symmetry of the few-body system at unitarity. Interestingly, two recent experiments [TJGJ$^+$14, HSGH14] succeeded in measuring beyond the first Efimov resonance, thus they are the first evidence of discrete-scaling symmetry in few-body systems. However, the quench technique of the magnetic field (two-body scattering length) makes possible to measure the bound state energy of the Efimov states at large scattering lengths. These types of quenching techniques share similar logic as some high-energy experiments (*e.g.* the creation of QGP), where measurement of the fast strong interaction is inferred from the slow and long-wavelength asymptotes, and the strong interaction regime is generated by collisions at large energies.

1.3 Outline of This Thesis

This thesis focuses on the few-body approach to describe the dynamics of ultracold quantum gases. My thesis covers two topics, one is about scattering and bound states in ultracold Bose-Fermi mixture and the other is about quasi-1D scattering with general transverse confinement.

1.3.1 Ultracold Bose Fermi Mixtures

Bose-Fermi mixtures possess important roles from both many-body and few-body point of view. From the many-body physics point of view, Bose-Fermi mixtures in optical lattices are described by Bose-Fermi Hubbard model [TW00, JBC$^+$98, LSBF04, OdMF$^+$04]. Rich phase transitions are predicted in the large parameter space of the tunnelings, nearest-neighbor interactions and on-site interactions [KS03, KS03, AIE03, MWH$^+$04, CEI04, PTVHR06, TSH08, TSH09, MJP09, CWZ10, AWT$^+$12, STBH11a, Cra11]. Experimental studies of the quantum phases in Bose-

Fermi mixutre in optical lattices, include Mott insulator-superfluid transition [GSM$^+$06, OOH$^+$06, SIT$^+$nt, HGK$^+$11], disorder and Anderson localizations [SPLnt]. Few-body subsystems are the starting point of exploring exotic many-body phases [WBB$^+$11], like polaron excitations *etc*

From the quantum chemistry point of view, creating fermonic dipolar molecules and loading them into optical lattices is another approach to studying the quantum phases that are emerging from anisotropic interactions [NOdM$^+$08, YMG$^+$nt]. These heteronuclear molecules are fermonic, which potentially allows for experimental studies of a molecular Fermi sea in the quantum degenerate regime. The weakly bound heteronuclear molecules can be transferred to their ro-vibrational ground state, which has a much larger dipole moment than weakly bound Feshbach molecules [NOdM$^+$08, WPA$^+$12].

However, studying ultracold quantum gases in optical lattice is not the only way to investigate the the many-body physics in degenerate quantum gases. Without optical lattices, the Bose-Fermi mixture exhibits an even richer collective excitation spectrum and non-equilibrium dynamics. Traditionally, the dynamics of Bose-Fermi mixtures in the weakly interacting regime are described by the effective equation of motion of the quantum gases, namely the Bose-Fermi Gross-Pitaevskii equation. However, both the collective excitations and single-particle excitations play an important role in the dynamics of Bose-Fermi mixtures in general. In the hydrodynamic theory, elementary excitations in gases or liquids are classified into collisional excitations (short lifetime) and long-wave-length excitations (longer lifetime). However, in ultracold quantum gases, the distinction between those two regimes is not so clear. Intriguing behaviors show up in both adiabatic and quench dynamics.

Few-body systems are the building blocks for dilute quantum gases. Theoretical understanding of the three-body system with short-range potential has been well developed[JRFG04, BHvK00, BH06]. The theoretical understanding covers three-body systems where the pairwise interaction are zero-range [BH06, RMG10] or finite-range or with a long-range van der Waals tail [WDEG12, WWDG12]. However, a large part the parameter space of studies into four-body systems is still open, compared to the level of understanding in three-body systems. The exploration

of four-body problem started in nuclear physics [BB36] dated back to 1930s, and was extensively explored in the quantum chemistry community [HS06, Kup97] in the 1990s and later. Studies from the few-body perspective have been into ultracold quantum gases after the realization of BEC-BCS crossover [RvSD$^+$11].

One striking finding in the four-boson system is that the bound states in this system are attached to the three-boson bound state. The Faddeev-Yakubovsky equations approach [YTDF06, FTD$^+$11, HYT$^+$11, HYT$^+$12, FHY$^+$13, FDH$^+$13] in momentum space and the hyperspherical potential approach [vSDGnt] in real space have both realized this subtly. However, there are qualitative and quantitative discrepancies among the existing theories, which is still a topic of active research. These studies indicate that no four-body parameter is needed, thus the three-body parameter is probably a unique length scale that determines cluster bound states(three-, four- and so on). The absence of four-body parameter may be one starting point to study how the microscopic and macroscopic length scales in many-body systems emerge and connect to one another.

In my thesis work, the energetics of few-body Bose-Fermi mixtures are systematically studied. Based on the energy spectra of four-body Bose-Fermi mixtures, the time evolution of the few-body system in both the adiabatic and quench limits is studied. Effective scattering properties of the various subsystems in four-body Bose-Fermi mixtures are studied, including the effective trimer-fermion (BBF-F) and dimer-dimer (BF-BF) scattering.

1.3.2 Quasi-1D Confinement Induced Resonances

While quantum statistics play a fundamentally important role in ultracold collisions, the dimensionality and curvature of space-time could also play important role in low energy scattering. When the dimensionality and metric tensor of the space in which particles live are neither three-dimensional nor Cartesian, even non-interacting particles exhibit peculiar behaviors. One example is electrons moving in a two-dimensional space. The dispersion relation of the electrons is drastically different from the three-dimensional case, exhibiting Dirac cone in the band structure rather than a parabola that are in their 3D counterparts. Another example is identical particles

moving in one-dimensional space. Because of the 1D geometry, the original definition of bosons and fermions in terms of permutation symmetry in wave functions are drastically different from their 3D counterparts, resulting in a boson-fermion duality in 1D systems.

However, strict 1D and 2D systems are not possible experimentally, so the practical experimental technique for exploring low-dimensional physics is creating a reduced dimensional system in ultracold atoms or in solid-state materials. In the context of solid state materials, reduced dimensional systems are achieved in layer of of chemical composite or quantum wire or quantum dot structures. The transport properties in these reduced dimensional material setups are measured to examine the structure of the reduced-dimensional systems. In ultracold atomic systems, quasi 1-D and quasi 2-D systems are achieved by adjusting the trapping geometry and temperature. Instead of transport properties, exotic behaviors of reduced dimensions in ultracold atoms are measured by time-of-flight or in situ image experiments.

Particularly for one-dimensional systems, solvable models have been worked out in the 1950s and 1960s for many-body [Gro63, Gir60, Gir65, Dod70, McG64]. Many of these conclusions can be connected to theoretical explorations from the mathematics community into the nature of scattering in a space of arbitrary dimensions [Ada71], dating even farther back in time.

However, for a long time, the creation and observation of reduced dimensional systems were hampered by limits on existing experimental techniques. Later, after laser cooling and trapping techniques were developed for ultracold atomic gases [GWO00], many experimental quasi-1D and quasi-2D [GBM$^+$01, GVL$^+$01, BSM$^+$07, SCE$^+$12] quantum systems were realized and a number of theoretically-predicted novel behaviors were observed. In quasi-1D fermionic ^{40}K [MSKE03, GSM$^+$05a] and bosonic ^{87}Rb [GVL$^+$01], various properties from pure-1D theory have been confirmed. By tuning the ratio(s) of trapping frequencies in different directions (ω_ρ/ω_z *e.g.*), the shape of an ultracold gas can be engineered and varied continuously from a nearly isotropic 3D geometry to a quasi-1D or quasi-2D geometry. Cross-dimensional effects have been observed [EM04, LCB$^+$10] and also theoretically studied [Nis10, GDB12a]. These phenomena in low-dimensional systems have recently been reviewed by [MVR12, DMBO11, YOW08, BDZ08, Pos06].

After achieving success in creating reduced-dimensional systems, physicists began to explore the scattering properties of atoms, hoping to find additional tunability of interactions in ultracold gases. The confinement-induced resonance(CIR) is one such useful tunability of particular interest. From an experimental point of view, the CIR adds another way to manipulate and control low-dimensional systems. Dunjko *et.al* [DMBO11] has reviewed developments related to CIR for a variety of systems. The CIR is unique in the sense that the system exhibits the unitarity limit at a non-resonant value of the 3D scattering parameters (*i.e.* the scattering length for s-wave, and the scattering volume for p-wave).

The CIR in a harmonically transverse-confined quasi-1D system was predicted theoretically by Olshanii [Ols98], and later extended to fermions by Granger and Blume [GB04]. In realistic atomic interactions, the incoming wave in the z-direction will not only couple to the s-wave (or p-wave for fermions) component of the interaction, but also to higher partial waves components.

In the treatment of s-wave scattering, Olshanii [Ols98] derived the exact wave function and phase shift for a regularized zero range potential that are associated with low energy s-wave scattering. This problem can also be treated using Green's function methods[BEKW98, MEGK04, NTMJ07, ZZ11]. However for higher partial waves, different mathematical models of the zero-range interaction are needed in the Olshanii treatment [IC06]. In an alternative treatment, Granger and Blume [GB04] used the frame transformation method, in which the 3D phase shift information directly determines the 1D reaction matrix K. Thus the frame transformation approach avoids the need to design a zero-range model potential for higher partial wave scattering, which has some conceptual advantages.

As the exeperimental techniques of laser trapping have grown in sophistication, various confinement potentials beyond the harmonic trap have been realized, *e.g.* optical lattice traps [HGM$^+$09], uniform trap [GSG$^+$13]. In these systems, a more general theory of CIR beyond a harmonic trap is needed. Kim *et. al* gave a general description of a symmetric cylindrical hard wall trap [KSS05] using a Green's function method.

The goal of work in the second part of the thesis is to develop a systematic description of quasi-

1D scattering in arbitrary transverse confinement. Specifically, we consider the situation in which one light particle is scattered off an infinitely massive particle in the center of the confinement. We apply the local frame transformation method [Fan81], and solve the divergence problem occurring in this method. Because this divergence also arises in many other ananlytical and numerical applications of this method, we believe that the systematic discussion presented here yields valuable insights. To illustrate our implementation of the method, we treat the CIR in a square well transversely-confined system as an example. The development of our regularization method can be generalized to higher partial waves interacting through short-range potentials.

Chapter 2

Few-body Theory of Ultracold Bose-Fermi Mixtures

2.1 Introduction

Among all the ultracold mixtures of quantum gases, Bose-Fermi mixtures are unique in many aspects. Table 2.1 enumerates the classifications of atomic mixtures and phases in different interaction regimes.

Away from unitarity ($|a_{sc}| \ll n^{-1/3}$, a_{sc} refers to the inter species scattering length, n is the mean density of atomic gases), Bose-Fermi mixture can be described by a BEC interacting with a Fermi sea. Interspecies interactions could result in depletion of the condensate and the deformation of the Fermi surface [PSB05]. Naturally, zero-temperature phase transitions are expected at some critical interaction strengths [AWT$^+$12]. Theoretical studies focused on exotic phases in Bose-Fermi mixtures in optical lattices are intensified particularly after the experimental realization of BEC and degenerate Fermi gases [KS03, KS03, AIE03, MWH$^+$04, CEI04, PTVHR06, TSH08, TSH09,

mixtures	$a_{sc} = 0^-$	$a_{sc} = 0^+$	$a_{sc} = \pm\infty$
$Boson_1\ Boson_2$	weakly interacting atomic condensate	weakly interacting bosonic molecular condensate	strongly correlated Bose-Bose mixture
$Fermion_1\ Fermion_2$	BCS	weakly interaction BEC of molecules	strongly correlated Fermi-Fermi mixture
$Fermion_1\ Boson_1$	weakly interacting BEC and Fermi sea	weakly interacting molecular Fermi sea	strongly correlated Bose-Fermi mixture

Table 2.1: Table of ultracold quantum gas mixtures, classified by particle statistics. a_{sc} is the inter species scattering length.

MJP09, CWZ10, AWT$^+$12, STBH11a, Cra11]. In addition, the experimental studies of the quantum phases in Bose-Fermi mixtures in optical lattices focused on the exploration of the Mott insulator-superfluid transition [GSM$^+$06, OOH$^+$06, SIT$^+$nt, HGK$^+$11], disorder and Anderson localization [SPLnt].

Few-body subsystems are the starting point of studying exotic many-body phases [WBB$^+$11]. The experiments on Bose-Fermi mixture in optical lattices conducted by Bloch *et al.* showed that one single fermion imbedded in a few-body bosonic field can modify the effective boson-boson interactions. The measurements of the few-body subsystem in each lattice site are the prerequisite for realizing novel many-body phases.

Particularly in the regime $0 < a_{sc} \ll n^{-1/3}$, weakly bound Feshbach molecules can exist in Bose-Fermi mixture. These heteronuclear molecules are fermonic, which potentially allows for experimental studies of the molecular Fermi sea in the quantum degenerate regime. The weakly bound heteronuclear molecules can be transferred into their ro-vibrational ground states, that have much larger dipole moment than the Feshbach molecules [NOdM$^+$08, WPA$^+$12]. As a consequence, the interactions between ro-vibrational ground state molecules are long-range ($\sim r^{-3}$) and highly anisotropic. The electronic dipole-dipole interaction between the molecules can be controlled by external electric field. This unique feature of controllability makes fermonic dipolar molecules promising candidate to study quantum magnetism. Although the experimentally realized fermonic molecular gases have not yet reached the deep quantum degenerate regime (T$\sim 1.0T_F$), magnetic quantum phases have already been observed [YMG$^+$nt]. (Use of the electric dipole moments of the dipolar molecule in order to study quantum magnetism lies in the fact that the magnetic dipole moment is much smaller than the electric dipole moment particularly in heteronuclear alkali molecules.)

In the unitary regime ($a \sim \pm\infty$), the Bose gas and the Fermi gas exhibit strong correlations. This regime imposes several challenges on the theoretical and experimental investigations. Theoretically, a fundamental question that rises is how to properly describe the inter-particle interactions in the unitary regime. In the few-body picture, it is clear that the bound state energies of

any two-body system that interact through realistic potentials are well defined when the two-body scattering length diverges. The bound state emerges at $a = \infty$, and grows as $\propto -a_{sc}^{-2}$. In the many-body mean field theory, the interparticle interaction energy is characterized by the scattering length. Without proper modification to the first order mean field theory, this Hamiltonian may not have a definite energy. Various renormalization mechanisms of summing scattering amplitude and perturbation expansion techniques of correlation functions have been derived to approach the unitary regime [LH12]. Another technical challenge is that although many existing theoretical methods are capable of solving the ground state of a many-body system at any given interparticle interaction strengths, excited states are usually difficult to treat.

Experimentally, approaching the unitary regime in ultracold Bose-Fermi mixtures is challenging too. The reason is that both the Feshbach molecular states and atomic states can decay into low-lying bound states through three-body recombination, resulting in enormous atom losses from either magnetic or optical traps [SZS$^+$04, EGS01]. Similar issues are manifested also in the realization of strongly interacting bosonic systems. Thus, the experimental approaches to study unitary regime in Bose-Fermi mixture can be grouped into two categories. One method is ramping the quantum gases across unitary. The other method is quenching the system to unitarity and quenching back within short enough time-of-stay at unitarity [MKG$^+$13]. (Note that, for some cases, some atomic mixtures are easier to realize than others due to their special molecular structure near unitarity [HWC$^+$12].) In summary, both the quantum statistics and the nature of the anisotropic inter-particle interactions make Bose-Fermi mixtures an intriguing system to study.

This chapter of the thesis will focus the study of the few-body Bose-Fermi mixture, in terms of their scattering properties and bound state properties. We also study the dynamics of few-body Bose-Fermi mixtures, both in the adiabatic limit and the quench limit. The main numerical methods are briefly introduced and discussed at the beginning of the chapter. Next comes the discussion of few-body systems. Two-body and three-body systems in Bose-Fermi mixture are compared with existing theoretical results. They set the foundations to explore four-body system and beyond. Following that is the discussion of four-body systems. Dynamical evolutions of the few-

body systems are also presented and discussed, focusing on interpreting and proposing experimental observations of unitary Bose-Fermi mixtures.

The structure of the chapter is as follows:

(1) Brief introduction and review of correlated Gaussian basis functions and hyper spherical methods.

(2) Discussion of the spectra and dynamics of two- and three-body systems in a Bose-Fermi mixture.

(3) Discussion of the spectra and dynamics of four-body systems in Bose-Fermi mixture.

(4) Summary and outlook.

In Fig. 2.1 we provide the schematic representation in the structures of the study of the few-body Bose-Fermi mixtures. This chapter has used verbatim paragraphs from [ZvSG12].

2.2 Method

2.2.1 Correlated Gaussian Basis

In this section, the standard correlated Gaussian basis functions are briefly introduced. A more complete collection of correlated Gaussian matrix elements expressions can be found in Appendix A of Suzuki's book [SV98]. The eigenstates of the few-body systems (three-body and four-body) are expanded on the correlated Gaussian basis.

The correlated Gaussian basis function has the general form:

$$f_{klm}(\mathbf{x}) = (\sum_i v_i \mathbf{x}_i)^{2k+l} Y_{lm}(\hat{\mathbf{v}}) \exp(-\frac{1}{2}\mathbf{x}^T A \mathbf{x}), \tag{2.1}$$

where $\mathbf{x}$ are a set of spatial vectors written in Jacobi coordinates (Jacobi vectors), $\mathbf{v} = \sum_i v_i \mathbf{x}_i$, v_i are a set of C-number, A is a positive definite matrix, the power $2k + l$ refer to the inner product $(\sum_i v_i \mathbf{x}_i) \cdot (\sum_i v_i \mathbf{x}_i)$ to the $k + l/2$ power. The Jacobi coordinates constitutes a unitary transformation of the particles' spatial coordinates: $\mathbf{x} = U\mathbf{r}$, $\mathbf{r} = \{\mathbf{r}_1, \cdots, \mathbf{r}_n\}$, where n is the number of particles.

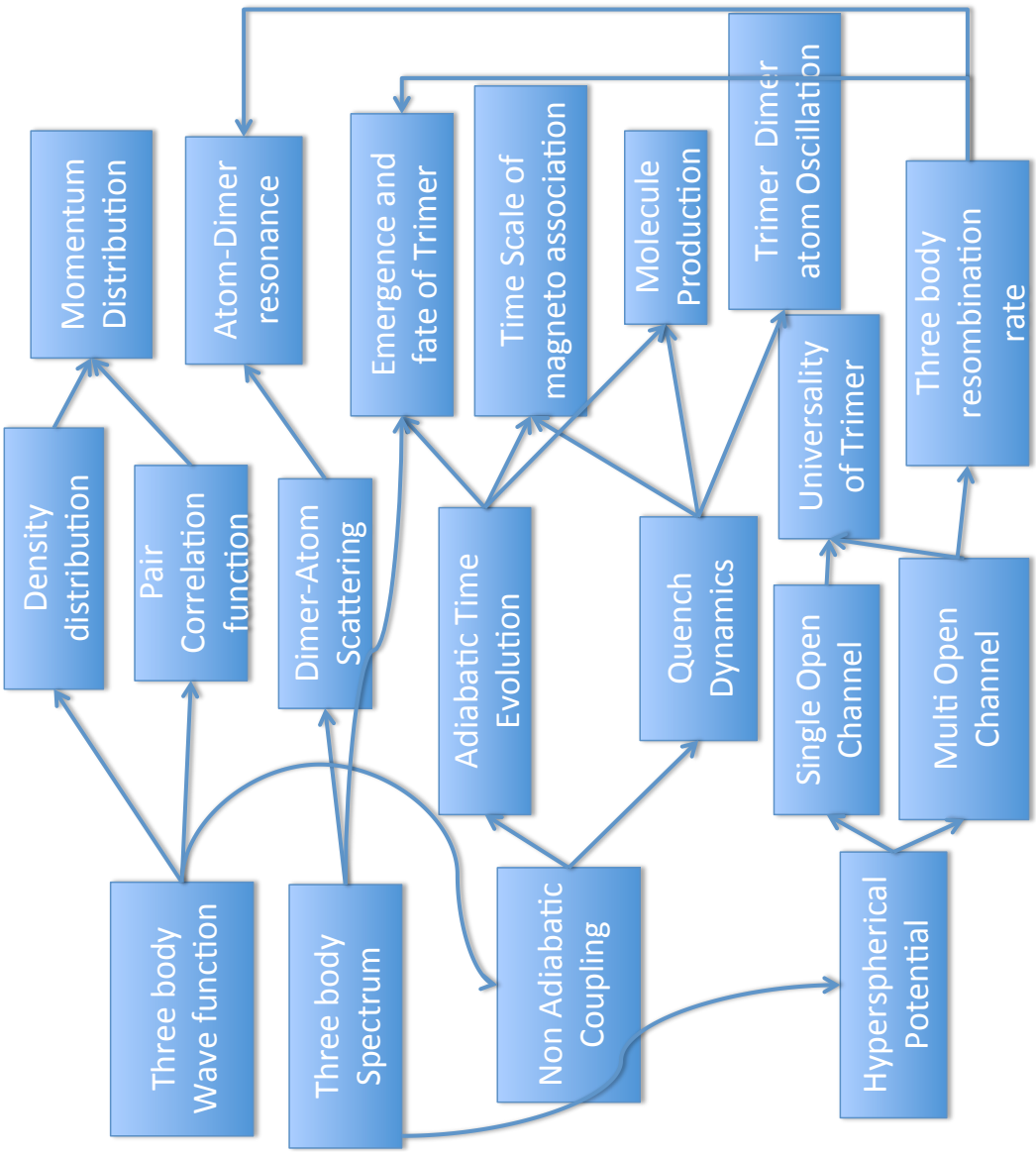

Figure 2.1: A diagrammatic scheme of the theoretical investigations in the three-body problem in ultracold Bose-Fermi mixture.

In this thesis, each basis function is generated by randomly selecting interparticle distances $\{d_{ij}\}$. A matrix in each basis is transformed from the random set of $\{d_{ij}\}$ subsequently. Hence the selection of the Jacobi tree structure, does not affect the results. More details with respect to Jacobi tree definition can be found in Rittenhouse's Ph.D thesis [Rit09].

The interparticle distances vector are defined as follows (for an n-particle system):

$$\begin{pmatrix} \mathbf{r}_{12} \\ \mathbf{r}_{13} \\ \vdots \\ \vdots \\ \mathbf{r}_{n-2,n-1} \\ \mathbf{r}_{n-1,n} \end{pmatrix} = \begin{pmatrix} 1 & -1 & 0 & \cdots & \cdots & \cdots & 0 \\ 1 & 0 & -1 & \cdots & \cdots & \cdots & 0 \\ \vdots & \vdots & \vdots & \vdots & \vdots & \vdots & \vdots \\ 0 & \cdots & \cdots & \cdots & 1 & -1 & 0 \\ 0 & \cdots & \cdots & \cdots & 0 & 1 & -1 \end{pmatrix} \begin{pmatrix} \mathbf{r}_1 \\ \mathbf{r}_2 \\ \vdots \\ \mathbf{r}_{n-1} \\ \mathbf{r}_n \end{pmatrix} \tag{2.2}$$

n(n-1) elements n×(n(n-1)) matrix T n elements

In matrix notation $\{\mathbf{r}_{ij}\} = T\{\mathbf{r}_i\}$. The interparticle distance vector enters the quadratic inner product in the exponential function in a quadratic form, thus resulting in the following expression:

$$\mathbf{x}^T A\mathbf{x} = \mathbf{r}^T U^T AU\mathbf{r} = \mathbf{y}^T D\mathbf{y}, \tag{2.3}$$

where $\mathbf{y} = \{\mathbf{r}_{ij}\}$, $D = diag(d_{ij}^{-2})$. Thus the A matrix and the randomly generated interparticle distance vectors are connected through the following relation:

$$A = (U^T)^{-1} T^T DTU^{-1} \tag{2.4}$$

Most matrix elements (overlap, kinetic energy, potential energy and interpaticle interactions) of the correlated Gaussian basis functions have analytical expressions, which significantly reduce the time consumed on numerical optimization. Suzuki [SV98] gave a more complete collection of matrix elements between basis functions having arbitrary angular momentum L, arbitrary number of nodal nodes L.

The Hamiltonian $\mathcal{H}$ of the interacting few-body Bose-Fermi mixture in an isotropic harmonic

trap has the following general form:

$$\mathcal{H} = -\sum_i \frac{\hbar^2 \nabla_i^2}{2m_i} + \frac{1}{2} m_i \omega^2 r_i^2 + \sum_{i_B, j_F} V(\mathbf{r}_{i_B} - \mathbf{r}_{j_F}) \tag{2.5}$$

The eigenfunctions of the few-body system are expanded in the correlated Gaussian basis:

$$\Psi_{KLM}(\mathbf{r} = \sum_j C_j f^j_{KLM}(\mathbf{x}), \tag{2.6}$$

in which f_{KLM} is a correlated Gaussian basis function, K is the number of radial nodes, L is the total angular momentum, M is the magnetic quantum number of the total angular momentum. The corresponding eigenvalue problem for calculating the C_j vectors is:

$$\underline{H} C = E \underline{O} C. \tag{2.7}$$

$\underline{H}$ is the Hamiltonian matrix, $H_{ij} =< f^i|\mathcal{H}|f^j >$. $\underline{O}$ is the overlap matrix, $O_{ij} =< f^i|f^j >$. Exact diagonalization of the generalized eigenvalue problem gives eigenvalues and eigenstates of the few-body system.

2.2.2 Hyperspherical Coordinates and Hyperspherical Correlated Gaussians

The method of correlated Gaussian basis expansion provides us with eigenstates and eigenenergies of a variety of few-body systems with enough accuracy as it is demonstrated in Suzuki's book [SV98] and a recent review by Varga *et. al.* [MBH$^+$13]. However, the multidimensional wave functions of a few-body system are hard to visualize. One way to understand the structure of a few-body eigenstate (configuration) is calculating the pair-correlation functions for this state. A generic pair correlation function has the form of Eqn. 2.8

$$\rho_{ij}(\mathbf{r}) = \int \Pi_{i=1}^N d\mathbf{r}_i |\Psi(\mathbf{r}_1, \mathbf{r}_2, \cdots, \mathbf{r}_N)|^2 \delta^{(3)}(\mathbf{r}_i - \mathbf{r}_j - \mathbf{r}) \tag{2.8}$$

However, this definition of a pair correlation function indicates that it will not help to understand the scattering of one configuration into another, nor the elastic scattering within one channel.

Thus, to have a convenient and efficient description of the scattering procedures of the few-body systems, a new coordinate system is desirable. Ideally, the new coordinate system should be

able to capture the structure of all the asymptotic channels of the few-body system, and should allow for describing transitions between channels during the scattering process.

The hyperspherical coordinates have been shown to be one of the best coordinate systems to describe a few-body scattering processes. An adiabatic representation in these coordinates was first proposed by Macek in 1968 to study the auto-ionizing states of helium [Mac68]. The key idea of the hyperspherical coordinates is to characterize the internal motion of a few-body system (center of mass motion removed) using a single length (hyperradius R) and several angles (hyperangles Ω). All the channels asymptotically at large hyperradii correspond to the system's different breakup thresholds. Each interparticle distance can be represented by the hyperradius multiplied by trigonometric functions of hyperangles. For example, in a three-body system $\{\mathbf{r}_1, \mathbf{r}_2, \mathbf{r}_3\}$, in the hyperspherical representation $\sqrt{m_{12}}|\mathbf{r}_{12}| = \sqrt{\mu}R\sin\alpha$, $\sqrt{m_{12,3}}|\mathbf{r}_{12,3}| = \sqrt{\mu}R\cos\alpha$. Table 2.2 shows some simple Jacobi tree structures.

The hyperangles are considered as the fast variables while the hyperradius is the slow one in the few-body system asymptotically. Thus the hyperradial and hyperangular degrees of freedom are adiabatically separated. Transitions between different configurations are characterized by nonadiabatic couplings between different configurations.

The criteria of "fast" and "slow" variables are not strictly appropriate in all regions, especially in the region where all particles are close to each other. Nevertheless, although the adiabatic separation concept does not work well, numerical methods that do not assume strictly adiabatic evolution are developed to solve the few-body problem, *e.g.* DVR basis (discrete variable representation). Jia Wang's Ph.D thesis has a more detailed description of the implementation of DVR basis [Wan12]. In principle, the adiabatic representation is an exact recasting of the original Schroedinger equation, since it is an expansion of the wavefunction onto a complete, orthonormal set of hyperangular functions.

The squared hyperradius is defined as a mass weighted summation of the Jacobi vector $\mathbf{x}_i$

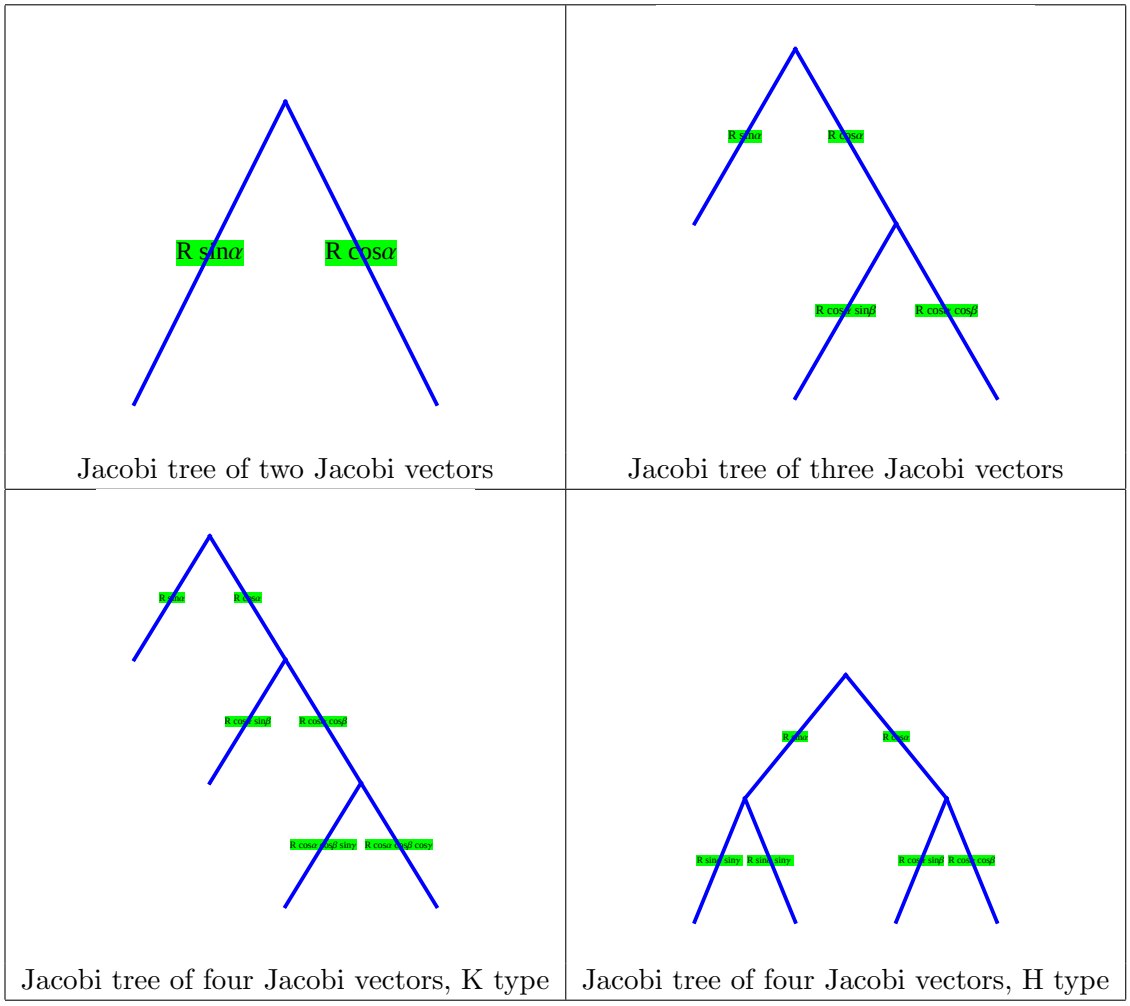

Jacobi tree of two Jacobi vectors | Jacobi tree of three Jacobi vectors

Jacobi tree of four Jacobi vectors, K type | Jacobi tree of four Jacobi vectors, H type

Table 2.2: Jacobi Tree structure. Each leaf in the tree represents a Jacobi vector. Their lengths are listed on the edge.

norms:

$$\mu R^2 = \sum_i m_i x_i^2. \tag{2.9}$$

The hyperradius is invariant under Jacobi tree rotations (Jacobi trees refer to different definitions of the Jacobi vector sets for a few-body system, and Jacobi tree rotations refer to unitary transformations between different definitions of Jacobi vectors sets).

The Hamiltonian of an interacting few-body system in free space represented in the hyperspherical coordinate reads:

$$\mathcal{H} = -\sum_{j=1}^{N}\sum_{i=1}^{d}\frac{1}{2m_j}\frac{\partial^2}{\partial x_{j,i}^2} + \sum_{ij} V(r_{ij}) = \mathcal{H}(R,\Omega) = -\frac{1}{2\mu}\frac{1}{R^{Nd-1}}\frac{\partial}{\partial R}R^{Nd-1}\frac{\partial}{\partial R} + \frac{1}{2\mu}\frac{\mathbf{\Lambda}^2}{R^2} + V(R,\Omega), \tag{2.10}$$

where i denotes the spatial coordinates and j denotes the index of the Jacobi coordinate, d is the number of dimensions each particle lives in, and N is the number of Jacobi coordinates.

$\mathbf{\Lambda}$ is the grand angular momentum operator [Smi60]. It is a generalized angular momentum operator involving both spatial angles and hyperangles.

$$\mathbf{\Lambda}^2 = \sum_{p>q} -\Lambda_{pq}^2, \Lambda_{pq} = x_p\frac{\partial}{\partial x_q} - x_q\frac{\partial}{\partial x_p}, \tag{2.11}$$

in which p and q run over every degree of freedom in the system (Nd in total).

Usually the last two terms of Eqn. 2.10 together are called the adiabatic part ($\mathcal{H}_{ad}$) of the Hamiltonian:

$$\mathcal{H}_{ad} = \frac{1}{2\mu}\frac{\mathbf{\Lambda}^2}{R^2} + V(R,\Omega) \tag{2.12}$$

The terms involving derivatives of the hyperradius act like the kinetic energy of particles moving in the potential created $\mathcal{H}_{ad}$.

Although the angular momentum introduced by the spatial dimensions or the hyperangles appear indistinguishable in this definition in Eqn. 2.11, the rotational symmetry of interaction terms and the permutational symmetry of particles in the Hamiltonian distinguish them. More details of various definition conventions of hyperangles and details about how hyperangular momenta couple to each other are discussed in Rittenhouse's thesis [Rit09].

With the property of asymptotically well separated hyperradius and hyperangular degrees of freedom, it is straight forward to consider the adiabatic evolution of the system in the hyperradial potential. This concept also shows up in the usual molecular Born-Oppenheimer approximation (BO), where the "fast" motion is the electronic degrees of freedom. Integrating over the electronic motion results in an effective potential for the nuclear motion. The potentials are calculated at every spatial configuration of the nuclei. Thus the BO potential is often a multi-dimensional potential surface, rather than a simple potential curve.

One difference between BO approximation and hypersherical approximation is that, BO separates slow and fast motion solely based of mass ratio of the electrons and nuclei. The hyperspherical approximation does not rely on the smallness of a mass ratio of the particles in the system. Thus, whereas the BO approximation fails in systems where particles have comparable masses, the hyperspherical adiabatic representation still works, at least in principle, provided nonadiabatic couplings are fully incorporated.

The hyperspherical Gaussian method uses the correlated Gaussian basis to compute the eigenstates of the adiabatic part of the Hamiltonian $\mathcal{H}_{ad}$ in Eqn. 2.12.

$$\underline{H_{ad}} C_{ad} = E \underline{O_{ad}} C_{ad}, \Psi_n(R,\Omega) = \sum_i (C_{ad})_i^n f^i, \tag{2.13}$$

in which $(\underline{H_{ad}})_{ij} = \langle f^i | \mathcal{H}_{ad} | f^j \rangle_\Omega$, $(\underline{O_{ad}})_{ij} = \langle f^i | \mathcal{I} | f^j \rangle_\Omega$. Here the brackets$\langle | \, | \rangle_\Omega$ mean integrations are carried out only over the hyper angular degrees of freedom.

The eigenvalues of $\mathcal{H}_{ad}$ are referred to as hyperspherical potentials $\{u_n(R)\}$ and the eigenstates $\{\Psi_n(R,\Omega)\}$ are referred to as the corresponding eigenfunctions. Ideally, with the full knowledge of the hyperspherical potentials and their corresponding eigenstates, the Nd-dimensional few-body problem is reduced to a set of coupled 1D ODEs for the $F_n(R)$.

$$\Psi = \sum_n F_n(R) \Psi_n(R,\Omega). \tag{2.14}$$

Practically, the hyperspherical potentials and channels are solved numerically. As a consequence, the numerical accuracy of E is determined by the number of converged potential curves

and channels of $\mathcal{H}_{ad}$. The solution of F needs first and second order derivatives of the channel functions, this imposes even higher demand of the numerical accuracy of the number of the converged hyperspherical potentials. So efficient numerical basis functions are needed.

2.2.3 Stochastic Optimization

With the analytical expressions of matrix elements at hand, we still have to face extensive numerical challenges in solving the eigenvalue problem efficiently. One reason is that for interacting few-body systems, the range of interactions, the size of bound states and other length scale of the system (trap length *e.g.*) could be quite distinct. An extensive number of basis functions characterizing different length scales are expected. Appropriate selection and optimization of a relatively small set of basis functions are important.

The selection of the parameters in each correlated Gaussian basis function can be categorized into two main approaches. One is selection from desired configurations, *e.g.* trimer or atom-dimer configurations in three-body systems, dimer-dimer and atom-trimer configurations in four-body systems. The other is starting from a completely random configuration, stretching or squeezing at one or more of the d_{ij}s. Both methods raise trials in optimizations, and the criteria to test the trials is whether they give lower energy compared to the existing basis in addition to their linear independence from the rest of the basis.

The test can be done either by adding basis functions, or by replacing each basis function with one which provides a more converged energy. Keep adding basis may not be on the right track, because it would bring in more numerical difficulties in diagonalization of a large initial basis set. So a trial-select algorithm are implemented in OpenMP to test replacements rather than increment of an initial basis. Tens of trials are carried out simultaneously by using multi-CPUs, and their corresponding Hamiltonian matrix elements and overlap elements are stored. The eigenenergies are calculated for each trial. Finally the trial gives the lowest eigenenergies is selected to replace the old one.

Although finding the eigenenergies for each trial seems to be a diagonalization at first glance,

this procedure in fact only involves a root finding. The time cost of a diagonalization and a root finding are drastically different, which is part of the reason why this trial-select method works efficiently.

The root finding algorithm works as follows. We assume that there are n existing basis functions (in a practical calculation, this number is the number of correlated Gaussian basis, from 100-5000), and the first basis function needs optimization. The sub Hamiltonian matrix (generated by the 2nd-nth basis) is already diagonalized. Matrix elements of each trial of the 1st basis are calculated and stored. To find the eigenvalues of each trial is equivalent to find the root of the following polynomial:

$$det\begin{pmatrix} A_{n,n} & A_{n-1,n} & A_{n-2,n} & A_{n-3,n} & \cdots & \cdots & A_{2,n} & A_{1,n} \\ A_{n-1,n} & b_{n-1} & 0 & 0 & \cdots & \cdots & 0 & 0 \\ A_{n-2,n} & 0 & b_{n-2} & 0 & \cdots & \cdots & \vdots & \vdots \\ \vdots & \vdots & 0 & \vdots & \vdots & \vdots & 0 & 0 \\ A_{2,n} & 0 & \vdots & \cdots & 0 & 0 & b_2 & 0 \\ A_{1,n} & 0 & 0 & 0 & 0 & 0 & 0 & b_1 \end{pmatrix} = 0 \tag{2.15}$$

$$\Rightarrow \Pi_{i=1}^{n-1} b_i (A_{n,n} - \sum_{i=1}^{n-1} \frac{A_{n-i,n}^2}{b_{n-i}}) = 0,$$

in which

$$A_{ij} = H_{ij} - \epsilon O_{ij}, b_i = \epsilon_i - \epsilon O_{ii}, \tag{2.16}$$

ϵ is the eigenvalue corresponding to one of the trial basis functions, ϵ_i is the eigenvalue of the sub Hamiltonian. Finding the n roots of the above polynomial is much faster than solving eigenvalue problem for each trial function. And the root finding calculation can be easily adapted to a large number of trial functions by parallelization without costing significant computation time. Details of this rooting finding process are also in Suzuki's book [SV98].

2.3 Two-body and Three-body States in an Isotropic Harmonic Trap

As we mentioned in the introduction of this chapter, the purpose of this section is to provide a solid understanding on the two-body and three-body systems, which in the future are essential conceptual paradigms to understand the dynamics of the four-body systems at ultracold temperatures. In this section, the numerical calculations are benchmarked by comparisons with existing analytical and numerical results in the literature.

2.3.1 Adiabatic Spectrum of Two-body States in an Isotropic Harmonic Trap

Two trapped particles interacting through a zero-range interaction has a well known solution by Busch *et al.* [BEKW98]. The reasons to elaborate the two-body system are as follows:

The first reason is that Busch's study assumed a regularized zero-range potential in his study. However, in the present thesis we employ various short-range model potentials. Comparison between the two-body analytical result and result from model potentials help us to decide the boundaries of the universal regime of the scattering lengths that the model potentials provide.

The second reason is that Busch's study does not cover any higher partial wave bound states in a harmonic trap. At some point, higher partial wave bound states are needed [HGS02, KB04]. Numerical model potentials would help to extract the relation between the bound state energy and higher partial wave scattering parameters.

The wave function for zero-range interaction $V(\mathbf{r}) = \dfrac{2\pi a_{sc}\hbar^2}{\mu}\delta(\mathbf{r})\dfrac{\partial}{\partial r}(r\times)$ in a 3D isotropic harmonic trap is [BEKW98]:

$$\psi_\nu(\mathbf{r}) = \exp(-\frac{r^2}{2a_{ho}^2})\Gamma[-\nu]U(-\nu,\frac{3}{2},\frac{r^2}{a_{ho}^2}), E_\nu = \hbar\omega(2\nu+\frac{3}{2}),$$

$$\Gamma[-\nu]U(-\nu,\frac{3}{2},\frac{r^2}{a_{ho}^2})\text{Expansion around } r\to 0 \Rightarrow \sqrt{\pi}(\frac{1}{r} - \frac{2\Gamma[-\nu]}{\Gamma[-\frac{1}{2}-\nu]} + (-\frac{3}{2}-2\nu)r + o(r)^2), \tag{2.17}$$

in which ν denotes the radial quantum number, U is the Tricomi's (confluent hypergeometric)

function.

$$
\begin{aligned}
U(a;b;z) &= \frac{\Gamma[1-b]}{\Gamma[a-b+1]}M(a,b,z) + \frac{\Gamma[b-1]}{\Gamma[a]}z^{1-b}M(a-b+1,a-b,z) \\
M(a,b,z) &= \textstyle\sum_{n=0}^{\infty}\dfrac{a^{(n)}z^n}{b^{(n)}n!} =_1 F_1(a;b;z) \\
U(a;b;z) &= -\frac{(b+az)\Gamma[-b]}{\Gamma[1+a-b]} + \frac{z^{1-b}\Gamma[b-1]}{\Gamma[a]} + \cdots .
\end{aligned}
\tag{2.18}
$$

The relation between the scattering length and ν is determined by:

$$
\frac{a_{ho}}{a_{sc}} = \frac{\Gamma[-\nu]}{\Gamma[-\nu-\frac{1}{2}]}. \tag{2.19}
$$

Integer ν corresponds to $a_{sc} = 0$ and half-odd-integer values of ν corresponds to $a_{sc} = \infty$.

A comparison between eigenenergy from the analytical expression and model potential calculation is shown in Fig. 2.2. In the universal regime near $a_{sc} \sim \pm\infty$, agreements between the two curves are good. However, deviations due to the finite range effect of the model potential show up at small a_{sc} on both sides of the unitarity.

Two important positions on the spectrum are $a_{sc} = 0$ and $a_{sc} = \pm\infty$, the reason is that the wave functions and energies in these two positions are not dependent on a_{sc}. Although in the two-body sector the results are relatively simple, extension to a few-body system or even a many-body system may not be that straight forward. Table 2.3 summarizes the properties of two-body eigenstates at these two points. Fig. 2.2 shows wave functions corresponding to some non-interacting and unitary two-body states in an isotropic 3D trap.

The wave functions for $\nu = n + \dfrac{1}{2}$ states have a $1/r$ divergence near $r = 0$. This is consistent with the boundary condition interpretation of the zero-range potential: $\dfrac{(\psi r)'}{(\psi r)} = -\dfrac{1}{a_{sc}}$. Infinite a_{sc} implies zero logarithmic derivative of the scaled wave function near the origin. Although for s-wave two-body scattering, no other parameters of the short-range potential are needed to determine the bound state energy, this conclusion is not always generally true for the higher partial waves.

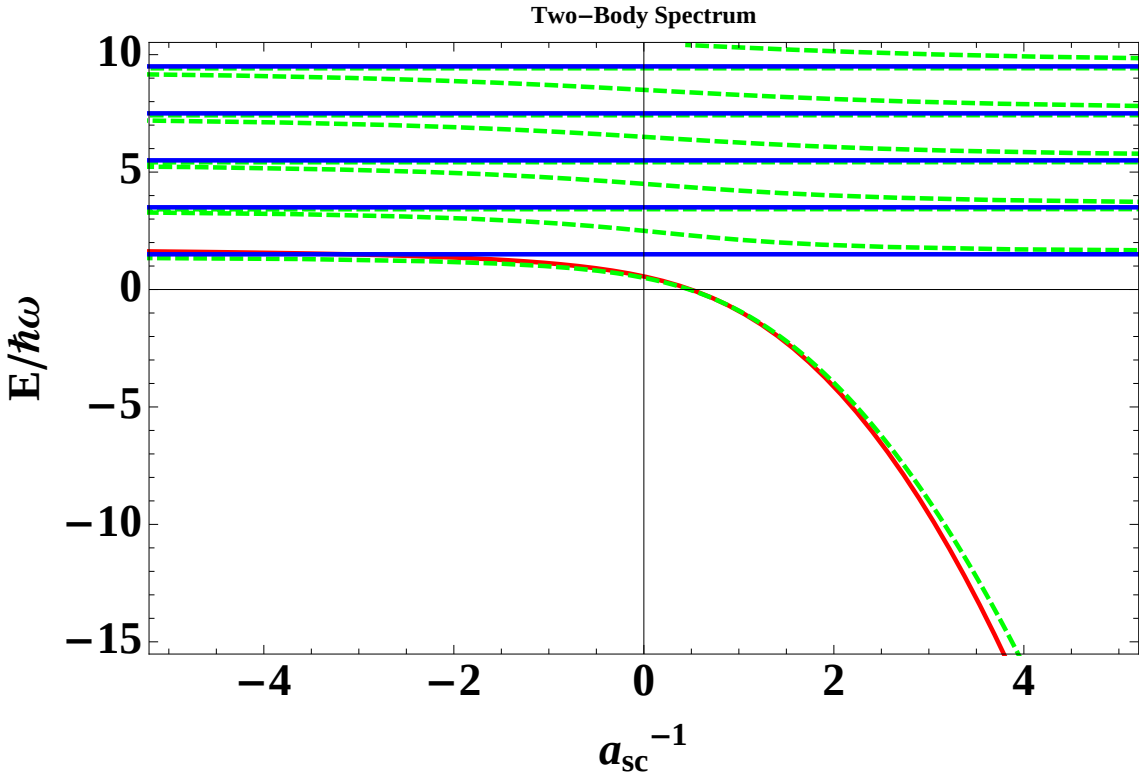

Figure 2.2: Two-body spectrum in a 3D isotropic harmonic trap. The green dashed line is from the analytical expression $\frac{a_{ho}}{a_{sc}} = \frac{\Gamma[-\nu]}{\Gamma[-\nu-\frac{1}{2}]}$, the red solid line is from an attractive short-range Gaussian model potential calculation. The short-range potential that has been used in this spectrum is $V(r) = V_0 \exp(-\frac{r^2}{2d_0^2})$, where $d_0 = 0.01 a_{ho}$.

	$a_{sc} = 0$ $(\nu = 0)$	$a_{sc} = \pm\infty$ $(\nu = \frac{1}{2})$	$a_{sc} = \pm\infty$ $(\nu = \frac{3}{2})$
Feature	Non-interacting	Molecular Branch	Atomic Branch
Wave function near $r \to 0$	$\exp(-r^2/2)$	$\exp(-r^2/2)\Gamma[-\nu](-\frac{1}{2r} + r + O(r))$	$\exp(-r^2/2)\Gamma[-\nu](\frac{3}{4r} - 3r + O(r))$
Energy	$\frac{3}{2}$	$\frac{1}{2}$	$\frac{5}{2}$
Energy of nearby states	$\frac{3}{2} + \frac{a_{sc}}{a_{ho}} A_\nu$	$\frac{1}{2} + \frac{a_{ho}}{a_{sc}} B_\nu$	$\frac{5}{2} + \frac{a_{ho}}{a_{sc}} B_\nu$

Table 2.3: Properties of the two-body system in the non-interacting and the unitarity.

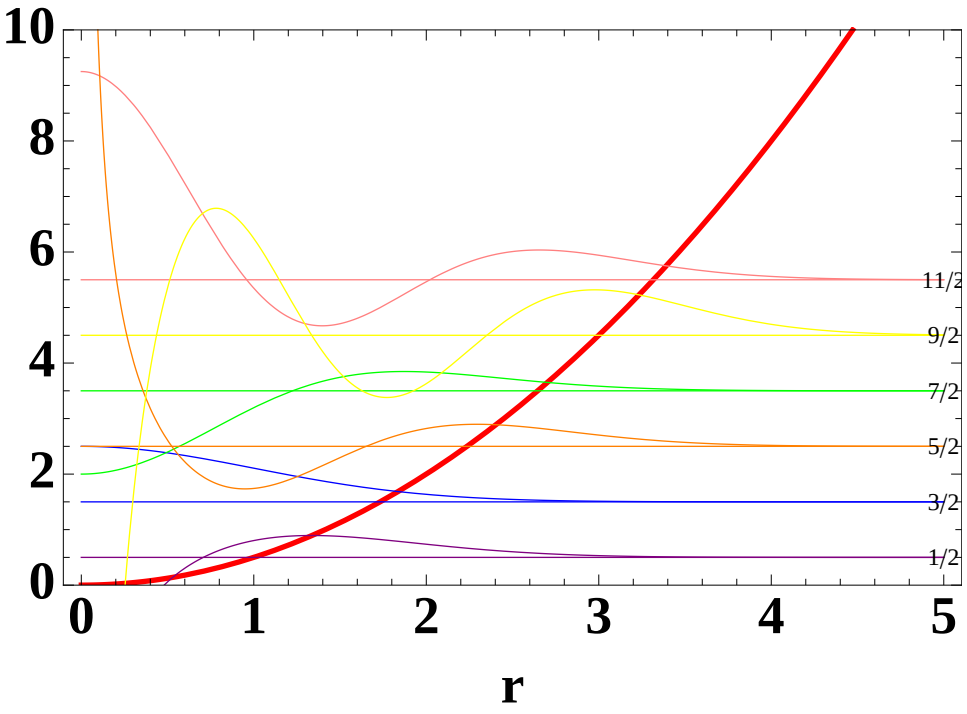

Figure 2.3: Two-body wave functions correspond to quantum number $\nu = -\frac{1}{2}, 0, \frac{1}{2}, 1, \frac{3}{2}, 3$. The red solid line represents the harmonic trap. Eigenenergies $E = \hbar\omega(2\nu + \frac{3}{2})$ are listed on the right hand side of the figure. The wave functions are plotted using the same color as the energy.

For a three-body system, even s-wave bound states needs additional boundary conditions in the hyperadius to determine the bound state energy.

2.3.2 Adiabatic Spectrum of Three-body States in an Isotropic Harmonic Trap

To understand the few-body scattering processes in ultracold Bose-Fermi mixtures, the starting point is the three-body system. Extensive theoretical works have been done in three-body systems, both homonculear and heteronuclear, various mass ratios, zero-range and long range interactions. Jesen, Nielsen, Fedorov and Garrido *et al.* developed a systematic description of the three-body system in the context of nuclear physics [ZDF$^+$93, NFJG01, NFJ98, JCF$^+$99, JRFG04]. Their series of works have focused on structures and reactions of the quantum halo, which refers to clusters of particles with a radius extending well into classically forbidden regions.

So the purpose of this chapter is to compare my results to existing analytical, numerical and experimental results. Stable and convergent three-body energetics serve as the numerical prerequisites for understanding the scattering processes in four-body systems and beyond.

Since the ultracold experiments are often in the low-energy scattering regime, we limit our calculation to the low partial waves ($L = 0$ and $L = 1$) in the total angular momentum. The weakly bound states treated here are associated with a broad Feshbach resonance, as narrow resonances are not considered. Losses due to relaxation and recombination into deep molecular states are not considered within the scope of this thesis.

In Efimov's early few papers, exotic trimer states were predicted [Efi70b, Efi70a, Efi73], the so called Efimov states. Before the observation of three-boson Efimov trimers in ultracold quantum gases [KMW$^+$06, KFM$^+$nt, PDH09, ZDD$^+$nt], candidate systems to observe Efimov states were proposed in [JRFG04, BHvK00] and nuclear scattering experiments have been interpreted in the context of Efimov states [TZ94]. The helium trimer was observed in [CG86] in molecular potential surface calculations. The authors proposed that the trimer states they found could be Efimov trimers, based on their breakup energy thresholds. A hyperspherical theory was applied to identify the homo- and hetero- nuclear Efimov trimers in helium later [ELG96].

Nowadays, there are two main classes of theoretical methods to understand Efimov states. One is functional renormalization group theory [BH06], as is discussed in the Introduction chapter. The other is analytical and numerical hyperspherical theory. While there are many ways to theoretically understand the three-body systems, a Green's function method developed by Rittenhouse *et al.* has been proved to be general and easy to implement [RMG10]. This method separates boundary conditions in hyperangles and particle permutation symmetry. So the scheme of this method works well for generic three-body systems. However, one limitation of this method is that it only gives a simple analytical solution for zero-range pairwise interactions. The two-body potentials are handled by Bethe-Peierls boundary conditions ($-\frac{1}{ru}\frac{d(ru)}{dr} \to \alpha$). This method does not predict the bound state energies of Efimov states at unitarity unless an additional three-body parameter is introduced.

Natrually, the question arises: How about finite-range interactions? In systems where two-body interactions have van der Waals tails, it is shown that the bound state energy of homo- and hetero- nuclear Efimov states have a universal relationship with the C_6 coefficient of the van der Waals potential, both experimentally and theoretically [WDEG12, WWDG12, Chi12]. The motivation of particularly exploring van der Waals type potentials is that they represent the typical interaction form found in ultracold atoms [CGJT10].

Interestingly, the shape of the pairwise interaction potential does not affect the universal scaling factor s_0 (the scaling factor is defined as from the eigen energies of the Efimov states at unitarity: $E^{(n)} = E_0 exp(-2n\pi/s_0)$), although it can affect the formation position of the lowest few Efimov states. So the Green's function method [RMG10] can be widely applied to all system with short-range interactions, and is not limited to pure zero-range interactions. The independence of scaling factor s_0 to details of the interaction potentials manifests Efimov states' universal behavior. As long as the interactions are nearby a resonance, details of the interactions should not affect the universal scaling behavior.

Before diving into calculations, some estimations of the three-body systems in a Bose-Fermi mixture are presented below. Table 2.4 summarizes estimations of the ground state energies of

		Ground State Energy		
Three-body System	angular momentum	$a_{sc} \sim 0^-$	unitarity	$a_{sc} \sim 0^+$
BBF	0	3	2	E_{BBF}
BBF	1	4	3	$E_{BF} + \frac{5}{2}$
FFB	0	5	?	$E_{BF} + \frac{3}{2}$
FFB	1	4	3	$E_{BF} + \frac{5}{2}$

Table 2.4: Perturbative estimation of ground state energies for different three-body systems in a mixture of fermionic K and bosonic Rb in an isotropic harmonic trap, frequency ω. Unitarity means that the two-body $l = 0$ a_{sc} diverges to $\pm\infty$. All the energies are in units of $\hbar\omega$.

different configurations from the perturbation perspective. Among all listed systems, Efimov states are only allowed in BBF L=0 configuration for KRb. In the non-interacting limit (unbound atoms) and in the molecular limit (dimer+atom), the configurations and energies could be estimated by a simple symmetry argument. While in the unitary limit, for some cases, the strong couplings between the three particle do not allow estimations based on the energetics of the two-body sectors.

Fig. 2.4 is a collection of the three-body system's energy spectrum as a function of the inter species scattering length. In the limits $a_{sc} \sim 0^+$ and $a_{sc} \sim 0^-$, the three-body systems show excellent agreement with the estimations in Table 2.4. In the unitary regime, detailed discussions are presented for each systems below.

The model potentials that we employ in this section are the Gaussian short range model potentials $V(r) = V_0 \exp(-\frac{r^2}{2d_0^2})$ and $V(r) = V_i \exp(-\frac{r^2}{2d_i^2}) + V_o \exp(-\frac{r^2}{2d_o^2})$, namely the attractive Gaussian and the repulsive core Gaussian. Thus, we do not expect the absolute value of the three-body bound state energies to have universal behavior, in contrast with those discovered with systems having van der Waals long-range interactions.

The BFF system is expected to have a relatively simple energy spectrum. So the BFF of the part calculation is used as a simple check. In the BFF system, the atom-dimer scattering is the most important scattering process. In Petrov's earlier work and in a recent experimental observation in the Grimm group, a repulsive atom-dimer interaction is observed in the $L = 0$ channel, and a attractive atom-dimer interaction is observed in the $L = 1$ channel. Grimm *et al.* identify the

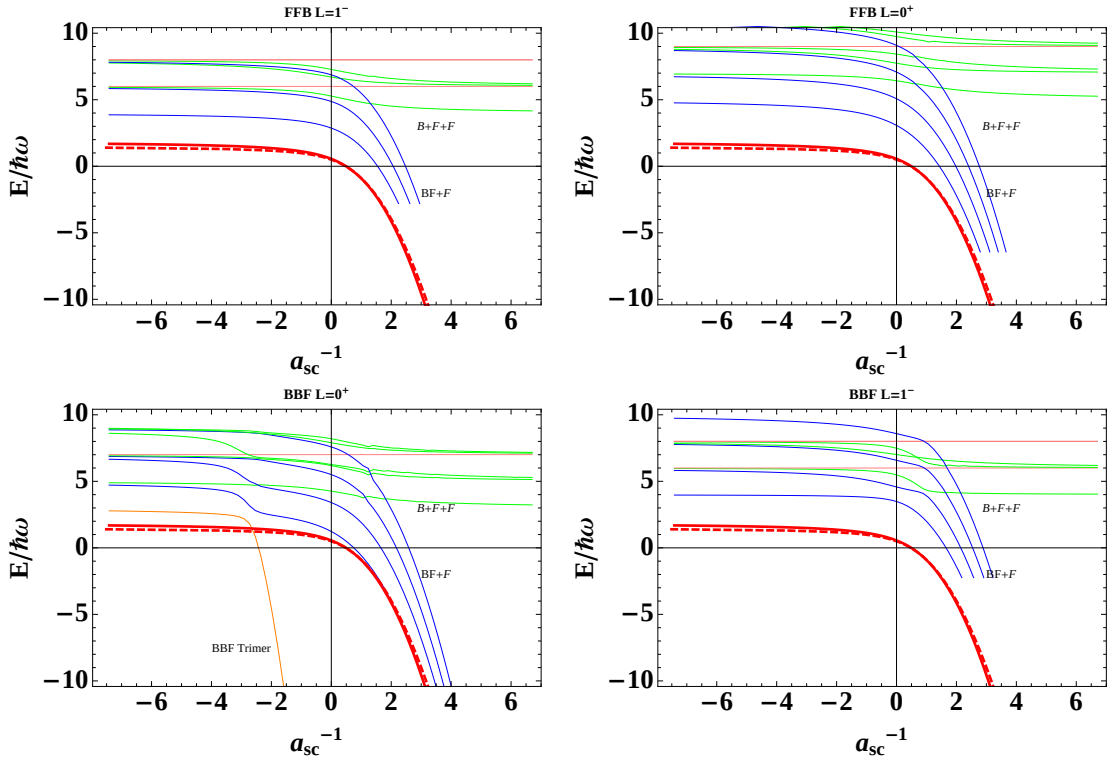

Figure 2.4: Spectrum of FFB and BBF total angular momentum L=1^- and L=0^+. Orange line: the Efimov trimer state, Red line: the two-body spectrum of one boson and one fermion in an isotropic harmonic trap. Red dashed line: the spectrum from zero-range two-body potential. Blue lines: the class of dimer-fermion, the green lines: the trap bound states. In this calculation, the boson is ^{87}Rb, the fermion is ^{40}K. The short-range model potential is $V = V_0 \exp(-\frac{r^2}{2d_0^2})$, $d_0 = 0.01 a_{ho}$. The spectrum is diabatized from the pure adiabatic spectrum, so that unphysical sharp avoided crossings are eliminated.

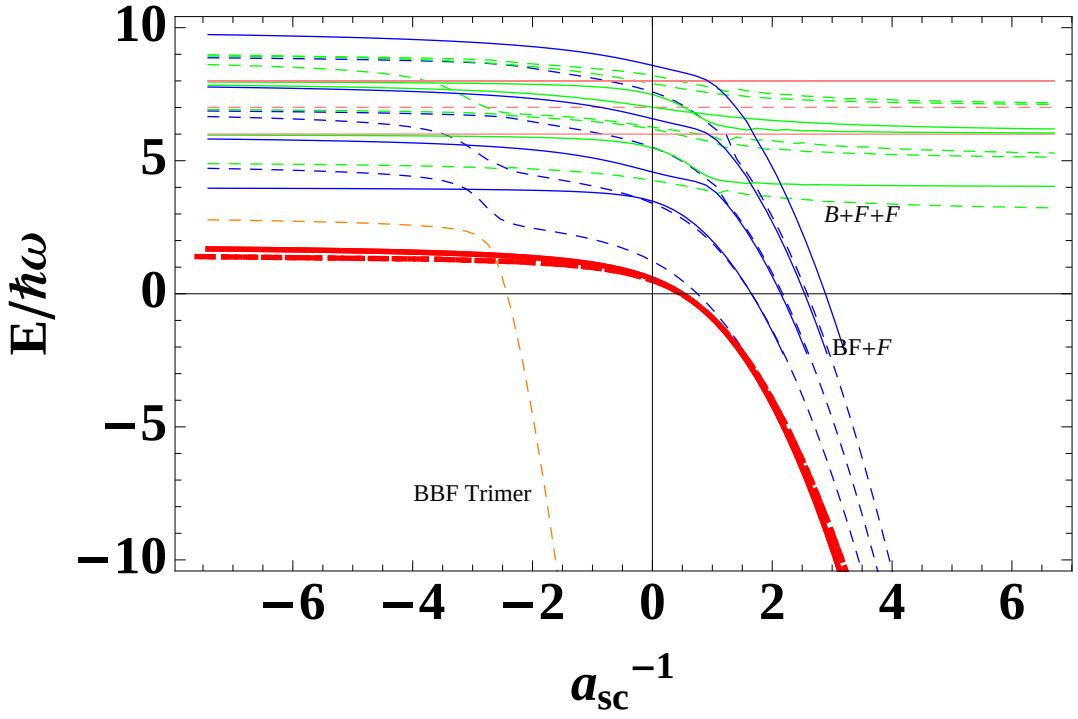

Figure 2.5: The spectrum for the BBF system, overlapping spectra of $L = 0^+$ and $L = 1^-$ symmetries. Dashed lines: L=0 spectrum; solid lines: L=1 spectrum.

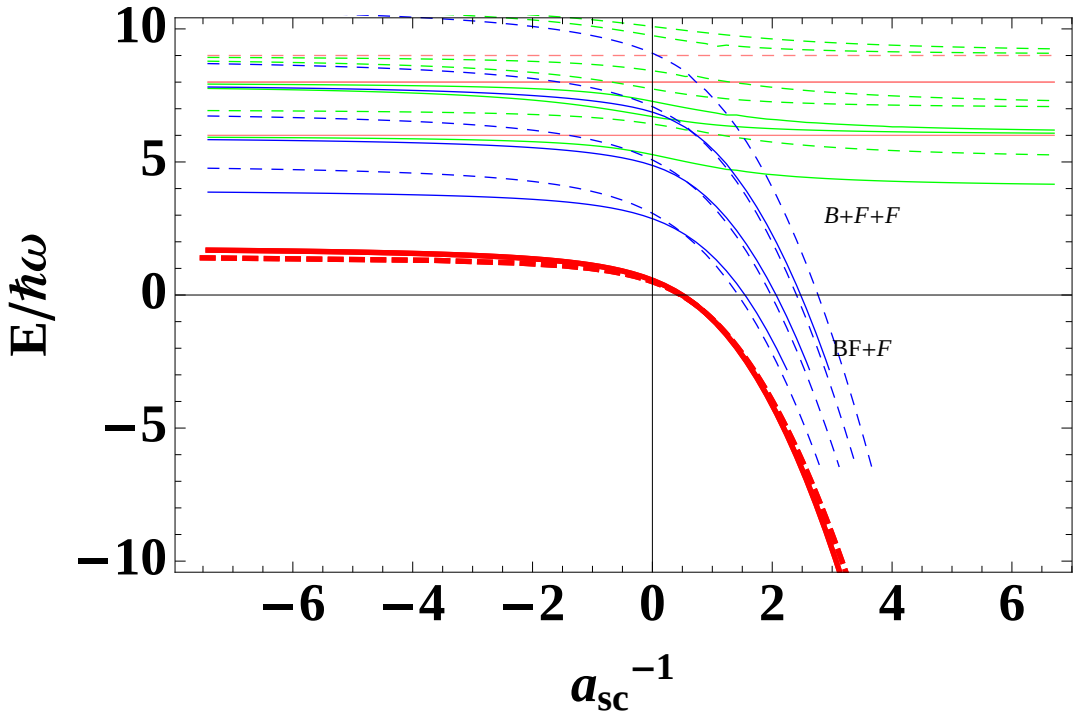

Figure 2.6: The spectrum for the FFB system, overlapping spectra of $L = 0^+$ and $L = 1^-$ symmetries. Dashed lines: L=0 spectrum; solid lines: L=1 spectrum.

attractive interaction as the dominant mechanism in their experiments [JZC$^+$13].

The BFF system in KRb is expected to be much simpler than BBF. One argument is that the Pauli repulsion between the fermions forbids the formation of a three-body bound state for mass ratio below $m_B/m_F = 8.17$. The Born-Oppenheimer and hyperspherical approximation do not show big differences in this case. The spectrum of both $L = 0$ and $L = 1$ BFF systems are shown in Fig. 2.3.2.

On the contrary, the BBF system has a richer spectrum in terms of three-body bound states. For the ^{87}Rb^{87}Rb^{40}K case, the geometrical scaling constant $s_0 \approx 0.653$, meaning $\exp(\frac{\pi}{s_0}) \approx 122.85$. (For three identical bosons, this number is ≈ 22.7.) Table 2.5 lists the values of s_0 for some heteronuclear systems [DE06a].

Besides geometric scaling in binding energies at unitarity, Efimov states have other signatures both in spectrum and hyperspherical potential curves. The positions (on interparticle scattering length a_{sc} axes) at which each Efimov trimer become bound also follow a geometric scaling rule. The scaling factor is $\exp(-\pi/s_0)$. In terms of determining the scaling factor, these trimer formation positions are equivalent to observing the eigenenergies at unitarity. The reason is that they are also affected by the harmonic trap. In general, an ultracold mixture system with larger scaling factor poses more challenges in observing the scaling factor experimentally and numerically.

Can we determine more precisely the scaling factor from short-range model potential calculations? Yes, by examining the asymptotic behavior of the hyperspherical potentials. In hyperspherical potentials, determining where a three-body system supports Efimov states is more direct. The criteria is the hyperspherical potential curve has an attractive R^{-2} tail with the coefficient $s_0^2+1/4$. This is expected even in the WKB picture. An attractive R^{-2} potential at unitarity provides us with the number of bound states from the quantization condition of the WKB potential.

The hyper spherical potential curve is also generated from correlated Gaussian basis. Unfortunately, the integrals of correlated Gaussian basis over hyperangles do not have analytical expressions in general. von Stecher have implemented the integration over hyperangles numerically. K. M. Daily showed that the integrals for even spatial dimensions have full analytical expressions, while

Trimer	s_0	$\exp(\pi/s_0)$
$^{174}Yb_2$ ^{6}Li	2.246	4.05013
$^{133}Cs_2$ ^{6}Li	1.983	4.87569
$^{87}Rb_2$ ^{6}Li	1.633	6.84704
$^{41}K_2$ ^{6}Li	1.154	15.216
$^{23}Na_2$ ^{6}Li	0.875	36.2483
$^{87}Rb_2$ ^{40}K	0.653	122.856
$^{133}Cs_2{}^{87}Rb$	0.535	355.006
$^{41}K_2{}^{87}Rb$	0.246	351759.

Table 2.5: Table of heternuclear Efimov state scalling factor.

for odd spatial dimensions would involve at least one dimensional numerical integration [DG14].

2.3.3 Quench Dynamics of Three-body Systems in an Isotropic Harmonic Trap

A long standing question about experimental observations of Efimov states, at least from the theoretical point of view is, whether it is possible to directly measure the bound state energy of an Efimov trimer. Unlike measuring the binding energy of a Feshbach molecule, the Efimov trimer's binding energy is not directly related to the interparticle scattering length. This comes from the fact that determination of the three-body parameter strongly depends on the short-range detail (the short-range cut off in hyperradius) of the hyperspherical potential.

Another challenge is that even if we know the exact functional form of the three-body parameter as a function of the two-body potential, accessing the unitary regime and staying there long enough to do a photo-dissociation type measurement of the Efimov trimer's binding energy is difficult and suffers from atomic losses.

However, the quantum beats experiment inspire us to consider, whether we can transfer the measurement of bound state energy to the measurement of the oscillation period of a quantum beat between different eigenchannels of the three-body system. The observable in the quantum beat experiment below is the number of atoms remaining in the ground state of a weakly repulsive BEC gas. The quantum beat can be qualitatively viewed as an oscillation between Efimov states at unitary and all unbound states at unitarity in the three-body system. As we will show below,

this quantum beat experiment work. In Fig. 2.7, we point out the critically important interparticle scattering lengths in the spectrum of a three-body system in the quantum beat experiment scheme, depicted in Fig. 2.8.

An example of the quantum beat oscillation is presented in Fig. 2.9 and Fig. 2.10. The low-frequency oscillation is from the trap frequency, which is $\omega = 1$, the period is in the unit $t = \frac{2\pi}{\omega}$. The high-frequency oscillation is from the binding energy of the lowest Efimov trimer at unitarity. In this oscillator unit for this particular pairwise interaction potential, this energy is$-44.0\hbar\omega$. The distinction of the fast and slow oscillations of the quantum beat enable us to infer the bound state energy of deep Efimov trimers at any given scattering length after its formation.

Fig. 2.10 shows that the contrast of this quantum beat is controlled by the time at a_{hold}. By tuning the time that the system stays at a_{hold}, the best contrast scheme can be chosen. The quantum beat experiment is in principle a sequence of sudden projections of between the sets of eigenstates of different Hamiltonian. So in contrast to the adiabatic dynamics, the quench dynamics is not only able to measure the ground state energies, but also able to measure properties of excited states. However, as a trade off, the quench system is no longer guarantee to be in a thermal equilibrium. So the micro canonical ensemble average we apply before may not be legitimate any more.

Particularly for the quench sequence, the sudden change of the wave function can be viewed as projections to eigenstates at different scattering lengths.

$$\Psi(a^{(j)}, t) = \sum_{\nu} c_{\nu}^{(j)} \psi_{\nu} \tag{2.20}$$

The three-body system is prepared to be an eigenstate of nearly noninteracting boson gas, thus is described by the lowest oscillator state in the trap. After the quench to a_{hold}, the system is allowed

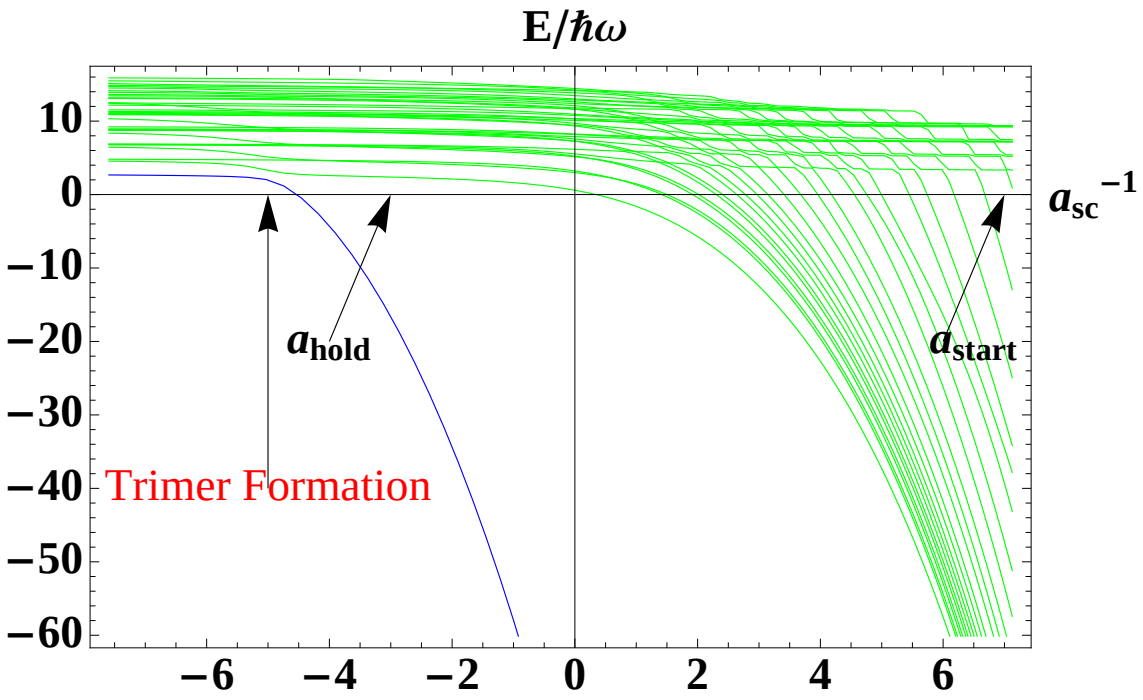

Figure 2.7: Energy spectrum of a three-body system, in which a quantum beat experiment could be performed to measure the bound state energy of an Efimov trimer at unitarity.

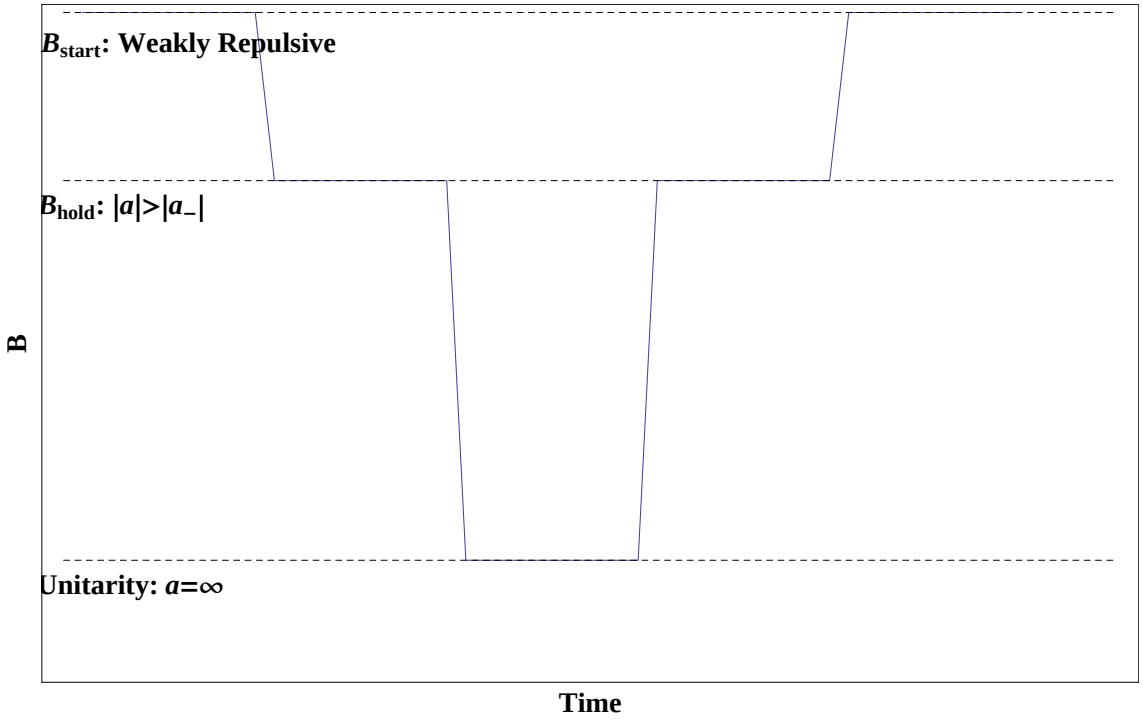

Figure 2.8: The scheme and steps of a quench experiment to measure the quantum beat period between the Efimov trimer state and the continuum.

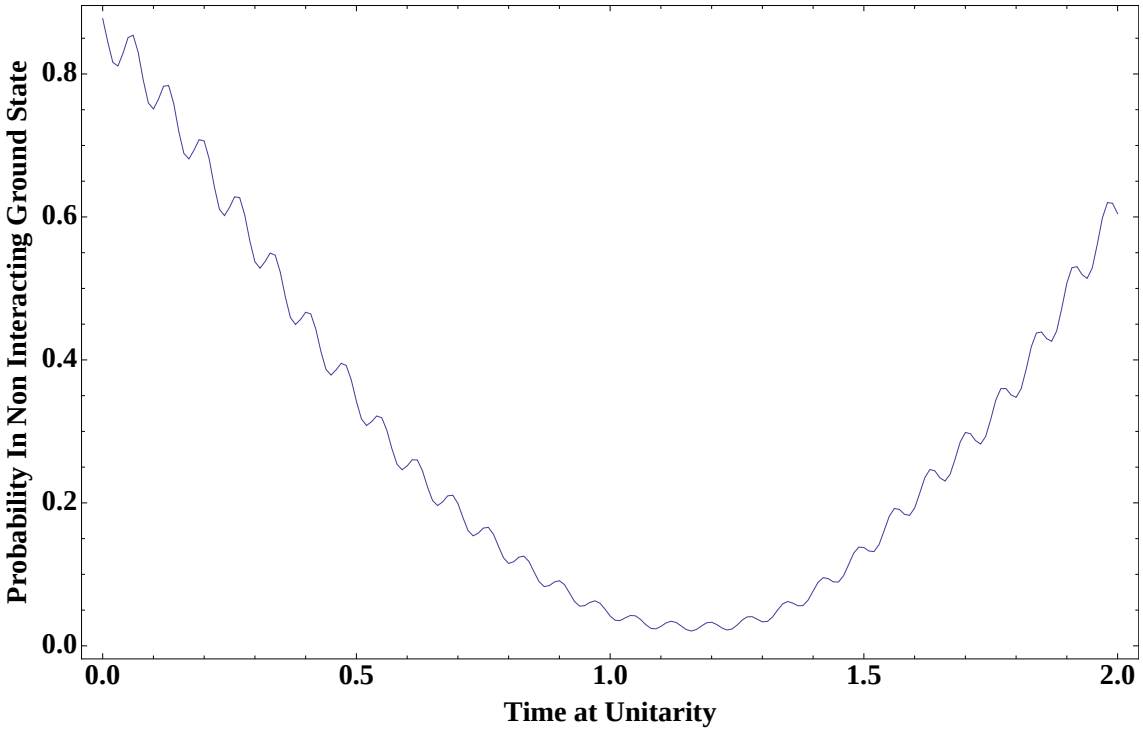

Figure 2.9: A quantum beat experiment between an Efimov trimer at unitarity and a weakly interacting three-body system.

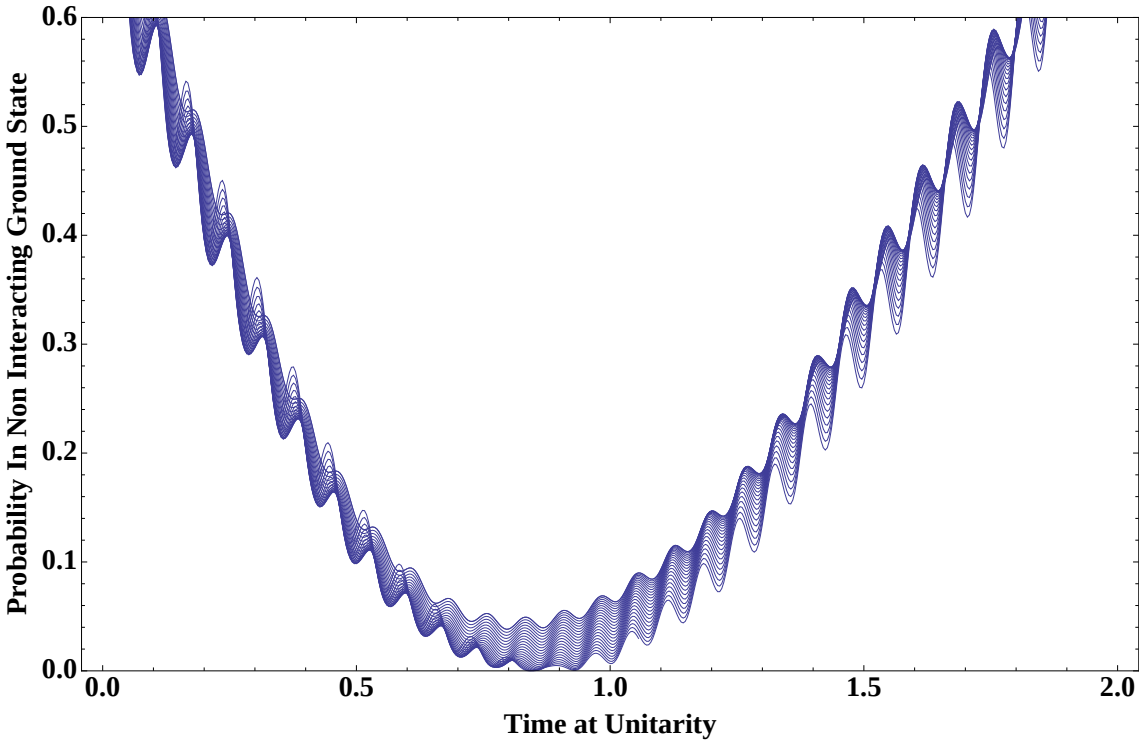

Figure 2.10: A collection of quantum beat profiles predicted that display interference in ramps between an Efimov trimer at unitarity and a weakly interacting three-body system. Different curves start with different holding times at a_{hold}.

to evolve at a_{hold} for t_{hold}.

$$\begin{aligned}
&\Psi(a_{hold}, t=0) = \Psi(a=0, t=0) = \textstyle\sum_{\nu=1}^{N} \langle \Psi(a=0,t=0)| \, |\psi_\nu(a_{hold})\rangle \, \psi_\nu(a_{hold}) \\
&\Psi(a_{hold}, t_{hold}) = \textstyle\sum_{\nu=1}^{N} \langle \Psi(a=0,t=0)| \, |\psi_\nu(a_{hold})\rangle \, \psi_\nu(a_{hold}) e^{iE_\nu(a_{hold})t_{hold}} \\
&= \textstyle\sum_{\nu=1}^{N} \langle \Psi(a=0,t=0)| \, |\psi_\nu(a_{hold})\rangle \sum_{\mu=1}^{N} \langle \phi_\mu(\pm\infty)| \, |\psi_\nu(a_{hold})\rangle \, \phi_\mu(\pm\infty) e^{iE_\nu(a_{hold})t_{hold}}
\end{aligned} \tag{2.21}$$

Then the system will stay at unitarity to time t_{evolve}.

$$\begin{aligned}
&\Psi(a_{hold}, t_{hold}+t_{evolve}) = \textstyle\sum_{\nu=1}^{N} \langle \Psi(a=0,t=0)| \, |\psi_\nu(a_{hold})\rangle \, \psi_\nu(a_{hold}) e^{iE_\nu(a_{hold})t_{hold}} \\
&= \textstyle\sum_{\nu=1}^{N} \langle \Psi(a=0,t=0)| \, |\psi_\nu(a_{hold})\rangle \sum_{\mu=1}^{N} \langle \phi_\mu(\pm\infty)| \, |\psi_\nu(a_{hold})\rangle \, \phi_\mu(\pm\infty) e^{iE_\nu(a_{hold})t_{hold}} e^{iE_\mu(\pm\infty)t_{evolve}} \\
&= \textstyle\sum_{\nu=1}^{N} \langle \Psi(a=0,t=0)| \, |\psi_\nu(a_{hold})\rangle \sum_{\mu=1}^{N} \langle \phi_\mu(\pm\infty)| \, |\psi_\nu(a_{hold})\rangle \\
&\textstyle\sum_{\nu'} \langle \phi_\mu(\pm\infty)| \, |\psi_{\nu'}(a_{hold})\rangle \, \psi_{\nu'}(a_{hold}) e^{iE_\nu(a_{hold})t_{hold}} e^{iE_\mu(\pm\infty)t_{evolve}}
\end{aligned} \tag{2.22}$$

Then the system is quenched back following a reversed order of the ramping procedure described above.

$$\begin{aligned}
&\Psi(a_{hold}, t_{hold}+t_{evolve}+t_{hold}) = \textstyle\sum_{\nu=1}^{N} \langle \Psi(a=0,t=0)| \, |\psi_\nu(a_{hold})\rangle \sum_{\mu=1}^{N} \langle \phi_\mu(\pm\infty)| \, |\psi_\nu(a_{hold})\rangle \\
&\textstyle\sum_{\nu'} \langle \phi_\mu(\pm\infty)| \, |\psi_{\nu'}(a_{hold})\rangle \, \psi_{\nu'}(a_{hold}) e^{iE_\nu(a_{hold})t_{hold}} e^{iE_\mu(\pm\infty)t_{evolve}} e^{iE_{\nu'}(a_{hold})t_{hold}}
\end{aligned} \tag{2.23}$$

This series of quenches can also be described by transformation between basis set and unitary time evolutions in the matrix formalism, which is much more succinct.

$$\begin{aligned}
&G = U(a=a_{hold}\to a=0) T(a_{hold}, t_{hold}) U(a=\pm\infty \to a=a_{hold}) T(\pm\infty, t_{evolve}) \\
&U(a=a_{hold}\to a=\pm\infty) T(a_{hold}, t_{hold}) U(a=0 \to a=a_{hold}) \\
&\Psi(t_{hold}+t_{evolve}+t_{hold}) = G\Psi(t=0) \\
&T(a,t) = diag(\exp(iE_i(a)t))
\end{aligned} \tag{2.24}$$

In this wave, we can see that during the quench dynamics, the initial state goes through a non unitary transformation as well as unitary time evolution. The phase difference accumulated during these quench steps give rise to oscillations of amplitude in different eigenstates of $a = 0$ as we change the time that the system stays at unitarity.

2.4 Four-body States in an Isotropic Harmonic Trap

2.4.1 Review of Research in Four-boson Systems

As we discussed in the last section of this chapter, three-body systems interacting through short-range potentials have been well understood both analytically and numerically. However, the level of understanding in four-body system is not as high as the three-body systems.

First of all, why we would like to address four-body systems? Arguments from the few-body and many-body community vary.

From a simplistic viewpoint in renormalization group (RG) theory of a spin-zero bosonic field, the four-body bound states correspond to the four-momentum coupling. RG theory in many systems predicts that this coupling is always irrelevant in describing the phase transitions and many other critical phenomena. However, calculations from RG show that four-body bound states in spin-zero bosonic systems should be present [HP07, PHM04, Pla09]. Besides the existence of four-body bound states, another important conclusion is that unlike in the case of three-body systems, four-body parameter that determines the cutoff length scale of the considered system is not needed for an identical boson system. In other words, the three-body parameter is sufficient to predict the four-body bound state energies. This conclusion is expected due to the fact that each three-body bound state is associated with one or several four-body bound states in the four-body spectrum. Although effective field theory provides essential insights on the energy spectrum of four-body systems at unitarity, the early works from this perspective have not predicted the full spectrum at all scattering lengths. Recently, functional RG theory attempted to predict the positions of formation in the two-body scattering length and the decay of the four-body bound states by assuming different pairwise interacting potentials [SM10].

However, the full spectrum of the four-boson system possesses more global and subtle structures. The corresponding energy spectra in Fig. 2.11 and Fig. 2.12 depict several important conclusions, suggesting, however, several fundamental questions on the generic aspects of a four-body system.

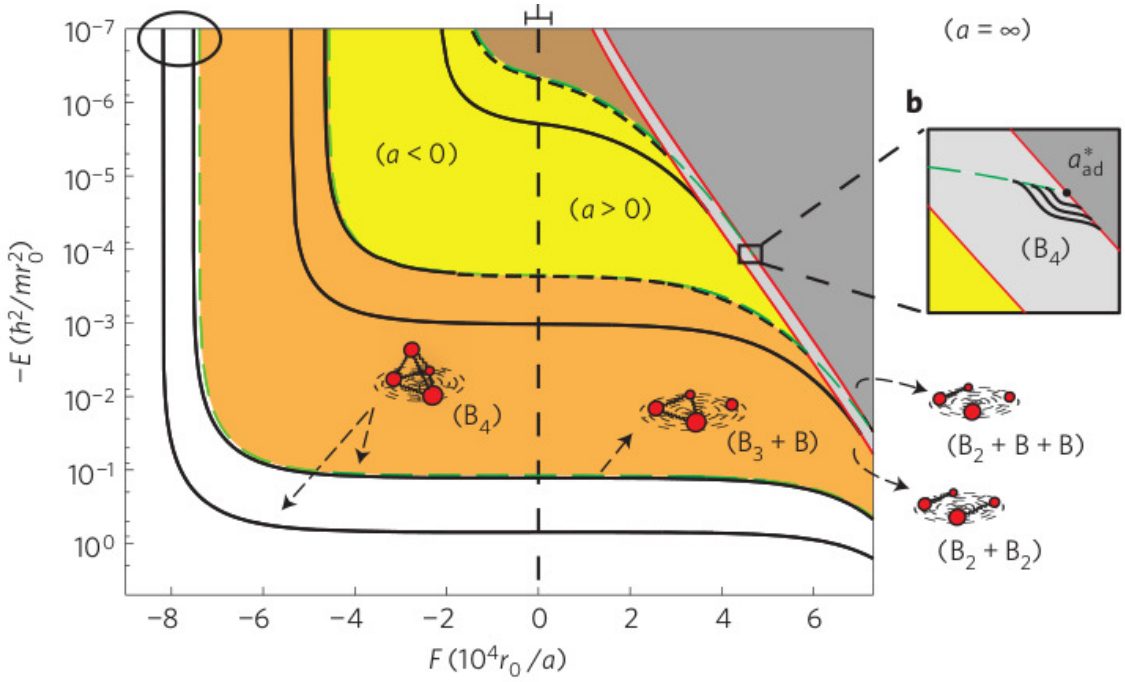

Figure 2.11: Four-boson energy spectrum. From von Stecher *et al. Nature Physics* **5**, 417 (2009) [vSDGnt]. The spectrum is plotted on a log scale in energy, as a function of the inverse boson-boson scattering length. The length unit of the spectrum is the extent of the short-range interpartice interaction r_0, and the energy unit of the spectrum is $\hbar^2/mr_0^2$. Dashed lines: Efimov trimer; solid lines: tetramers attached to each Efimov trimer. The formation positions of the trimers and tetramers are in the regime of $a < 0$, each indicating a three/four-body resonance. The positions where trimer/tetramer curves merge into the dimer curve indicate dimer-atom/dimer-dimer resonances.

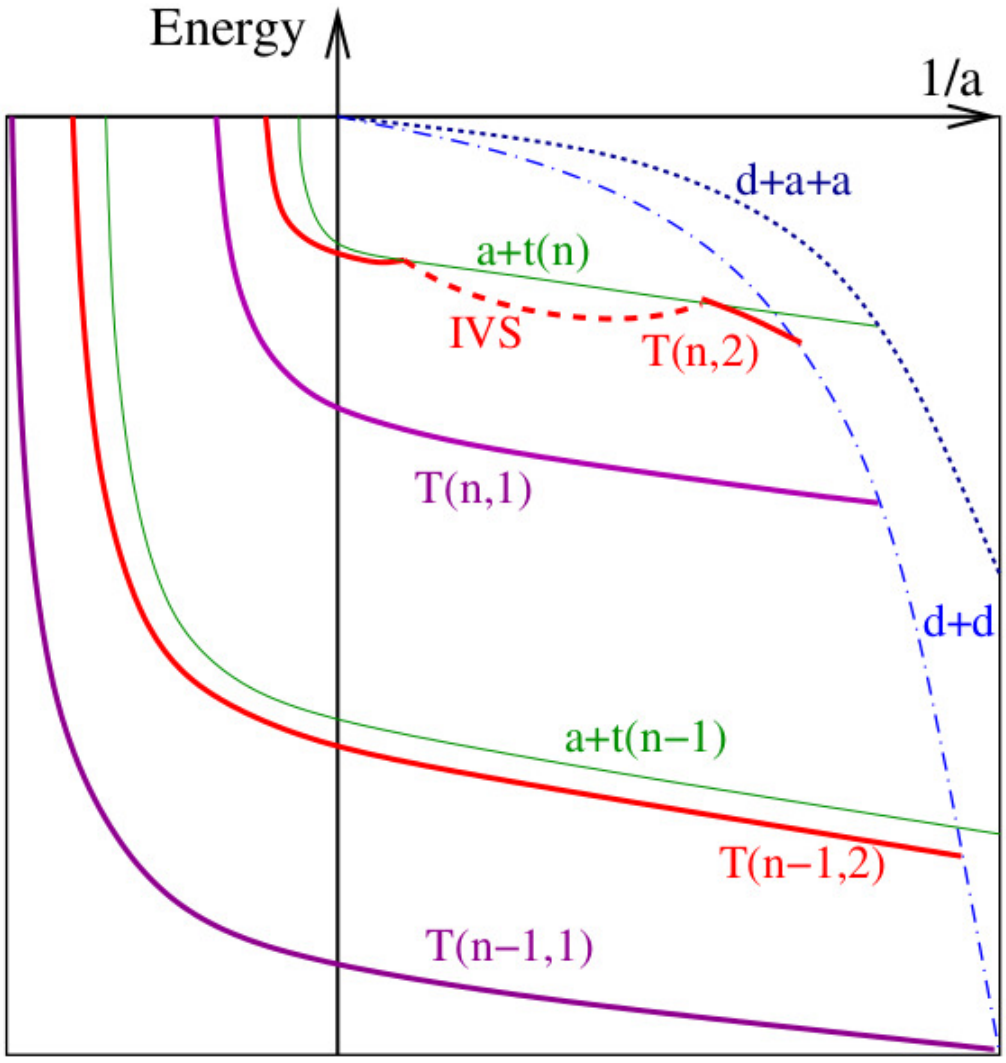

Figure 2.12: Four-boson spectrum. From Deltuva EPL (Europhysics Letters) **95**, 4(2011) [Del11]. Thin lines: Efimov trimer; thick lines: tetramers attached to each Efimov trimer, dash-dotted line: two dimer; dotted line: one dimer.

Both of Fig. 2.11 and Fig. 2.12 are spectrum of a four-boson system near unitarity. However, they do not exactly agree with each other. One main difference is that Deltuva suggested in Fig. 2.12 that in some high lying tetramer channels (four-body bound states), the tetramer forms at some negative large scattering length, then dissociate to an atom-trimer state, then goes back to a tetramer states again at some large positive scattering length. This feature was not observed in von Stecher's work, shown in Fig. 2.11.

Despite all the differences in Fig. 2.11 and Fig. 2.12, both of them present several features of the four-boson system. In a four-boson system, there are two tetramer states attached to each Efimov trimer state. Their energies possess a universal relation with the corresponding Efimov state, $E^m_{4,1} \approx 4.58 E^m_3$ and $E^m_{4,2} \approx 1.01 E^m_3$. The scattering lengths at which these two tetramer states form are $a^m_{4,1} \approx 0.43 a^m_3$ and $a^m_{4,2} \approx 0.90 a^m_3$.

Recall that the full spectrum of the three-boson system exhibits a universal geometric scaling relation of the bound state energies and formation point of each Efimov trimer. This universal relation contains two conclusions. Specifically, the universality exhibited by the three-boson system includes: (1) at unitarity $E^m_3 = 22.7^2 E^{m+1}_3$, m are counted from the lowest Efimov trimer in a bosonic gas; (2) $1/a^m_3 = 22.71/a^{m+1}_3$, a^m_3 and a^{m+1}_3 refer to the formation position of the mth and $m+1$th Efimov trimer.

In the full spectrum of the four-boson system, one might wonder whether the bound state energies of the tetramer states have similar universal relations in both the bound state energies and formation positions. Table 2.6 compares the bound state energy and formation positions of the tetramer states with the bosonic Efimov trimer. These data are from calculations in [vSDGnt]. Hence, the same universal relations in both the binding energies and formation positions are expected for the tetramers as for the trimer states. However calculations in [vSDGnt] have shown slight differences. Platter *et al.* have pointed out that the tetramer's binding energies can be solved through the Faddeev-Yakubovsky equations (FY eqns) [PHM04] for the four-boson system.

As we can see from Table 2.6, the four-body scaling factors that are extracted from the binding energy at unitarity and from the formation position of the cluster states are not exactly

	E/E_3^m	a/a_3^m
$m+1$th Trimer	22.7^2	$1/22.7$
mth Tetramer 1	$4.58(\neq (0.43)^{-2} = 5.04)$	$0.43(\neq (1/4.58)^{1/2} = 0.47)$
mth Tetramer 2	$1.01(\neq (0.90)^{-2} = 1.23)$	$0.90(\neq (1/1.01)^{1/2} = 0.995)$

Table 2.6: Table of comparison between trimer and tetramer energies in four-boson systems. Data collected from [vSDGnt].

consistent with each other, but with a slight error.

The investigations into the universal relations of tetramers in the four-boson system are not completed. Frederico, Hadizadeh, Yamashita, Tomio, Delfino *et al.* have solved the FY equation for a four-boson system [YTDF06, FTD$^+$11, HYT$^+$11, HYT$^+$12] and summarized the solutions by different methods in their recent papers [FHY$^+$13, FDH$^+$13]. Although these calculations does not scrutinize the accuracy of the ratios in Table 2.6, their interpretation of the functional form of E_4/E_3 enrich our theoretical understandings of the four-body problem. Frederico, Hadizadeh, Yamashita, Tomio, Delfino *et al.* proposed the functional of tetramer energy and trimer energy, pushing forward the research of general four-body problem. The functional form they proposed is as follows:

$$\sqrt{(B_4^{N+1} - B_3)/B_4^N} = \mathcal{F}^N(B_3/B_4^N), \tag{2.25}$$

where Bs refer to the binding energy of the three- and four-body systems. $\mathcal{F}$ refers to the tetramer scaling function in their theory. Frederico, Hadizadeh, Yamashita, Tomio, Delfino *et al.* have also provided the relation of the formation point of trimer and tetramer [FHY$^+$13, FDH$^+$13]:

$$a^T_{N_3,N+1}/a^-_{N_3} = \mathcal{A}(a^T_{N_3,N}/a^-_{N_3}), \tag{2.26}$$

where as are the formation position of trimer/tetramer states, T refers to tetramer, $-$ refers to trimer, Ns are the index of the trimer/tetramer states. Their result is summarized in [HYT$^+$11]. However, the theory in [HYT$^+$11] assumes one of the tretramer state $E^N_{4,2}$ has identical energy as the trimer E^N_3. This assumption would contradict the findings in the work of von Stecher [vSDGnt, vS10] and Deltuva [Del11].

Interestingly, the four-boson spectrum shows signatures of similarity in the position where

the trimer-atom channels merge into the dimer-atom-atom channels as where the latter system become bound. The dimer-atom-atom configuration can be perceived as a new three-body system. Thus this system resonantes with the two-body system of a trimer and an atom. This position can be viewed as a trimer-atom resonance. This feature is also found by Frederico, Hadizadeh, Yamashita, Tomio, Delfino *et al.* in [YTDF06, FTD$^+$11, HYT$^+$11, HYT$^+$12, FHY$^+$13, FDH$^+$13]. Note that these features can be experimentally observed. As the temperature of the bosonic gases is lowered, these features should be visible if errors can be reduced in comparison with the earlier experiments.

2.4.2 Heteronuclear Four-body Systems

In the active theoretical studies of four-boson systems, the difficulties in a generic four-body system have already showed up, as discussed below. For a generic few-body system with zero-range two-body interactions, the boundary conditions and permutational symmetries of the particles are coupled together. Can we separate two-body boundary conditions from the permutational symmetries? In the three-body sector, Rittenhouse *et al.* have achieved it using a Green's function method and tree rotations. The striking beauty of that method in the three-body problem is that this method completely separates the boundary conditions and quantum statistics [RMG10]. However, the generalization of this method to a four-body system suffers from coupled boundary conditions in the 2D hyperangular space (here the spatial angles are still trivially separated out, the number of hyperangles that are not from true angular degrees of freedom is two.).

On the other hand, the FY equation approach has to impose symmetry of the particles before numerical solution to reduce the dimension of the problem in momentum space. The functional RG approach is essentially a field theory approach, thus boundary conditions no longer exist in their Lagrangian. Instead, the quadratic term in the Lagrangian incorporates the two-body interactions.

Unlike in the case of the three-body system where there is only one hyperangle, a four-body system has two hyperangles. A simple generalization of Rittenhouse's method to four-body system will result in a non-separable boundary conditions in the two hyperangular degree of freedoms,

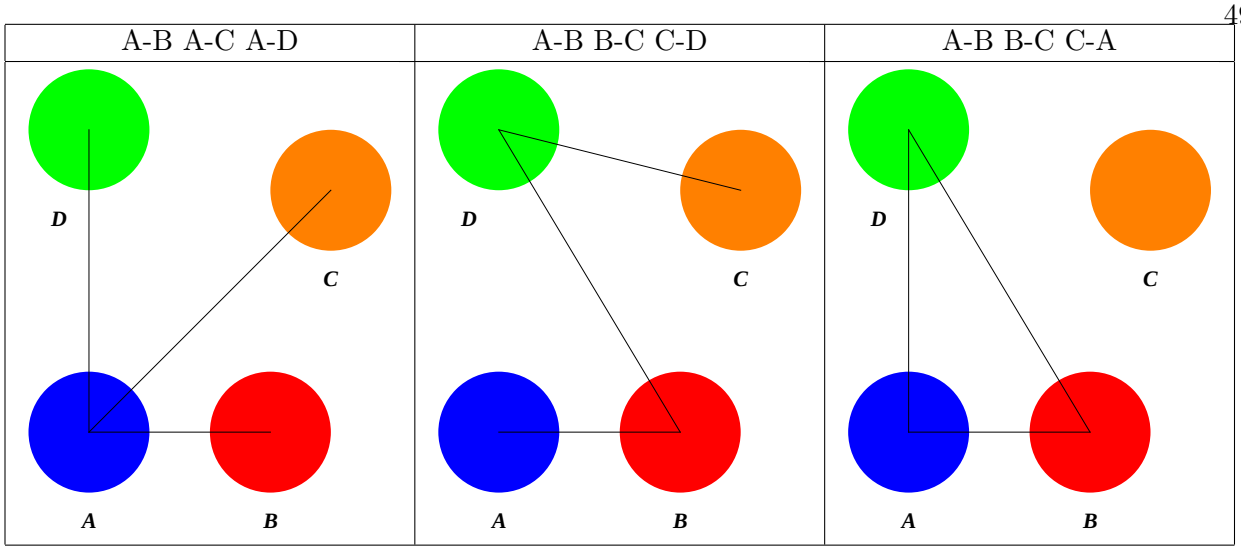

Table 2.7: Table of configurations of three pairwise boundary conditions in a generic four-body system. A B C D refer to different particles. We remark that they do not necessarily have permutation symmetry.

independent of the number of pairwise interactions in the system. In order make a non-trivial three-body system, at least two pairwise short-range interactions is required, which corresponds to two boundary conditions in the hyperangle. On the other hand, in order to create a non-trivial four-body system, the boundary conditions are more complicated, resulting in at least three two-body boundary conditions. The configurations for three two-body boundary conditions are listed in Table 2.7 and Table 2.8.

Table 2.7 and Table 2.8 show that in order to form a four-body bound state, a minimum number of 3 pairwise interactions are necessary, while 4 pairwise interactions are sufficient. Six pairwise interactions are automatically turned on in a four-boson problem due to the permutation symmetry of the particles. The four-identical-boson system certainly has a higher symmetry, however it may not be the simplest non-trivial four-body system in terms of correlations.

Particularly in a Bose-Fermi mixture, the most interesting non-trivial four-body systems include BBFF, BFFF, BBBF if pairwise interactions between boson and fermions are in the unitary regime. BBBF [WLvSE12] and BFFF [CMP10] systems are non-trivial because the resulting four-body Efimov related bound states are predicted to exist in both of them.

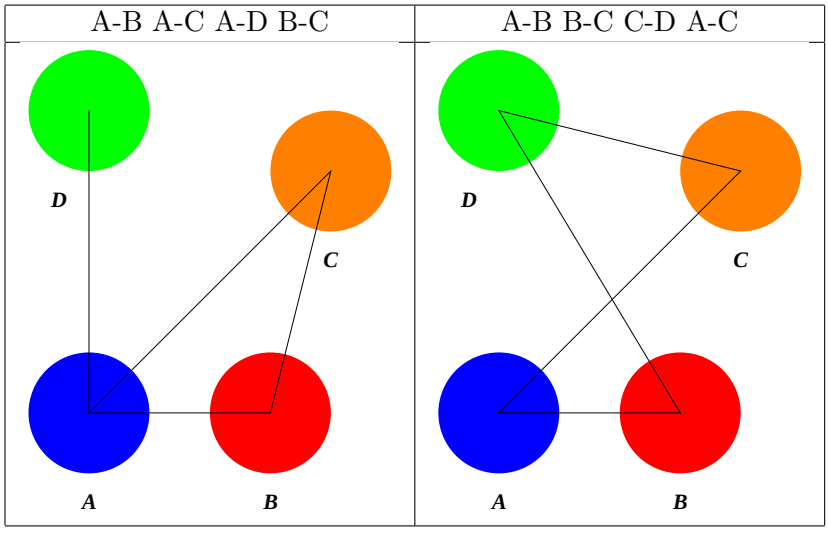

Table 2.8: Table of configurations of four pairwise boundary conditions in four-body system. A B C D refer to different particles. We remark that they do not necessarily have permutation symmetry.

However, the calculation of Wang *et al* [WLvSE12] was carried out in the BO approximation framework, and did not predict accordingly any of the mass ratios that have been in experimentally realized in the ultracold quantum gases (LiCs, KRb, NaK). The calculation of Castin *et al.* predicted a mass ratio ($13.384 < M/m < 13.607$, the heavier is a fermion) at which a four-body Efimov state can exist. This mass ratio is still different from any experimentally realized atomic species. A numerical solution of the BBBF system will help to clarify the range of validity of the BO approximation in [WLvSE12] and compare its predictions with the corresponding experimental realizations of possible four-body resonances in LiCs mixtures [TJGJ$^+$14].

Fig. 2.13 from Wang *et al.* [WLvSE12] showed the BBBX spectrum in the BO limit, where $m_B/m_X > 30$. Wang *et al.* predicted that there is only one tetramer bound state in BBBX system, and the $E_4^m/E_3^m \approx 4.34^2$. Numerical calculations in Wang's work suggests this ratio is independent of the mass ratio as long as $m_B/m_X > 30$. One immediate question is whether this conclusion applies to systems beyond BO approximation, in which m_B/m_X is not necessarily that small. One more fundamental question about four-body systems is whether the existence of a second tetramer state in the four-boson system is accidental or it is a consequence of bosonic permutation symmetry or particle-particle correlations. These questions are still open, both for theory and experiments, stimulating the interest of ultracold gas community.

While the BBBF and BFFF systems are important from the few-body perspective, the BBFF system is important in both few-body and many-body viewpoints. In the BBFF system, the BBF trimer states play an important role in scattering processes. Moreover, because the BF molecules (BF) are fermonic, in $L = 0^+$ BBFF system, only one fermonic Feshbach dimer is allowed in the regime $a_{sc} > 0$. On the other hand, in $L = 1^-$ BBFF system, two BF Feshbach dimers are allowed in the molecular regime of the spectrum. As a consequence, unlike the identical bosons, Bose-Bose mixtures, Fermi-Fermi mixtures, the ground states of BBFF system are different in different scattering length regimes. Mapping the dynamical evolutions from the few-body to the many-body BBFF systems needs knowledge of both the $L = 0^+$ and $L = 1^+$ spectra.

In the remainder of this chapter, our studies in BBFF in KKRbRb will be presented. Pre-

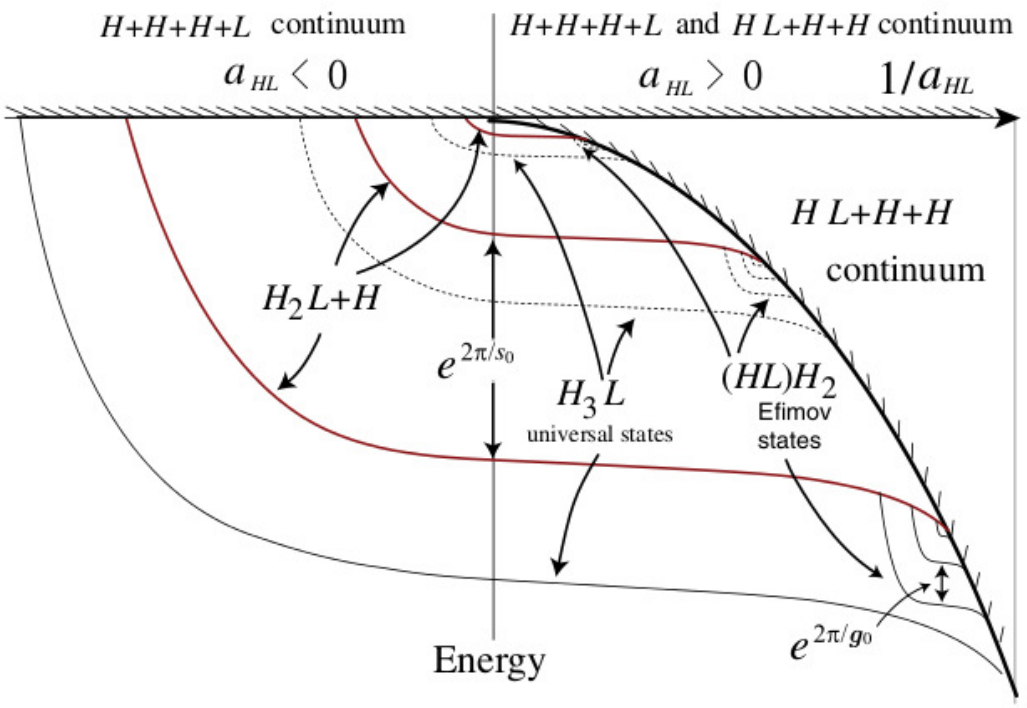

Figure 2.13: The BBBX spectrum in the BO approximation, from Wang *et al. Phys. Rev. Lett.* **108**, 073201 (2012) [WLvSE12]. H in the plot denotes the heavy bosonic particle, L denotes the other light particle X.

liminary studies of BBBF in LiCsCsCs will also be presented afterwards.

2.4.3 Spectra and Dynamics of a Bose-Fermi mixture (KRb)

In this subsection, studies of spectra and dynamics of RbRbKK systems are presented. Two total angular momentum states are considered, namely $L = 0^+$ and $L = 1^-$. The structure of this subsection is as follows:

(1) the adiabatic energy spectra as a function of interspecies scattering length are presented;

(2) the P-matrix analysis and adiabatic time evolution of the BBFF system across a broad Feshbach resonance are presented. This adiabatic time evolution is employed in order to mimic the magneto association of the weakly bound KRb molecules;

(3) the effective trimer-atom and dimer-dimer scattering parameters are extracted from the energy spectra;

(4) the hyperspherical potential curves are presented. The hyperspherical potentials constitute a complementary test to determine whether the system supports four-body Efimov states.

The first and the second point are also discussed in our published work [ZvSG12]. The third and fourth point are in preparation for publication.

The few-body Hamiltonian which corresponds to a Bose-Fermi mixture is written as follows:

$$\mathcal{H} = \sum_i \left(-\frac{\hbar^2}{2m_i}\nabla_i^2 + \frac{1}{2}m_i\omega_0^2\mathbf{r}_i^2 \right) + \sum_{i_B,j_F} V(\mathbf{r}_{i_B,j_F}), \tag{2.27}$$

where B refers to bosons, F refers to fermions, and the inter-particle interaction potential V are attractive Gaussian or repulsive core Gaussian. The boson-boson scattering length is considered to be much smaller than the trap length since the magneto association has been performed away from any boson-boson Feshbach resonance, *e. g.* the KRb experiment by Olsen *et al.* [OPCJ09]. Thus, for simplicity, only noninteracting bosons are considered in this calculation.

The eigenfunctions and eigenenergies for the few-body Hamiltonian are determined by a variational approach. The eigenfunctions are expanded in a correlated Gaussian basis as discussed in the Methods section of this chapter. This method has been previously applied in the two-

component fermion system [vSG07, Blu08, BR09, BD09, DB10, BD10a, BD10b, DB12, DRB12, GDB12b, Blu12] and in the identical boson system [DvSG09a, vS11, vSG09].

Systems which involve many bosons are in general more difficult to treat numerically, because the boson cluster states could have energies of very different scales. However, many-body fermionic systems have an energy spacing comparable to the trap energy or two-body bound energy in most of the cases. In this sense, the Bose-Fermi mixture system is also numerically challenging, because cluster states like Efimov trimers, and tetramers have very distinct sizes. In the meantime, the numerical methods are required to give good descriptions for Fermi sea of heteronuclear molecules.

After the determination of the adiabatic spectrum, the time-dependent Schrodinger equation is solved numerically using the diabetic by sector method [vSG07].

Table 2.9 summarizes the allowed configuration for $L = 0^+$ and $L = 1^-$ system.

With the optimization method discussed elsewhere in this chapter, a numerically convergent basis functions are obtained. With the optimized basis set, the spectra are calculated as functions of a_{sc}^{-1}. Fig. 2.4.3 and Fig. 2.4.3 illustrate the spectra of BBFF system as functions of inverse scattering length. Both spectra display a series of avoided crossing between the adiabatic level concentrated especially near the formation position of Efimov trimer and near unitarity.

The diabatized spectrum preserves the important physical avoided transitions while the narrow ones are eliminated by ignoring the coupling between those channels at the crossing points.

A more quantitative way to describe each avoided crossing is to evaluate the changing speed of eigenstates near that point, namely, the P-matrix elements between the two channels. The P-matrix is the non-adiabatic coupling between two adiabatic states (denoted as i and j in the following discussions):

$$P_{ij} =< \Psi_i | \frac{d\Psi_j}{d\lambda} >, \tag{2.28}$$

where λ is the adiabatic parameter in the system. A narrow avoided crossing corresponds to a narrow and sharply peaked P-matrix curve as a function of the adiabatic parameter, centered at the crossing point. On the contrary, a wider avoided crossing corresponds to a broad and smooth

		$L = 0^+$	$L = 1^-$
trimer+atom	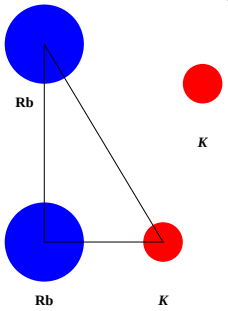	v	v
dimer+atom+atom	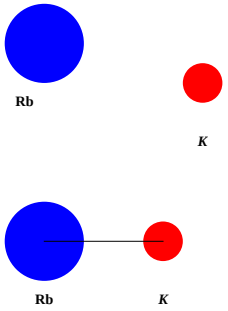	v	v
dimer+dimer	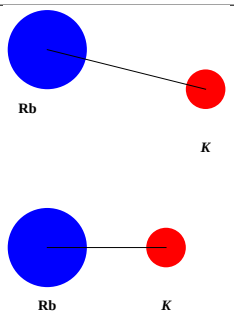		v
unbound atoms	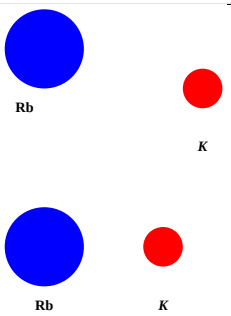	v	v

Table 2.9: Allowed configurations for the BBFF system. v means possible configuration.

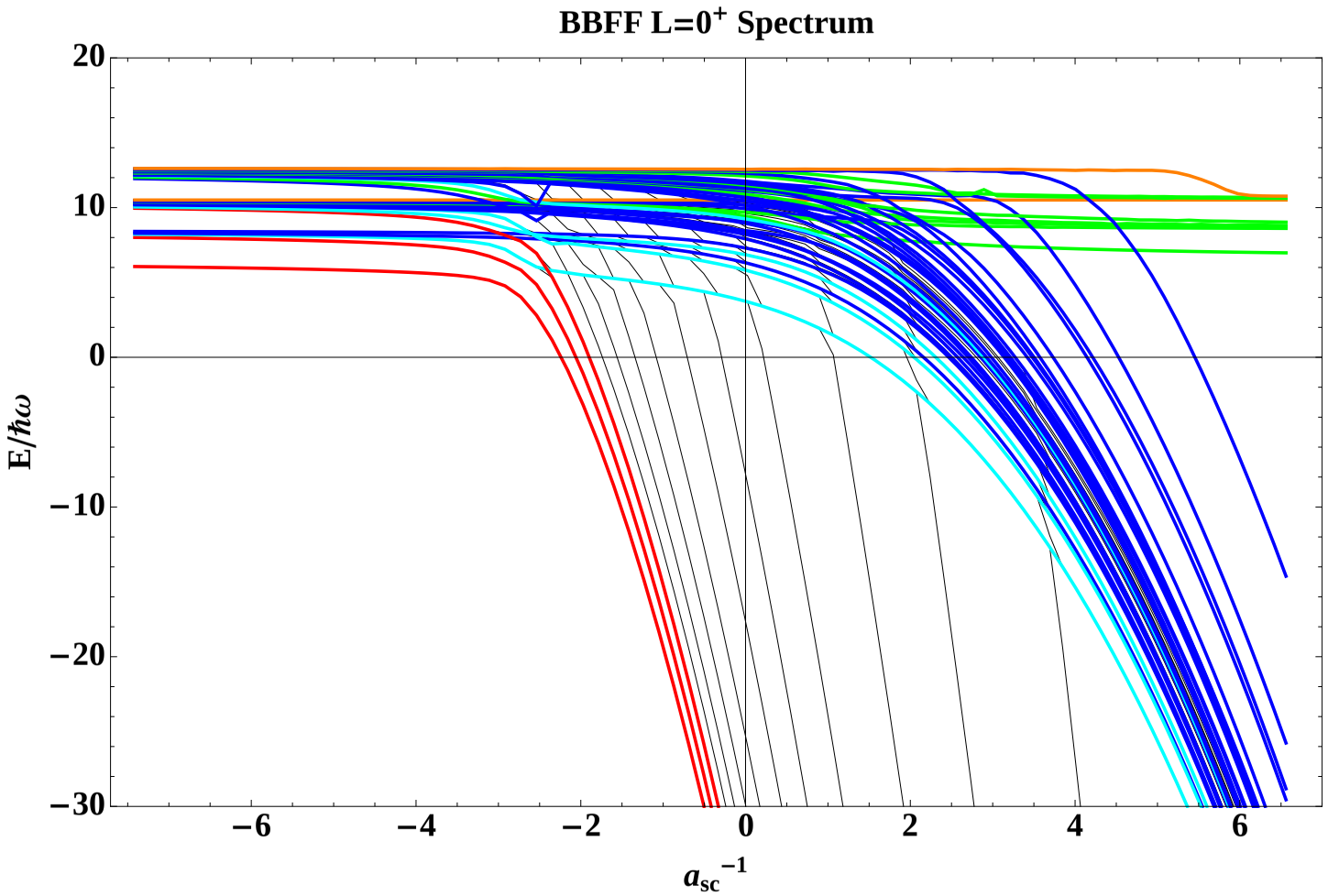

Figure 2.14: BBFF $L = 0^+$ spectrum. Black thin curves are from the adiabatic spectrum. Thick curves are the partially diabatized spectrum, different colors refer to different configuration channels. Red: trimer+atom; blue and cyan: dimer+atom+atom; green and orange: unbound atoms. The difference between blue and cyan is that near the trimer's formation point, blue lines do not have avoided crossings with the trimer class, while cyan lines have significant avoided crossings with the trimer class. The difference between green and orange lines is that the green lines resemble the features of two particle interacting through s-wave zero-range potential in an isotropic harmonic trap, while orange lines corresponds to higher partial wave two-body channels. The scattering length a_{sc} is in oscillator length unit, and the reduced mass of one boson and one fermion is defined as 1/2.

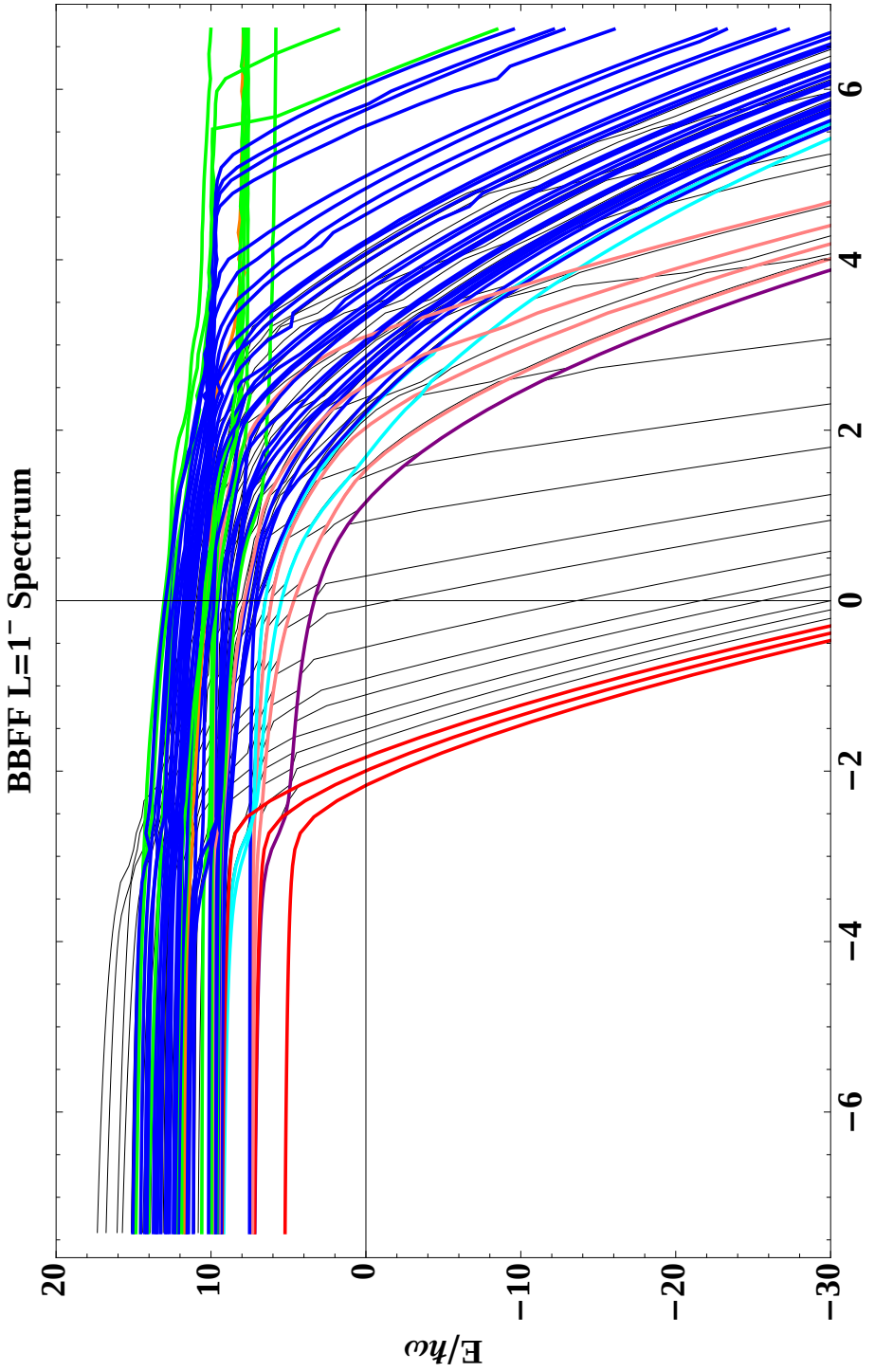

Figure 2.15: BBFF $L = 1^-$ spectrum. Black thin curves are from the adiabatic spectrum. Thick curves are the partially diabatized spectrum, different colors refer to different configuration channels. Red: trimer+atom; blue and cyan: dimer+atom+atom; green and orange: unbound atoms; purple and pink: dimer+dimer. Differences within each channel class show their differing avoided crossing behavior near the trimer formation point.

P matrix curve in the whole range of the adiabatic parameter. The diabatization procedure could also be carried out by calculating the P matrix elements connecting each pair of adiabatic states and selecting those that are sufficiently wide according to some quantitative criteria. However, this method works only in principle, it is not so effective in practical calculations.

The adiabatic parameter can be anything that has time dependence and is smoothly changing over the ramping procedure. We choose the inverse scattering length to be the adiabatic parameter $\lambda = a_{sc}^{-1}$. In the adiabatic limit, the Landau-Zener approximation is applied to interpret the time evolution result. This approximation predicts that a transition from the adiabatic eigenchannel i to j happens near the crossing point, and the probability of this transition is $T_{ij} = \exp(-\chi_{ij}/\chi)$. χ is the rate of change of the adiabatic parameter with respect to time. χ_{ij} is the characteristic rate of change for channel i and j near the crossing point. The quantity χ_{ij} is referred to as the Landau-Zener parameter.

The nonadiabatic coupling controls the probability of transitions between adiabatic channels. Clark has shown that if a transition has the form that can be approximated by the Landau-Zener model, the P matrix element for the transition from channel i to j has a Lorentzian shape for whose width, along with the corresponding eigenenergies, characterizes the Landau-Zener parameter [Cla79]. The framework of a general adiabatic transition theory was originally coined by Dykhne [Dyk62], and was later widely applied to many problems.

The important P matrices are evaluated numerically, and the fitted into Lorentzian shape to obtain a simplified Landau-Zener prediction that we can compare with the time-evolution result. The low-lying channels P matrices exhibit an approximately Lorentzian shape. However, the couplings between high-lying configurations usually do not have Lorentzian shape at all. They can be multi peaked and asymmetric near the transition point. Examples of important P matrices are shown in Fig. 2.16 and Fig. 2.17. The indices of the channels (configurations) and of the P matrix follow the definition in Table 2.10. Comparisons among Landau-Zener parameters that are fitted from a incoherent sequential transition and that are calculated from the P-matrix are in Table 2.11. Incoherent transitions series refer to the scenario that after a sequence of transitions, the

system	Channels	Final Probability Distributions
BBFF $L = 0^+$	1 (trimer+ atom)	$(1-T_{12})(1-T_{13})$
	2 (dimer+atom+atom)	$T_{12}(1-T_{23})$
	3 (4 atoms)	$T_{12}T_{23}+(1-T_{12})T_{13}$
BBFF $L = 1^-$	1 (trimer+ atom)	$(1-T_{12})(1-T_{13})$
	2 (dimer+dimer)	$T_{12}(1-T_{23})(1-T_{24})$
	3 (dimer+atom+atom)	$(T_{12}T_{23}+(1-T_{12})T_{13})(1-T_{34})$
	4 (4 atoms)	$T_{12}T_{23}T_{34}+(1-T_{12})T_{13}T_{34}+T_{12}(1-T_{23})T_{24}$

Table 2.10: The final probability distribution after the time-evolution from $a_{sc} \sim 0^-$ to $a_{sc} \sim 0^+$ across unitarity. The final probabilities are represented as sequences of Landau-Zener transitions. T_{ij} is defined as $\exp(-\chi_{ij}/\chi)$, where χ_{ij} is the fitted Landau-Zener parameter from the time-evolution calculation, χ is the ramping rate of the adiabatic parameter $\chi = \frac{d\lambda}{dt}$, $\lambda = 1/a_{sc}$.

final probability distribution into different configurations only rely on the transition probability at each transition point (in the BBFF system, the two transitions points are the trimer formation and unitarity).

In the BBFF system, there are two important transition regimes, formation point of trimer and unitarity respectively. Thus, P matrix are expected to have peaky behavior near both of them. This two-peak nature of the spectrum may potentially cause Stueckelberg type oscillation between in the formation of dimer states.

To approximately connect our few-body calculation to various many-body experiments, we construct a dimensionless ramping speed which has the density information of the system built in: $\chi = \frac{M}{\hbar\rho}|\frac{d\lambda}{dt}|$, in which M is the total mass of the molecule, ρ is the density of boson-fermion pair in the noninteracting system, and $\lambda = (1/a_{sc})$ is the inverse scattering length. This follows an analogous procedure carried out by von Stecher [vS08] in his PhD thesis research. Our calculation provides the probability distributions for creating various final states in a ramp across a Feshbach resonance as functions of the dimensionless ramping speed χ. At the same time, χ could be extracted from experimental data at each value of $\frac{dB}{dt}$, where B is the magnetic field, and our calculation predicts the molecule formation at that ramping speed. The above definition of dimensionless ramping speed is appropriate for a homogeneous system, however, we propose to use the peak density for an inhomogeneous system analogously, such as an ultracold gas in a harmonic trap.

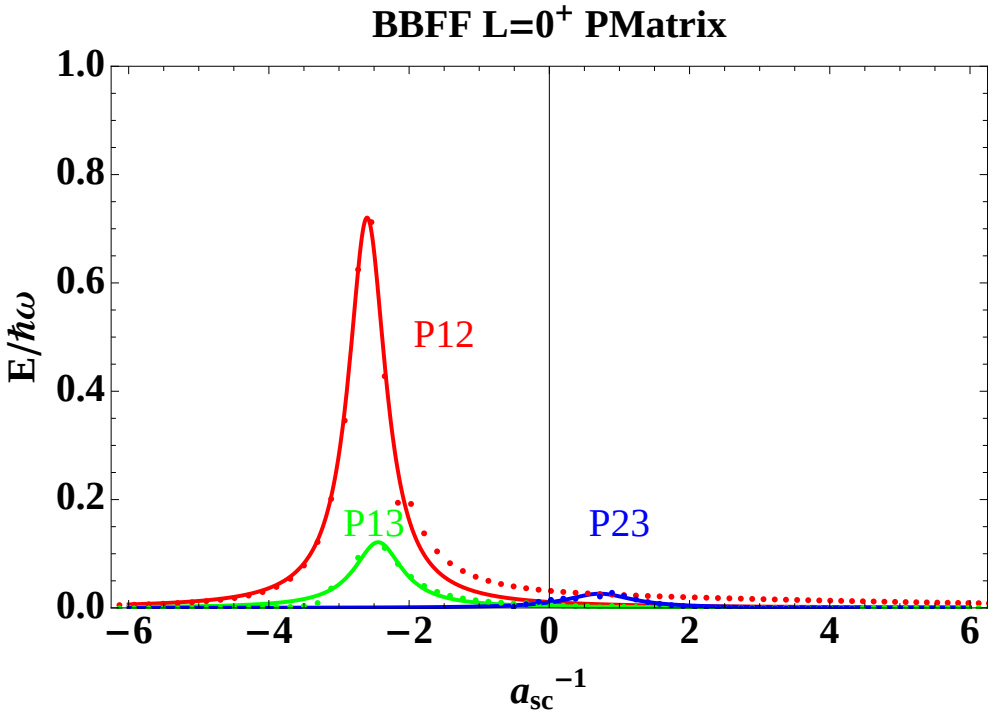

Figure 2.16: Nonadiabatic coupling P-matrix for the BBFF $L = 0^+$ system. The i j indices of the P matrix follows the index definitions in Table 2.10.

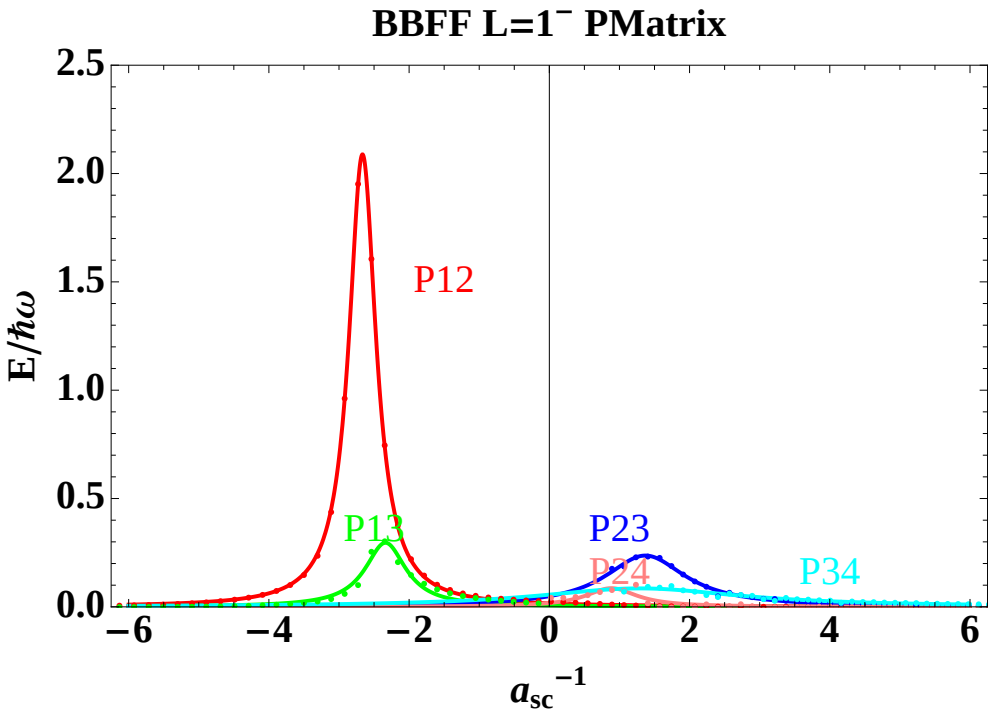

Figure 2.17: Nonadiabatic coupling P-matrix for the BBFF $L = 1^-$ system. The i j indices of the P matrix follows the index definitions in Table 2.10.

	χ	P-matrix(width)	P-matrix (height)	time-evolution
BBF $L = 0^+$	χ_{12}	1.18	1.12	0.98
	χ_{23}	22.4	47.8	19.9
BBFF $L = 0^+$	χ_{12}	1.57	1.89	2.06
	χ_{13}	11.7	110	19.1
	χ_{23}	11.8	371	43.3
BBFF $L = 1^-$	χ_{12}	1.23	1.21	1.09
	χ_{23}	6.15	76.5	4.07
	χ_{13}	6.25	28.8	13.3
	χ_{24}	3.94	48.4	15.3
	χ_{34}	29.7	92.5	28.5

Table 2.11: Comparison of the Landau-Zener parameter fitted from the time-evolution and from the P-matrix calculation. The indices follow definitions in Table 2.10.

In other words, the connection between the few-body and many-body system is realized by solving a few-body problem in an artificial trap tight enough so that the peak density of the few-body system is the same as the peak density of the many-body system. The rescaled oscillator length depends on the peak density of the many-body system, namely $a_{ho}^{RS} = (\overline{\rho}/\rho_{exp})^{1/3}$, where $\overline{\rho}$ is the dimensionless peak density $\overline{\rho} = \rho * (a_{ho})^3$ from the few-body calculation, ρ_{exp} is the peak density measured in experiments. For our calculation, the ratio of the artificial trap frequency to the experimental trap frequency $\frac{\omega_{art}}{\omega_{exp}}$ is around 30.

In our calculation, the following units are used: $\hbar = 1$, the boson-fermion reduced mass is $\mu = \frac{m_B m_F}{m_B + m_f} = 0.5$, the mass ratio is $\frac{m_B}{m_F} = \frac{87}{40}$, boson mass $m_B = 1.5815$, fermion mass $m_F = 0.72988$, total mass of the molecule is $M = m_B + m_F = 2.31$, the trap frequency is $\omega = 1$, the oscillator length of the boson-fermion relative motion is $a_{ho} = (\frac{\hbar}{2\mu\omega})^{1/2} = 1$, which is set to be the length unit, and the time unit is $\frac{2\pi}{\omega}$. The number density ρ of molecules is defined such that: $\int \rho d^3r = N$. For the experimental system, N is around $10^4 \sim 10^5$ [OPCJ09, Ols09], while for our calculation, N is 2. The dimensionless peak density is $\overline{\rho} = 1.066$.

The artificially tight trap can be related to the number ratio of the few-body system to the many-body system. For typical experimental conditions, the temperature of the fermionic atoms is around $0.2 \sim 0.3T_F$, where the number of particles is large, around 10^4 to 10^5 [OPCJ09, Ols09], so the density profile of the system can be described by the zero temperature Thomas-

Fermi approximation [BB97]. The peak density of a zero temperature noninteracting Fermi gas in an isotropic harmonic trap is proportional to $N^{1/2}$, when the particle number of N is much larger than 1. Thus the relation between the experimental trap frequency and the rescaled trap frequency can be expressed in terms of the particle number ratio for the few-body calculation divided by that in the many-body experiments, i.e., $\frac{\omega_{ho}^{RS}}{\omega_{ho}^{exp}} \sim (\frac{N}{2})^{\frac{1}{3}}$. The temperature of bosons in the Bose-Fermi mixture is around $1.1 \sim 1.2T_c$, which implies that the boson's peak density has been tuned to match the fermion's peak density in the experiments under reasonable considerations. Therefore the fermion peak density itself provides a reasonable approximation to the maximum number of atom pairs near the center of the trap.

To relate our results to recent JILA experiments [OPCJ09], the Landau-Zener parameters $\delta = \chi_{mol}/\chi$ for transitions into configurations with trimers, dimer, and atoms are cast in terms of experimentally accessible variables. Since the trimer and the dimer are not distinguished experimentally, we present one analysis for which the trimer formation is included and another analysis where it is excluded from the count of molecules formed.

The adiabatic parameter in our calculation can be related to the ramping rate in experiments, through an assumption that the dependence of the two-body scattering length $a(B)$ on the magnetic field is approximated in the usual manner as $a_{sc}(B) = a_{bg}(1 + \frac{w}{B-B_0})$, whereby $\frac{d(1/a_{sc})}{dt} = (dB/dt)/(wa_{bg})$. Here, the resonance is assumed to be sufficiently broad that, in the ramping range of magnetic field, $\omega \gg B - B_0$, whereby the ramping speed $\frac{d(1/a_{sc})}{dt}$ can be simplified to $\frac{1}{a_{bg}}\frac{1}{\omega}\frac{dB}{dt}$.

The molecule fraction in the strongly interacting limit is the most relevant quantity to compare with experiments. For the present 4-body system, the molecular fraction is defined as the probability of ending up in the dimer-dimer configuration (for the symmetries considered here, this only occurs in the $L = 1^-$ case) plus half of the probability of ending up in the BF+B+F configuration following the ramp. If we also count each trimer as an experimentally detected molecular bound state, the trimer probability should be added.

The lowest channel in the BBFF $L = 0^+$ system is the ground state of the four-particle system

in the $a_{sc} \sim 0^+$ limit, whose energy asymptotically approaches E_{trimer} plus the zero point energy of the relative motion between the trimer and the fermion. On the other hand, the lowest channel in BBFF $L = 1^-$ system in the $a_{sc} \sim 0^-$ limit is the ground state of the four-particle system, where its energy asymptotically approaches 11/2 oscillator energy quanta. In this system a two-dimer configuration is allowed, potentially enhancing the formation rate of the fermionic dimers compared to that for the BBFF $L = 0^+$ symmetry. Because the dimers are identical fermions, the relative angular momentum between two s-wave dimers must be odd, implies that states with nonzero total angular momentum state can possibly be important for understanding experiments by Olsen *et al.* [OPCJ09]. This is different from the bosonic case [PW06, IGO$^+$04], where the $L = 0^+$ symmetry for four particles can already form two dimers, as well as the trimer and tetramer following a magnetic field ramp.

The prediction of the molecule formation ratio as a function of the inverse scattering length ramping speed χ is the strongest connection between our few-body calculation and the experimental many-body observations. Fig. 2.18 shows the molecule formation ratio in the BBFF $L = 0^+$ and $L = 1^-$ systems. Although the $L = 1^-$ system has a higher upper limit for its molecule formation ratio, the formation rates for the two symmetries are very similar at fast ramping speeds.

Various experiments have been carried out that have explored the maximum formation rate of heteronuclear Feshbach molecules in recent years, including ^{6}Li^{7}Li [TSM$^+$01, SKC$^+$01], ^{6}Li^{23}Na [HSD$^+$02], ^{40}K^{87}Rb [RRMI02b, MRR$^+$02, OPCJ09] and ^{6}Li^{133}Cs [MKS$^+$02]. The highest conversion through adiabatic magnetic field ramping across Fano-Feshbach resonance in ^{40}K^{87}Rb given by JILA [OPCJ09, GIO$^+$04] is around 36 percent of the minority (^{87}Rb). Our calculation gives the conversion rate as function of ramping speed in Fig. 2.18.

By comparing the Bose-Fermi mixture experiment to former experiments, we notice that in both of the two-component Fermi gas experiments and in the single-component BEC experiments [HTR$^+$05, PW06, GIO$^+$04], the formation rates of molecules (^{40}K$_2$, ^{87}Rb$_2$) are close to unity at zero temperature and sufficiently slow ramping speed. Also, the formation rate as a function of temperature was found to be well-described by a stochastic phase-space pairing model [HTR$^+$05].

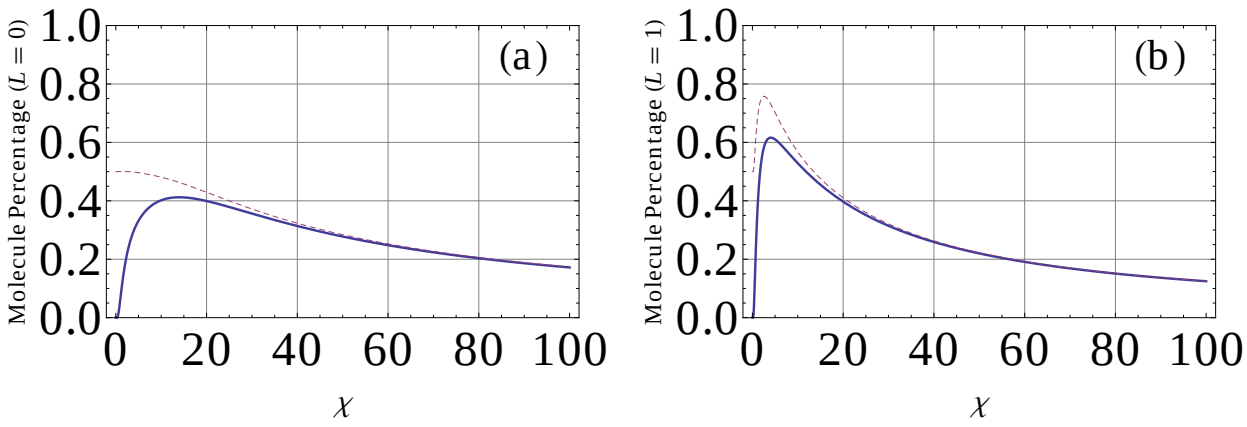

Figure 2.18: The molecule formation percentage is depicted as a function of the dimensionless ramp speed for (a) $L = 0^+$ and (b) $L = 1^-$ BBFF systems. Since the trimer and dimer were not distinguished experimentally, two separate analyses are presented here. In one analysis, a trimer is counted as a molecule (dashed) and in the other analysis the trimer is excluded from the molecules counting (solid).

However, in Bose-Fermi mixtures the experimental conversion rate of $^{40}K^{87}Rb$ dimers has never approached anywhere close to unity. The predicted molecule formation rate in the stochastic phase-space pairing model is in general higher than the observed rate in magneto-association experiments [OPCJ09]. In our few-body calculation, the possibility of trimer $^{40}K^{87}Rb_2$ formation provides a way to potentially understand why the observed molecule formation rate might be reduced: the trimer is more deeply bound than the Feshbach molecules, and might decay rapidly into one deeply bound dimer if struck by another atom, or if it pre-dissociates prior to detection, in which case the "spin flip" method for detecting the dimer [OPCJ09] would not be expected to detect a trimer bound state.

Our few-body calculations could be directly applied to understand optical lattice experiments when the tunneling between sites is small. Ideally, one boson and one fermion in one site is usually desired for such experiments, and the presence of additional bosons is likely to introduce three-body loss. However, our calculation suggests that within an appropriate sweeping speed range, the atoms in a single site containing more than 2 particles could be directly converted into a molecular bound state.

The Landau-Zener model yields a qualitative picture of the dynamical features of the trapped few-body system. It also offers some quantitative predictions for the transition probabilities and the characteristic range of ramping speeds that cause a change-over from a high rate of molecule formation to a low rate. However, the question of whether a Landau-Zener function is the appropriate functional form to describe the molecule formation fraction in a large system is still under debate [PTB$^+$05, CHT$^+$11]. Our Landau-Zener model (LZ) for three or four particles does not predict a single LZ function but rather a combination of different LZ terms that incoherently add up. Owing to its formulation in terms of the adiabatic eigenfunctions, the Landau-Zener model could identify each important transition into various possible final configurations reasonably well. Thus the functional form we have devised as a "sequence of transitions" appears to be consistent with our time dependent calculations. But a two-level Landau-Zener model cannot readily incorporate the effect of other nearby levels that may couple to one of the two levels and the fact that even

if other nearby levels do not contribute, the non-linear nature of the coupling is not captured in the simple linear Landau-Zener hamiltonian, while the final probability is regarded as a sum of the probabilities for transitions into all levels in each class, which is a limitation of the Landau-Zener model for analyzing our numerical results.

2.4.4 Scattering Properties of an Efimov Trimer near Unitarity (KRb)

In the last subsection, based on the spectrum of a BBFF system and its subsystems, the adiabatic evolution of a few-body Bose-Fermi mixture is discussed and compared to the magneto association of Feshbach dipolar molecules. However, experiments could not directly probe the trimer or tetramer bound state at unitarity back in 2009, when the experiments were performed. Although the probing of an Efimov trimer's scattering properties at unitarity is still challenging, the few-body ultracold Bose-Fermi mixture at unitary is interesting from a pure theoretical perspective.

The duality between unitarity ($a_{sc} \sim \pm\infty$) and the noninteracting system in the two-body sector is relatively well understood. However, the generalization of this idea to a Bose-Fermi mixture involves more characteristics of the system's generic properties. In a unitary two-component Fermi gas, the Fermi level sets the Fermi momentum k_F, and the order parameter and thermal dynamical quantities of the gas can be parametrized as a function of $k_F a$. The two component Fermi gas (where both spin have similar mass) is thus scaling invariant in the unitary limit. In a single component Bose gas, this scaling invariance is broken by the existence of Efimov trimers in the unitary regime. In a Bose-Fermi mixture, the relevant length scales include those from a bosonic and a fermonic system, and the ones characterizing the boson-fermion interaction. In a unitary few-body Bose-Fermi mixture, the characteristic length scales only include the density of each species and the cluster states' sizes (trimer, tetramer). Specifically in a BBFF system, since weakly bound tetramer states do not exist, the low energy elastic scattering properties of the Efimov trimer is ready to be studied.

To study the relation between the effective trimer-atom scattering length (BBF-F, referred to as a_{at} in the following discussion) and other length scales in the system, we performed calculations

for the BBFF system using a variety of pairwise interaction potentials. To extract the three-body parameter, we calculate the trimer's binding energy in free space at unitarity using various two-body model potentials. The three-body parameter κ is defined as $-\frac{\kappa^2}{2m} = E_{trimer}$, in which m is the reduced mass of the three-body system $m = \sqrt{\frac{m_B m_B m_F}{m_B + m_B + m_F}}$, E_{trimer} is the trimer's binding energy at unitary. The effective trimer-atom scattering length is extracted using the two-body in an harmonic trap:

$$a_{sc}(\epsilon) = a_{ho}\frac{\Gamma[-\frac{\epsilon}{2\omega} + \frac{1}{4}]}{\Gamma[-\frac{\epsilon}{2\omega} + \frac{3}{4}]}. \tag{2.29}$$

One may naturally think that the four particles could form a BBFF cluster state through this weak attractive interaction at unitarity. However, both the spectrum and the hyperspherical potential indicate that BBFF does not form a four-body cluster in free space. The hyperspherical potential curve of this system is in Fig. 2.19. The four-body system BBFF does not have an attractive $1/R^2$ behavior asymptotically in the atom-trimer channel. This already forbids the possibility of the four-body Efimov state in the BBFF system. Furthermore, the potential well in the atom-trimer channels is quite shallow. The term "shallow" means that a single channel calculation using this potential well does not support any bound states. So it is a further confirmation of the standard correlated Gaussian calculation that no four-body bound states will be supported in this system. This is equivalent to saying that the atom-trimer (F-BBF) scattering is far away from resonance. As a consequence, the lowest channel in the BBFF system at unitarity can be viewed as an Efimov trimer interacting with a fermion through a short-range interaction potential, parametrized by a zero-range effective atom-trimer potential. Fig. 2.20 depicts the universal relation between the trimer-atom scattering length a_{at} and the three-body parameter defined by the trimer's binding energy at unitarity.

In a few-body system, the trap length a_{ho} together with the particles number characterize the density at unitarity. For a many-particle system, it is common to apply the local density approximation to describe the in homogenous trapped system by using results from free space. However, in our treatment the quantum fluctuations in space are captured by the eigenfunctions

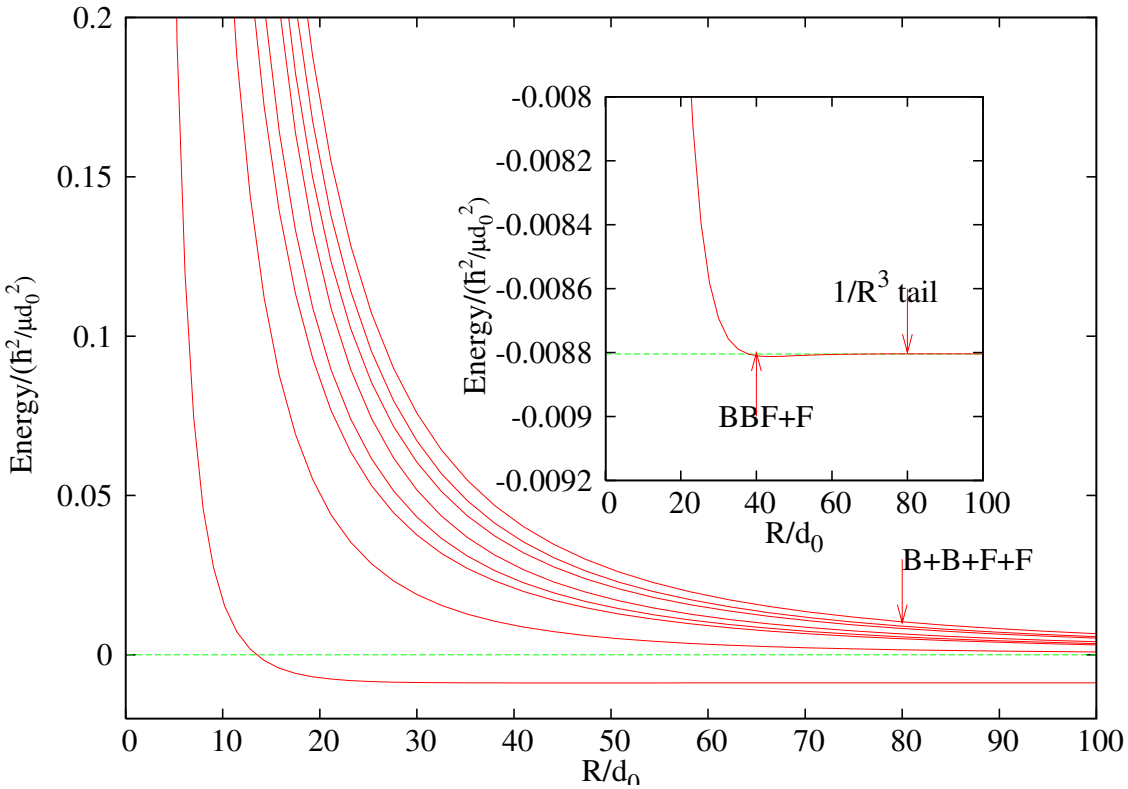

Figure 2.19: The hyperspherical potential curves of the BBFF $L = 0^+$ system at unitarity. d_0 is the extent of the short-range two-body interaction potential.

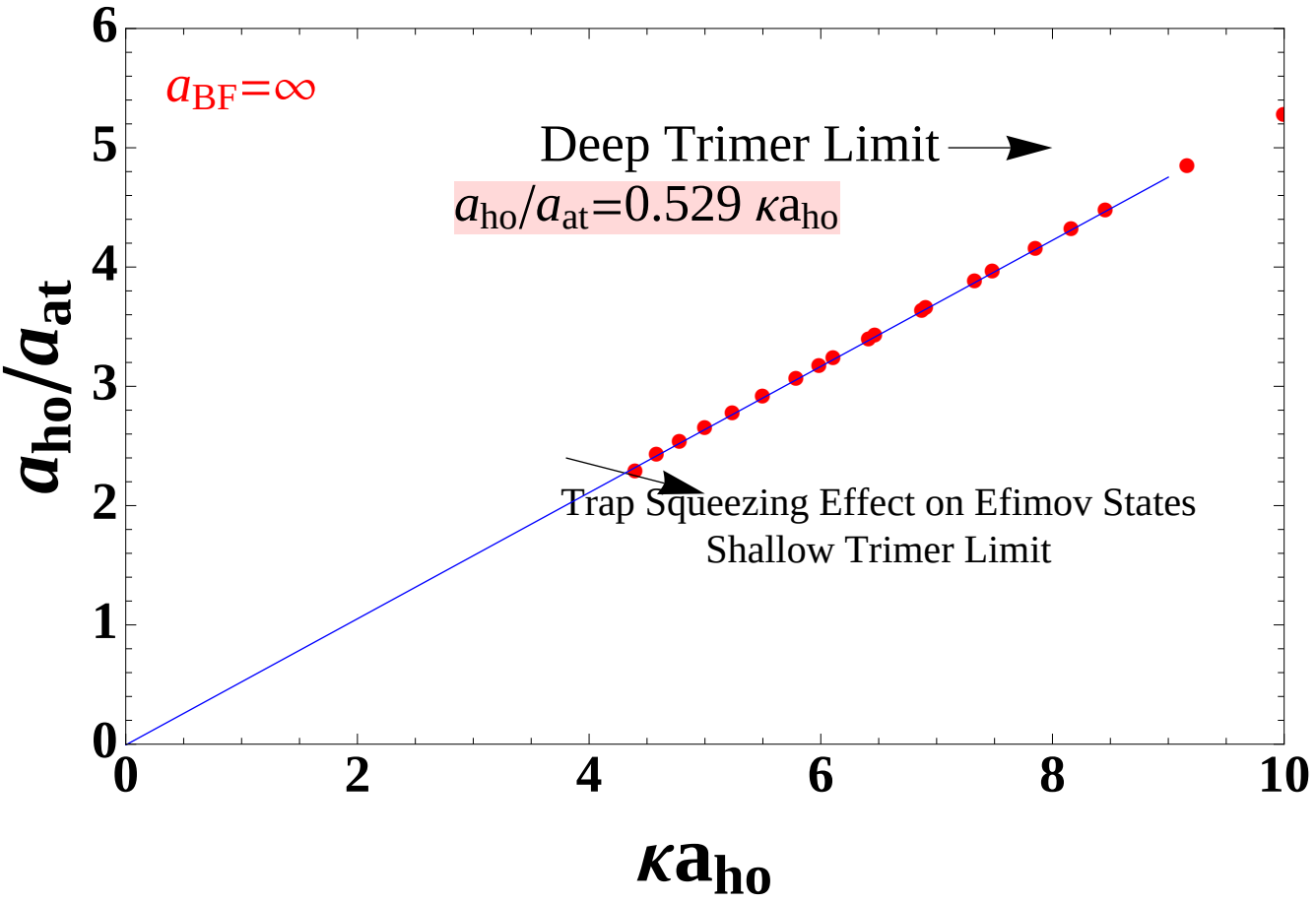

Figure 2.20: The universal relation between the trimer-atom scattering length a_{at} and the three-body parameter defined by the trimer's binding energy at unitarity ($a_{BF} = \infty$). The three-body parameter κ is defined as $-\frac{\kappa^2}{2m} = E_{trimer}$, in which m is the reduced mass of the three-body system $m = \sqrt{\frac{m_B m_B m_F}{m_B+m_B+m_F}}$, E_{trimer} is the trimer's binding energy at unitary in the oscillator unit. $a_{ho} = \sqrt{\frac{\hbar}{m_{at}\omega}}$, a_{BF} is the boson-fermion scattering length. m_{at} is the reduced mass of the trimer and the remaining fermion $m_{at} = \frac{(m_B+m_B+m_F)m_F}{m_B+m_B+m_F+m_F}$.

of the trapped gas, so no local density approximation is needed.

As is shown in Fig. 2.20, the relation between a_{ho}/a_{at} and κa_{ho} is highly linear when $\kappa a_{ho} \gg 1$. This suggests that in the deep trimer limit, the trap does not affect the bound state energy of the trimer. In the shallow trimer limit, despite setting the density of the gas, the harmonic trap also squeezes the trimer state's size.

This observation is consistent with Castin's earlier work on three-body in an harmonic trap [WC06] and Kokkelmans's later work [PK11]. In Castin's work, he presented how the trimer's binding energy spectrum, especially the high lying trimers, are affected by the trap. Castin's work on three-body system employed similar formulations as that in bosonic Laughlin states, namely, formulating the wave function in the following manner:

$$\psi = \exp(-\frac{r_i^2}{2a_{ho}^2})\Pi_{1\leq n<m\leq 3}[(x_n + iy_n) - (x_m + iy_m)]^{|\eta|}, \tag{2.30}$$

in which η characterizes the trap effect $\eta = \dfrac{E_{trimer}}{\hbar\omega}$. The limit $\eta = \infty$ is the free-space trimer system. In this limit, the Whittaker functions proposed as eigenstates in a trap go back to the BesselK functions, which describe the Efimov trimers in free space. Intuitively, we can imagine that deep trimers are less affected by the trap, whereas high lying trimers are squeezed or even destroyed by the trap. However, with only knowledge of the scaling factor, we cannot know the critical size of the trimer that the harmonic trap exhibits significant modification to the energy spectrum of the three-body system.

In the following, two methods can be employed to calculated the effective scattering length between the Efimov trimer and the remaining fermion. One method is based on a perturbation calculation in energy, assuming that the four-body system is in a weak 3D isotropic harmonic trap. The other method involves directly calculating the scattering phase shift of the effective atom-trimer scattering process, assuming that the four-body system is in free space.

The difference between these two methods is just like the difference between the variational calculation of the energy and the boundary conditions (introduced in the next chapter, variational R-matrix method). In the following discussion, we introduce the first one only.

The method of the energy variational principle works as follows. For simplicity, this method is demonstrated for the the total angular momentum $L = 0$ BBFF system in the following. The variational trial wave function of the atom-trimer bound state in the harmonic trap is:

$$\Psi = \Psi_{trimer}(1,2,3)\Psi_{sc}(\mathbf{R}_{123}, \mathbf{r}_4) - \Psi_{trimer}(1,2,4)\Psi_{sc}(\mathbf{R}_{124}, \mathbf{r}_3), \tag{2.31}$$

where the Ψ_{trimer} is the Whittaker function from Castin's work [WC06], Ψ_{sc} is the two-body wave function in a 3D harmonic trap. The wave function Ψ_{trimer} respect the boson-boson permutation symmetry, because the hyperangular part sums over two Jacobi tree contributions. Thus, the wave function only needs explicit antisymmetrization. The energy shift from the noninteracting trimer-atom system is the effective trimer-atom interaction energy.

$$\frac{<\Psi|H|\Psi>}{<\Psi|\Psi>} = E_{trimer} + E_{trimer-atom} \tag{2.32}$$

$$\begin{aligned} E_{trimer-atom} &= (N^2 - \langle\Psi_{trimer}(123)\Psi_{sc}(123,4)|\,|\Psi_{trimer}(124)\Psi_{sc}(124,3)\rangle)^{-1} \\ &(\langle\Psi_{trimer}(123)\Psi_{sc}(123,4)|\,E_k(123,4) + V(1,4) + V(2,4)\,|\Psi_{trimer}(123)\Psi_{sc}(123,4)\rangle \\ &- \langle\Psi_{trimer}(123)\Psi_{sc}(123,4)|\,E_k(124,3) + V(1,3) + V(2,3)\,|\Psi_{trimer}(124)\Psi_{sc}(124,3)\rangle). \end{aligned} \tag{2.33}$$

The trial wave function $\Psi_{trimer-atom}$ contains the effective trimer-atom scattering length. Thus, the equation above relates the three-body parameter, the scaling factor s_0 and the effective trimer-atom scattering length through an algebraic equation.

2.4.5 Spectra and Dynamics of a Bose-Fermi Mixture (LiCs)

Besides the ultracold mixture of KRb, we also considered the ultracold mixture of LiCs. Unlike KRb, LiCs has a much smaller scaling factor in the Efimov series. Thus LiCs mixtures are experimentally favorable to observe the Efimov series. In this subsection, we will present the LiCsCs Efimov spectrum calculated from short-range model potential interactions and compare to the universal scaling factor s_0 predicted in the zero-range range theory by Rittenhouse [Rit09].

The study of LiCsCs system is the starting point for studying LiCsCsCs system. First, this system is one of the most promising candidates for observation of universal scaling behaviors

of four-body cluster states. The reason is that the three-body subsystem of LiCs mixture has a relatively small scaling factor, allowing observation of more than one Efimov states. Moreover, the high-lying Efimov trimers are supposed to be more universal, suffering much less from the finite range interaction details. Thus, this system is much better than KRb in terms of observing the discrete scaling symmetry.

The scaling factor of LiCsCs system is $s_0 = 1.983$, $\exp(-\pi/s_0) = 4.87569$. This suggests at unitary, the energy scaling $E^{(n)}/E^{(n-1)} = \exp(-2\pi/s_0) = 23.7724$. From numerical model potential calculations, the first trimer state always suffer from finite-range correction, however, the second and the third trimer states already exhibit universal scalings, as is shown in Fig. 2.21 and in Table 2.12, Table 2.13.

From the two types of short-range model potential calculations, we can see that both of them give scaling factors close to that was predicted in the zero-range three-body solutions. However, there are discrepancies, and these discrepancies are strongly model dependent. This issue may arise in determining the four-body scaling factor as well, especially in the low-lying tetramer states.

With the three-body LiCsCs spectra in hand, we are ready to explore the four-body spectra of LiCsCsCs. In the four-body spectra, we are aiming at resolving the following fundamental questions:

(1) How many tetramer states can there be that are attached to each Efimov trimer?

(2) What is the scaling factor for each tetramer $E^{(4,i,n)}/E^{(3,n)}$?

(3) Does the scaling factor change as a function of the Efimov trimer index n?

2.5 Summary and Outlook

2.5.1 Summary

In this chapter, a study in the few-body theory of ultracold Bose-Fermi mixture is presented. Based on the energy spectrum of few-body systems (three- and four-body), adiabatic evolution of system is predicted. To connect the time evolution of a few-body system to its many-body counter

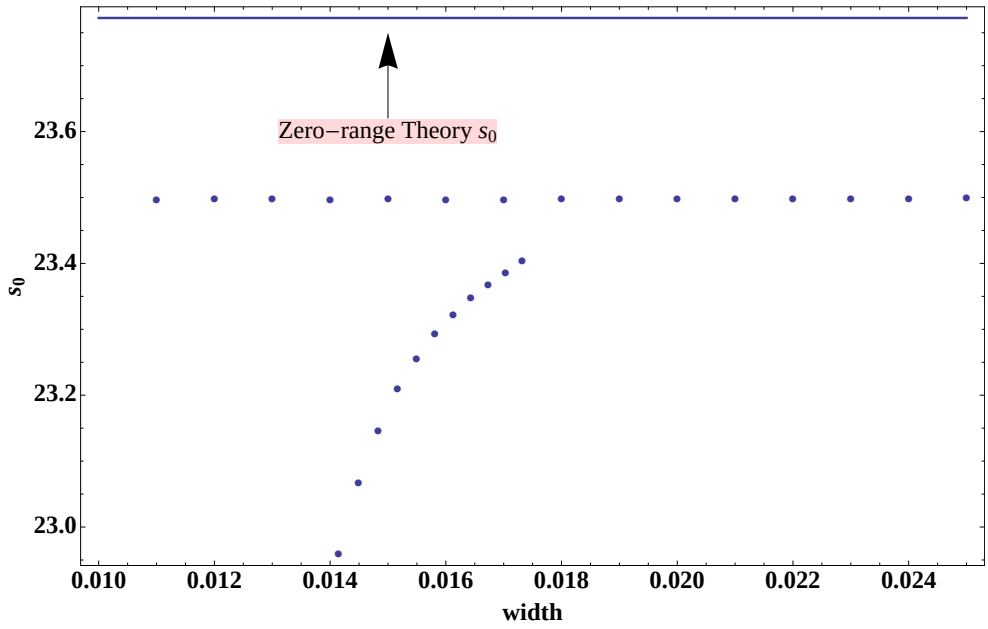

Figure 2.21: s_0 values extracted from various model potential calculations for the three-body LiCsCs systems.

d_0	$E^{(3)}/E^{(2)}$	$E^{(2)}/E^{(1)}$
0.011	15.46(56)	23.49(61)
0.012	15.46(56)	23.49(62)
0.013	15.46(56)	23.49(62)
0.014	15.46(56)	23.49(61)
0.015	15.46(56)	23.49(62)
0.016	15.46(56)	23.49(61)
0.017	15.46(56)	23.49(61)
0.018	15.46(56)	23.49(61)
0.019	15.46(56)	23.49(61)
0.02	15.46(56)	23.49(62)
0.021	15.46(56)	23.49(62)
0.022	15.46(56)	23.49(63)
0.023	15.46(56)	23.49(63)
0.024	15.46(56)	23.49(65)
0.025	15.46(56)	23.49(78)

Table 2.12: The ratio of energies of first three Efimov trimer states calculated using attractive Gaussian interactions $V(r) = V_0 \exp(-\frac{r^2}{2d_0^2})$.

d_0i	d_0o	$E^{(3)}/E^{(2)}$	$E^{(2)}/E^{(1)}$
0.01	0.02	14.26(63)	22.95(85)
0.01	0.021	14.92(87)	23.06(65)
0.01	0.022	15.42(11)	23.14(48)
0.01	0.023	15.78(55)	23.20(92)
0.01	0.024	16.05(32)	23.25(37)
0.01	0.025	16.24(77)	23.29(13)
0.01	0.026	16.38(66)	23.32(15)
0.01	0.027	16.48(31)	23.34(61)
0.01	0.028	16.54(73)	23.36(67)
0.01	0.029	16.58(68)	23.38(42)
0.01	0.03	16.60(75)	23.40(34)

Table 2.13: The ratios of energies of the first three Efimov trimer states calculated using repulsive core+attractive tail Gaussian interactions $V(r) = V_0 i \exp(-\frac{r^2}{2d_0 i^2}) - V_0 o \exp(-\frac{r^2}{2d_0 o^2})$. $V_0 i$, $d_0 i$ are the strength and width of the repulsive core, $V_0 o$, $d_0 o$ are the strength and width of the attractive tail.

part, we map the density between these two system while controlling the universal dimensionless ramping parameter χ. Although the few-body system is in principle a zero-temperature solution, the finite temperature observables can be calculated from the micro canonical ensemble average of energy eigenstates of the system.

Also based on the spectrum, specifically at unitary, the scattering properties of trimers are discussed. By testing various short-range pairwise interaction potentials, we show that in the unitary regime, the trimer-fermion scattering length has an universal relation with the three-body parameter.

Although accessing the unitary limit adiabatically is challenging, quenching the inter particle interactions by controlling external magnetic field opens the door to explore the unitary regime of a degenerate quantum gas. The quenching experiments have not been implemented for a Bose-Fermi mixture yet. However, we propose quenching experiments in Bose-Fermi mixture to directly probe the bound state energy of the Efimov trimer states.

2.5.2 Outlook

As discussed in this chapter, the future directions of research in ultracold Bose-Fermi mixture from a few-body perspective are pretty rich.

One direction is to explore systematically the structures and universal relations in terms of the heteronuclear clusters. Research in this direction will potentially resolve the debate on universalities in the tetramer bound state energies. Thus, more complete understanding in the larger cluster systems emerge in dilute quantum gases in the unitary regime will potentially be achieved.

Another direction is to explore the time adiabatic evolution of population balanced Bose-Fermi mixture systems with more particles. Research in this direction can potentially give a further understanding of how the many-body time scale emerges from a dilute system, beyond the two-body Landau-Zener picture and the simple density mapping picture.

Chapter 3

Quasi-1D Scattering in General Transverse Confinement

3.1 Introduction

The study of quantum mechanical reduced dimensional systems was started by Bethe in the early 1930s, in solving the one-dimensional(1D) Heisenberg spin chain model [Bet31]. After that, a new breed of exactly solvable models have been extensively studied in 1D spin chain models [Orb59, Wal59, dCP62, Gri64, YY66a, YY66b, YY66c]. Lieb and Liniger solved the 1D boson delta function interaction problem [LL63] in 1963. Yang and Gaudin independently solved the 1D fermion delta function interaction problem, by generalizing the Bethe ansatz [Gau67, Yan67] in 1967. The Calogero-Sutherland model and the Haldane Shatry-chain opened the door of fractional quantum statistics in 1D system [Cal71, Hal88]. Those seminal works constitute the foundations and incentives for the studies of 1D many-body physics. These advances in 1D systems were reviewed in [CCG$^+$11, GBL13].

In both many-body [Gro63, Gir60, Gir65, Hal81, DLO01] and few-body physics [Dod70, McG64, GDB12a], the predictions suggest that quantum states in reduced dimensional systems will show qualitatively different behavior from isotropic 3D systems in many nontrivial limits, *e.g.* in the zero-temperature limit and in the thermodynamic limit.

However, for a long time, the realization and observation of reduced dimensional systems were hampered by limits on existing experimental techniques. But the immense progress in laser cooling and trapping techniques in ultracold atomic gases [GWO00] enabled the exploration of reduced dimensional quantum systems. By adjusting the ratio(s) of trapping frequencies in dif-

ferent spatial directions (ω_ρ/ω_z *e.g.*), the shape of an ultracold gas can be engineered and varied continuously from a nearly isotropic 3D trapping geometry to a quasi-1D or quasi-2D geometry [MSG$^+$05a, GSM$^+$05b, GVL$^+$01]. Many experimental quasi-1D (Tonks-Girardeau gas [KWW04, PWM$^+$nt], super Tonks-Girardeau gas [HGM$^+$09, KWW05], modification of three-body recombination [TOH$^+$04],) and quasi-2D [GBM$^+$01, GVL$^+$01, DRB$^+$07, BSM$^+$07, GZHCnt, SCE$^+$12] many-body quantum systems were realized and a number of theoretically-predicted novel behaviors were observed.

The major difference between the reduced dimensional systems (quasi-1D , quasi-2D) and the pure low-dimensional systems are obviously the transverse dimensions. As a consequence, the reduced dimensional systems can be tuned close to pure low-dimensional. While tuning the trap geometry is a major knob, the temperatures and the short-range atomic potentials are also important. However, the critical values of these parameters should be deduced by incorporating the modified two-body scattering processes (by the trapping geometry and by the short-range potentials) into the reduced dimensional many-body models.

In the perturbative interaction regime, the effective 1D coupling constant in the effective 1D Hamiltonian is proportional to the the short-range interparticle scattering length in the s-wave approximation. However, when some of the length scales in the system are approaching each other in a quasi-1D (quasi-2D) systems, new resonant phenomena are expected. These resonances can be viewed as intermediate steps of continuously adjusting the dimensionality of an ensemble of quantum gas towards a pure 1D (or 2D) system. Thus, pure 1D and 2D models in general do not cover this point. The confinement-induced resonance(CIR) is a generic phenomenon that emerges from these quasi-1D (2D) systems.

From an experimental point of view, the CIR adds another way to manipulate low-dimensional systems. From a theoretical point of view, the CIR shows how the the hierarchy of length scales emerge from a competition between single particle dispersion relations and interparticle interactions. Olshanii [Ols98] first stressed the concept of CIR in the context of two particles in an elongated harmonic trap. Lieb [LSY03] gave a general discussion of the phases and thermal dynamics of bosons

moving in a quasi-1D system, raising the concept of dimensional crossover. This concept has been explored in ultracold quantum gases since then. In addition, cross-dimensional effects have been observed [EM04, LCB$^+$10] and theoretically studied [Nis10, GDB12a]. These phenomena in low-dimensional systems have recently been reviewed by [MVR12, DMBO11, YOW08, BDZ08, Pos06].

Dunjko *et.al* [DMBO11] has reviewed developments related to CIR for a variety of systems. The CIR is unique in the sense that the system exhibits the unitarity limit at a non-resonant value of the 3D scattering parameters (*i.e.* the scattering length for s-wave, and the scattering volume for p-wave).

The CIR in a harmonically transverse-confined quasi-1D system was predicted theoretically by Olshanii [Ols98], and later was extended to fermions by Granger and Blume [GB04]. Using realistic atomic interactions, the incoming wave in the z-direction will not only couple to the s-wave (or p-wave for fermions) component of the interaction, but also to higher partial waves components. Note that higher partial wave contributions to the CIR become increasingly important as the scattering energy increases. To address this point, Giannakeas *et.al* [GDS12] recently developed a method involving all partial waves, and pointed out a correction to the position of the s-wave CIR that derives from the d-wave component.

In the treatment of s-wave scattering, Olshanii [Ols98] derived the exact wave function and phase shift for a regularized zero range potential that are associated with low energy s-wave scattering. This problem can also be treated using Green's function methods. Implementation of an eigenfunction expansion of the Green's function for treating a bound state induced by a s-wave zero-range potential was discussed in [BEKW98]. A similar eigenfunction expansion of Green's functions is embedded in Olshanii's original work, although not explicitly emphasized. Later, a systematic discussion of the Green's function method and the corresponding Lippman-Schwinger equation was presented in [MEGK04, NTMJ07]. Recently the Green's function method was applied to a s-wave zero-range interaction in asymmetric transverse harmonic confinement [ZZ11]. However for higher partial waves, different mathematical models of the zero-range interaction [IC06, Der05] are needed in the Olshanii treatment. In an alternative treatment, Granger and Blume [GB04] used

the frame transformation method, in which the 3D phase shift information directly determines the 1D reaction matrix K. Thus the frame transformation approach avoids the need to design a zero-range model potential for higher partial wave scattering, which has some conceptual advantages. For example, a p-wave CIR was predicted, and later observed experimentally [dCDGC$^+$06].

As the exeperimental techniques of laser trapping have grown in sophistication, various confinement potentials beyond the harmonic trap have been realized, *e.g.* optical lattice traps [HGM$^+$09], uniform trap [GSG$^+$13]. In these systems, a more general theory of CIR positions beyond a harmonic trap is needed. Kim *et. al* gave a general description of a symmetric cylindrical hard wall trap [KSS05] using a Green's function method.

In this chapter, a systematic description is developed in order to understand the quasi-1D scattering in arbitrary transverse confinement. The structure of this chapter is organized as follows:

(1) A brief introduction to the local frame transformation [Fan81] is presented, followed by an introduction of numerical methods to solve the quasi-1D scattering problem we will employ in the rest of this chapter.

(2) The general formalism of quasi-1D confinement induced resonances is presented, in which we focus on solving the divergence problem occurring in the local frame transformation method.

(3) Example system 1: we consider the situation in which one light particle is scattered off an infinitely massive particle located in the center of the confinement.

(4) Example system 2: we generalize the concept of CIR to a scenario in which a matter wave interacts with lattice confined atoms, and we show that the system shares a common mathematical structure as in quasi-1D CIR.

(5) A summary of this chapter.

Some of the following results are discussed in the publications [ZG13a, ZG13b].

3.2 Methods

3.2.1 Local Frame Transformation

A physical system can often be divided into different regions in configurations space, where the relevant scattering channels differ. In each region, different symmetries of the interactions and the boundary conditions result in different sets of good quantum numbers.

Specifically, a quasi-1D system can be divided into two regions: $r \ll a_\perp$ and $|z| \gg a_\perp$, and the characteristic length $a_\perp$ of the transverse confinement is the relevant length scale to divide this system's configuration space (it is the oscillator length in the case of harmonic confinement, and the box side length for the square well confinement), r is the distance from the scattering center to the light particle, z is the distance in z-direction, which is the only asymptotic outgoing direction. At large distance ($|z| \gg L_\perp$) in any particular open channel ($E = \frac{\hbar^2 k^2}{2\mu} > E_{n_x,n_y}$ defines the term "open channel" with respect to its channel energy E_{n_x,n_y}, in which (n_x, n_y) are indices of the eigenstates (channels) in the transverse plane), the outgoing wave vector k_z is an asymptotically good quantum number. Thus the phase shift for each k_z asymptotically approaches to a constant. However, at very short range near the center of the confinement, where a scattering event occurs, the interaction potential imposes its full 3D spherical symmetry. Fig. is an example of the separation of length scales in a quasi-1D scattering process.

In order to connect the short-range scattering event and the large distance observables, we need to project the scattering information near the spherically symmetric scattering center onto the transverse channels yielding the quasi-1D scattering information in the z-direction. The determination of this projection is the starting point of the local frame transformation method.

The term "local" in this context was originally coined by Fano [Fan81] to distinguish this method from the usual unitary class of frame transformations (FT) in [GJ85, JR98]. Unlike the unitary frame transformation, local FTs are not unitary transformations. The two sets of eigenfunctions are actually solutions of the same Hamiltonian but with different boundary conditions. The bottom line is that they satisfy two different PDEs (partial differential equations). Thus,

the completeness of each set does not guarantee the transformation between them to be unitary, because one defines this transformation on a fixed-energy shell.

Harmin have applied this method extensively in the static Stark effect, namely, half-scattering of charged particles moving in external static EM field following an atomic photoionization event [Har81, Har82c, Har82a, Har84, Har86]. Later, this method was extended and applied to several scattering problems [Fan81, WRG88, Gre87], and in many cases it has resulted in excellent agreement with experimental observations with higher efficiency than previous theories. Note that whereas Zhao *et al.* [ZFDB12] claim to have identified a flaw in Fano's technique for the transformation of the solution that is irregular at the origin, the present application is tested numerically below and it exhibits no sign of any such discrepency.

Most of the early studies using local FT were applied in Stark or Zeeman effects, photoionization, photo-detachment problems in atom/electrons moving in external field. In recent years, interactions with a strong time-dependent laser field poses possible challenge to the local FT method, both conceptually and numerically. Conceptually, the pulse frequency and pulse duration both sets relevant energy scale and length scale of the system. However, these scales does not appear in spatial dimensions, the way they affect the matching point of the different regions may need to be reconsidered. Numerically, the number of closed channels needed to reach a convergent scattering amplitude in open channels might grow to a very large number or perhaps even diverge.

The local frame transformation is an approximation in treating scattering problems where there are well separated length scales in the system. The exact symmetries of wavefunction in the different regions of fields are not necessary, because the local FT only cares about the prevailing symmetry in each region. However, it is not expected to work well in systems where all the characteristic lengths are of the same order or magnitude. Unlike other adiabatic separation of degrees of freedom, the local FT does not rely on the existence of one particular adiabatic coordinate.

In Fano's FT theory of nonhydrogenic Stark effect [Fan81], the short-range part refer to the non-hydrogenic core having spherical symmetry, the long-range refer to the region in parabolic

coordinates $\eta \sim \infty$. The transformation is from spherical to parabolic coordinates.

$$\xi = r + z = r(1 + \cos\theta), \eta = r - z = r(1 - \cos\theta); \tag{3.1}$$

The wave functions are defined as:

$$\psi_{nm}(F, \epsilon; \xi, \eta, \phi) = N_{n\epsilon} u_{1m}(F, \epsilon, \beta_n; \xi) u_{2m}(F, \epsilon, 1 - \beta_n; \eta) e^{\pm im\phi} (2\pi)^{-1/2} \tag{3.2}$$

$N_{n\epsilon}$ are normalization constants of coordinate normalization, rather than the energy normalization used elsewhere. u functions are the eigen functions for the two ordinary differential equation of ξ and η, the β_n and $1 - \beta_n$ are the corresponding quantum numbers, F is the external electric field. Fano derived the FT theory from a K-matrix and Green's function formulation.

$$\Psi_{nm}(F, \epsilon; \xi, \eta, \phi) = \psi_{nm}(F, \epsilon; \xi, \eta, \phi) + \sum_{n'} \int_{-\infty}^{\infty} \psi_{n'm}(F, \epsilon'; \xi, \eta, \phi) \frac{\mathcal{P}}{\epsilon - \epsilon'} N^*_{n'\epsilon'} < n'\epsilon' | K_m^{(so)}(\epsilon) | n\epsilon > N_{n\epsilon} \tag{3.3}$$

The second term of the above formula is often referred to as the irregular part of a scattering wave function. In Fano's theory, the irregular part was reinterpreted as two steps: (1) acting on the free space solution sets by K-matrix; (2) acting on result from previous step the Coulomb-Stark Green's function.

$$\begin{aligned} G^{(CS)}(\mathbf{r}, \mathbf{r}') &= \textstyle\sum_{n',m} \int_{-\infty}^{\infty} d\epsilon' \psi_{n'm}(F, \epsilon'; \xi, \eta, \phi) \frac{\mathcal{P}}{\epsilon - \epsilon'} \psi_{n'm}(F, \epsilon'; \xi', \eta', \phi') \\ &= Trace(T(r) G T(r')) \end{aligned} \tag{3.4}$$

in which Ts are operators. Green's function in this case is tracing over quantum numbers. In the above formula, the value of Green's function is formulated as a trace in the quantum number space. T operator corresponds to a vector in the quantum number space (m, n), and G operator is a matrix in quantum number space.

$$\Psi_{nm}(F, \epsilon; \xi, \eta, \phi) = \psi_{nm}(F, \epsilon; \xi, \eta, \phi) + \textstyle\sum_{n'} \displaystyle\int_{-\infty}^{\infty} d\epsilon' \psi_{n'm}(F, \epsilon'; \xi, \eta, \phi) \frac{\mathcal{P}}{\epsilon - \epsilon'} N^*_{n'\epsilon'} < n'\epsilon' | K_m^{(so)}(\epsilon) | n\epsilon > N_{n\epsilon} \tag{3.5}$$

in which $W = N^*_{n'\epsilon'} < n'\epsilon'|K^{(so)}_m(\epsilon)|n\epsilon > N_{n\epsilon}$. Fano argued that at $\eta \to \infty$, ψ_{nm} oscillates so rapidly as a function of ϵ', so that its contribution vanishes except for $\epsilon' \sim \epsilon$. The TG part of the operator in Green's function reduced to:

$$G^{(CS)}(\mathbf{r}, \mathbf{r}') = \pi \sum_{n',m} \chi_{n'm}(F, \epsilon; \chi, \eta, \phi)\psi_{n'm}(F, \epsilon; \chi', \eta', \phi'), \eta > \eta', \tag{3.6}$$

in which χ is 90 degree different than ψ. Thus the TG part in the scattering wave function is:

$$\Psi_{nm}(F, \epsilon; \xi, \eta, \phi) = \psi_{nm}(F, \epsilon; \xi, \eta, \phi) + \pi \textstyle\sum_{n'} \chi_{n'm}(F, \epsilon; \chi, \eta, \phi) N^*_{n'\epsilon} < n'\epsilon'|K^{(so)}_m(\epsilon)|n\epsilon > N_{n\epsilon} \tag{3.7}$$

The K-matrix can also be derived in the spherical coordinate in the regime $r \to \infty$:

$$F^{F=0}_l Y_{lm}(\theta, \phi) = (f^0_l(\epsilon; r) + \pi g(\epsilon; r)|N_{l\epsilon}|^2 < l\epsilon|K^{(so)}(\epsilon)|l\epsilon >)Y_{lm}(\theta, \phi), \tag{3.8}$$

and it is diagonal in the spherical representation: $< l\epsilon|K^{(so)}(\epsilon)|l\epsilon >= -\pi^{-1} \tan^s_l(\epsilon)|N_{l\epsilon}|^{-2}$.

Transformation between the two coordinate sets will provide transformation of K-matrices.

$$\psi_{nm}(F, \epsilon; \chi, \eta, \phi) = N_{n\epsilon} \sum_l b_{nl}(F, \epsilon, m; r) Y_{lm}(\theta, \phi) \tag{3.9}$$

Up to this stage, the "local" approximation has not been applied yet. The two sets of eigenstates do not obey the same PDE. Thus an arbitrary function, which obeys the full Hamiltonian, can be expanded into both sets only within limited regime in space. This regime, intuitively, can be defined by the regime that the two Hamiltonians are approximately the same, referred as "local". For example, for the case of nonhyrdogenic Stark effect:

$$\begin{aligned} &b_{nl}(F, \epsilon, m; r) = a_{lm}(\beta_n, \nu) r^l [1 + O(r)]; \\ &u_{1m} u_{2m} \to (\chi\eta)^{m/2} = r^m \sin^m \theta \text{ as } \chi, \eta \to 0; \\ &f^0_l(\epsilon, r) \to r^l \text{ as } r \to 0. \end{aligned} \tag{3.10}$$

The "local" region refers to the common region of the above two. Fano's arguments not only made the idea of the frame transformation applicable, but also suggested the first order correction of this idea.

$$a_{lm}(\beta_n,\nu) = r^{-l}\int_{-1}^{1} d(\cos\theta)\sin^{2m}\theta P_l^m(\cos\theta)F(-\beta_n\nu+\frac{1}{2}(m+1),m+1,\frac{r(1+\cos\theta)}{\nu}) \\ F((\beta_n-1)\nu+\frac{1}{2}(m+1),m+1,\frac{r(1-\cos\theta)}{\nu}). \tag{3.11}$$

The integration was not required over the whole space, but only over the angular degree of freedom. This constraint makes the transformation mathematically valid. In Fano's formulation, the χ and ψ are referred to as solutions that have 90 degree phase shift with respect to each other. They are later referred to as regular and irregular solutions. It is true that ψ is the regular solution because it goes to 0 as $r \to 0$. However, the definition of irregular might be ambiguous if only examining the region $r \to 0$. Fano's original definition of χ is more appropriate in the context of local frame transformation.

3.2.2 Eigenchannel R-matrix Method

The eigenchannel R-matrix approach is a variational method of solving the scattering phase shifts or S-matrices. In stead of variationally calculating the energies of a bound state, this method calculates the scattering phase shifts in different scattering channel(s) variationally [Gre83]. This subsection follows conventions in Greene's 1983 development in the context of atomic photoionization in a strong magnetic field [Gre83].

The Ritz variational expression for the Schrodinger energy eigenvalue:

$$E = \frac{\int_\Omega \psi^* \left(-\frac{1}{2m}\nabla^2\psi + V\psi\right) d\omega}{\int_\Omega \psi^*\psi d\omega} \tag{3.12}$$

For a scattering problem, where we care about phase shift rather than the eigenenergy, boundary conditions can be expressed as:

$$\frac{\partial\psi}{\partial n} + b\psi = 0, \tag{3.13}$$

where n refers to the normal unit vector of the reaction volume Ω, b is the negative of the logarithmic derivative of the wave function on the boundary of the reaction volume. The reaction volume

is defined as a volume outside which the interactions between the particle goes either zero or asymptotic regime.

Thus, the Ritz variational expression for boundary conditions b is:

$$b = \frac{E\int_\Omega \psi^*\psi d\omega - \frac{1}{2m}\int_\Omega \nabla\psi^*\cdot\nabla\psi d\omega - \int_\Omega \psi^* V\psi d\omega}{\frac{1}{2m}\int_\Sigma \psi^*\psi d\sigma} = \frac{2m\int_\Omega \psi^*(E-V)\psi d\omega - \int_\Omega \nabla\psi^*\cdot\nabla\psi d\omega}{\int_\Sigma \psi^*\psi d\sigma} \tag{3.14}$$

If one chooses a trial basis function in the form of a linear combination of standard numerical basis (Bspline in this thesis), the following equations arise: $\psi = \sum_k c_k y_k$.

$$\begin{aligned} b[c_k] &= \frac{\sum_{kl} c_k \Gamma_{kl} c_l}{\sum_{kl} c_k \Lambda_{kl} c_l} \\ \Gamma_{kl} &= \int_\Omega \left(-\nabla y_k\cdot\nabla y_l + 2m y_k (E-V) y_l\right) d\omega \\ \Lambda_{kl} &= \int_\Sigma y_k y_l d\sigma \\ & N = \textstyle\sum_{kl} c_k c_l \Gamma_{kl}, D = \sum_{kl} c_k c_l \Lambda_{kl} \end{aligned} \tag{3.15}$$

The variational principle for the scattering phase shift leads to the condition $\frac{\delta b}{\delta c_k} = 0$. These result in a set of eigenvalue problem:

$$\frac{\partial b}{\partial c_k} = \frac{\frac{\partial N}{\partial c_k}D - \frac{\partial D}{\partial c_k}N}{D[c_k]^2} = 0 \Rightarrow \frac{1}{N}\frac{\partial N}{\partial c_k} - \frac{1}{D}\frac{\partial D}{\partial c_k} = 0 \tag{3.16}$$

$$\frac{\partial N}{\partial c_k} = \textstyle\sum_l \Gamma_{kl} c_l; \frac{\partial D}{\partial c_k} = \sum_l \Lambda_{kl} c_l; \tag{3.17}$$

$$\textstyle\sum_l \Lambda_{kl} c_l = \frac{D}{N}\sum_l \Gamma_{kl} c_l = \frac{1}{b}\sum_l \Gamma_{kl} c_l$$

$$\boxed{\Gamma \underline{c} = b\Lambda \underline{c}} \tag{3.18}$$

If the scattering process has more than one open or weakly-closed channels, the boundary condition b will be a diagonal matrix listing all the eigenchannel phase shifts.

The eigenchannel R-matrix approach is a numerically efficient method to solve a scattering problem. One of the many reasons is that, the boundary of the reaction volume Ω can be chosen as

small as several times the potential size, in a short-range potential scattering process. Compared to a full diagonalization in solving eigenenergies, the R-matrix does not have the so-called "box size" effect. Thus the box size in the scattering direction does not need to be as long as the spatial extent of the scattering wave, but is only controlled by the range of the scattering potential.

The Γ and Λ matrix can be reordered into open and closed channel blocks as follows:

$$\begin{pmatrix} \Gamma_{cc} & \Gamma_{co} \\ \Gamma_{oc} & \Gamma_{oo} \end{pmatrix} \begin{pmatrix} c_c \\ c_o \end{pmatrix} = b \begin{pmatrix} \Lambda_{cc} & \Lambda_{co} \\ \Lambda_{oc} & \Lambda_{oo} \end{pmatrix} \begin{pmatrix} c_c \\ c_o \end{pmatrix} = b \begin{pmatrix} 0 & 0 \\ 0 & \Lambda_{oo} \end{pmatrix} \begin{pmatrix} c_c \\ c_o \end{pmatrix} \tag{3.19}$$

It breaks to two matrix equations:

$$\begin{cases} \Gamma_{cc}c_c + \Gamma_{co}c_o = 0 & ① \\ \Gamma_{oc}c_c + \Gamma_{oo}c_o = b\Lambda_{oo}c_o & ② \end{cases} \tag{3.20}$$

$$\begin{aligned} ① \Rightarrow \quad & c_c = -\Gamma_{cc}^{-1}\Gamma_{co}c_o & ③ \\ ②, ③ \Rightarrow \quad & -\Gamma_{oc}\Gamma_{cc}^{-1}\Gamma_{co}c_o + \Gamma_{oo}c_o = b\Lambda_{oo}c_o & \\ & (-\Gamma_{oc}\Gamma_{cc}^{-1}\Gamma_{co} + \Gamma_{oo})c_o = b\Lambda_{oo}c_o & ⑤ \end{aligned} \tag{3.21}$$

The eigenvalue problem of b is transformed from $N_o + N_c$ dimensional into a simple N_o dimensional problem. N_c is the number of closed channels, N_o is the number of open channels in the problem.

Although the N_o dimensional problem involves Γ_{cc}^{-1}, this matrix inverse process can be replaced by a linear solver problem:

$$\Gamma_{cc}^{-1}\Gamma_{co} = A \Rightarrow \Gamma_{co} = \Gamma_{cc}A, \tag{3.22}$$

in which A can be solved using a linear solver rather than calculating a full matrix inverse.

By equating $b_{z\to R^-}$ and $b_{z\to R^+}$, we can find $\delta(k)$.

$$\boxed{\tan(\delta(k_z)) = \frac{-\frac{k_z}{b} - \tan(k_z R)}{1 - \frac{k_z}{b}\tan(k_z R)}} \quad \text{(Odd Parity)}$$

$$\boxed{\tan(\delta(k_z)) = \frac{\frac{b}{k_z} - \tan(k_z R)}{1 + \frac{b}{k_z}\tan(k_z R)}} \quad \text{(Even Parity)}, \tag{3.23}$$

$k_z = \sqrt{2 \times mass \times (Energy - Threshold_1)}$ is the momentum above the given threshold.

3.2.3 B-Spline Basis

To solve both the channel functions and the scattering functions, a basis expansion method is applied. In the numerical part of this chapter, B-spline basis functions are implemented to find the solutions of model potentials.

In this subsection, a brief introduction of B-spline basis will be presented. After defining the B-spline basis, the focus of this subsection is their advantages in solving the quasi-1D scattering problem that occurs in this chapter. More details on B-spline basis and their applications can be found in De Boor's book [DB78]. An iterative B-spline algorithm is publicly available for computer codes.

B-spline basis functions are a set of non-orthogonal piecewise polynomials spread in the region of interest. The input of B-spline basis can be well controlled, by inputing the support points. The number of basis functions, the highest order of the polynomials are also input. Each B-spline basis function does not oscillate in sign. These properties make B-spline basis functions flexible with respect to working regimes and numerically stable.

B-spline basis functions are defined in terms of polynomials of order k:

$$p(x) = a_0 + a_1 x + ... + a_{k-1} x^{k-1} \tag{3.24}$$

Each B-spline basis function and its derivatives $Df, \cdots, D^n f$ that are continuous on a given region $a < x < b$ are called class C^n. C^0 means only f is continuous and C^{-1} means f is not continuous.

Consider an interval $I = [a, b]$ divided into l subintervals $I_j = [\xi_j, \xi_{j+1}]$ by a sequence of $l+1$ points ξ_j ($Breakpoints$) in a strict ascending order:

$$a = \xi_1 < \xi_2 < ... < \xi_{l+1} = b. \tag{3.25}$$

Knots are a squence t_i, $t_1 \leq t_2 \leq ... \leq t_m$, μ is the multiplicity.

$$\begin{aligned}
&t_1 = t_2 = ... = t_{\mu_1} = \xi_1; \mu_1 = k \\
&t_{\mu_1+1} = ... = t_{\mu_1+\mu_2} = \xi_2, \\
&... \\
&t_{p+1} = ... = t_{p+\mu_i} = \xi_i; p = \mu_1 + \mu_2 + ... + \mu_{i-1} \\
&... \\
&t_{n+1} = ... = t_{n+k} = \xi_{l+1}; \mu_{l+1} = k; n = \mu_1 + ... + \mu_l
\end{aligned} \tag{3.26}$$

Different boundary conditions (zero value, zero derivative, open boundary) are handled by fixing the two B-spline functions with nonzero function value or derivative on each boundary, or in the case of open boundary conditions, not fixing them at all..

Expansion of wave function:

$$f = \sum_{i=1}^{n} c_i B_i \tag{3.27}$$

In the B-spline code given by de Boor, the function as is denoted bvalue(t,bcoef,n,k,x,jderiv).

bcoef: b coefficient sequence, length n.

$$\frac{d^j f}{dx} = \sum_i bcoef(i, j) * b(i, k - j, t) \tag{3.28}$$

where

$$bcoef(i, j) = \begin{cases} bcoef(i, 0) & j = 0 \\ \dfrac{bcoef(i, j-1) - bcoef(i-1, j-1)}{t_{i+k-j} - t_i} * (k - j) & j > 0 \end{cases} \tag{3.29}$$

$$B_i^1 = 1 \; t_i \leq x < t_{i+1}$$
$$B_i^1 = 0 \text{ other wise} \tag{3.30}$$

For $k > 1$, Property of B-spline basis:

$$B_i^k(x) = \frac{x - t_i}{t_{i+k-1} - t_i} B_i^{k-1}(x) + \frac{t_{i+k} - x}{t_{i+k} - t_{i+1}} B_{i+1}^{k-1}(x) \tag{3.31}$$

$$DB_i^k(x) = \frac{k-1}{t_{i+k-1} - t_i} B_i^{k-1}(x) - \frac{k-1}{t_{i+k} - t_{i+1}} B_{i+1}^{k-1}(x) \tag{3.32}$$

Since B-spline basis functions are highly localized, the region of numerical integrations are limited to several nearby basis rather than any pair of basis functions. This property results in several numerical advantages of B-splines:

(1) Both the Hamiltonian and the overlap matrices in solving for the bound state energies are banded: $\underline{H}C = E\underline{O}C$.

(2) Both the Γ and Λ matrices in solving for the phase shift are banded too.

(3) Multi-dimensional system can be solved by using a direct product of several 1D B-spline basis sets, which results in even more sparse banded matrix. Because of its sparsity, this banded matrix eigenvalue problem is suitable for sparse solvers.

Banded matrix storage can minimize computational needs for memory. Algorithms are also developed particularly for banded matrices, which are faster than dense matrix algorithms. Moreover, numerical linear dependence in the overlap matrix is in general weaker than that from dense matrices occur with a correlated Gaussian basis.

3.3 Confinement Induced Resonances in General Transverse Confinement

In this section, both the eigenfunction expansion and the frame transformation method are employed to solve for the quasi-1D scattering amplitude, in the presence of generic transverse confinements. Then two example systems are discussed and compared.

3.3.1 General Formalism

The quasi-1D Hamiltonian is:

$$\mathcal{H} = -\frac{\hbar^2}{2\mu}(\frac{\partial^2}{\partial x^2} + \frac{\partial^2}{\partial y^2}) + V_{trap}(x,y) - \frac{\hbar^2}{2\mu}\frac{\partial^2}{\partial z^2} + V(\mathbf{r}). \tag{3.33}$$

For an s-wave short-range interaction:

$$\mathcal{H} = -\frac{\hbar^2}{2\mu}(\frac{\partial^2}{\partial x^2} + \frac{\partial^2}{\partial y^2}) + V_{trap}(x,y) - \frac{\hbar^2}{2\mu}\frac{\partial^2}{\partial z^2} + \frac{2\pi a_{sc}\hbar^2}{\mu}\delta(\mathbf{r})\frac{\partial}{\partial r}(r\times), \tag{3.34}$$

The trapping potential V_{trap} determines the threshold and the characteristic length scale of the confinement $a_\perp$. We will see later in the comparison between the eigenfunction expansion method and the frame transformation method, the short-range interaction form is only required in the former one.

3.3.1.1 Eigenfunction Expansion Method

In the following, we first reformulate Olshanii's 1998 paper into a general scattering problem with a transverse confinement that fit into the goal of this chapter. The effective 1D Hamiltonian $\mathcal{H}_{1D}$, coupling constant g_{1D}, quasi-1D scattering amplitude f_{1D}, effective 1D transmission coefficient T_{1D} and scattering phase shift $\tan(\phi_{1D})$ are derived using the eigenfunction expansion method. The pole(s) of the effective 1D coupling constant give the location(s) of CIR in the corresponding quasi-1D system.

In the following, a one-open-channel scattering problem is considered first for simplicity. Then a trivial generalization to multi-open-channel scattering is presented.

The asymptotic wave function for a one-open-channel quasi-1D scattering problem has the general form:

$$\Phi = \phi_{00}(x,y)(e^{ikz} + f_{00}e^{ik|z|}) + \sum_{i\in closed} f_i\phi_i(x,y)e^{-k_i|z|}, \tag{3.35}$$

in which $(0,0)$ refers to the energetically lowest channel, i refers to channels with quantum numbers (i_x, i_y).

By applying Hamiltonian operator on the proposed form of the wave function $\mathcal{H}\Phi = E\Psi$, f_i can be calculated.

$$\begin{aligned}(H_{xy}+H_z+V)\Phi &= E_{00}\phi_{00}(x,y)(e^{ikz}+f_{00}e^{ik|z|})+\textstyle\sum_{i\in closed} f_i E_i\phi_i(x,y)e^{-k_i|z|} \\ &+\frac{\hbar^2k^2}{2\mu}\phi_{00}(e^{ikz}+f_{00}e^{ik|z|})-\frac{\hbar^2}{2\mu}2ik\delta(z)\phi_{00}f_{00}e^{ik|z|} \\ &+\textstyle\sum_{i\in closed}-\frac{\hbar^2k_i^2}{2\mu}f_i\phi_i e^{-k_i|z|}+\frac{\hbar^2}{2\mu}2k_if_i\delta(z)\phi_i e^{-k_i|z|}+V\Phi,\end{aligned} \tag{3.36}$$

in which H_{xy} contains the kinetic energy operator in the xy-plane and trapping potential in the xy-plane. H_z is usually the kinetic energy operator in the z-direction, since here we only consider transverse trap. The regular terms (terms without δ function or η function) cancel, the remaining terms are:

$$\begin{aligned}&V\Phi-\frac{\hbar^2}{2\mu}2ik\delta(z)\phi_{00}(x,y)f_{00}e^{ik|z|}+\frac{\hbar^2}{2\mu}\textstyle\sum_i 2k_if_i\delta(z)\phi_i(x,y)e^{-k_i|z|}=0 \\ &V\Phi=\frac{2\pi\hbar^2a_{sc}}{\mu}\delta^3(r)\frac{\partial}{\partial r}(r\Phi)\end{aligned} \tag{3.37}$$

After integrating over the xy degrees of freedom in Eqn. 3.37, we obtain a set algebraic equations of fs. For the open channel:

$$\begin{aligned}&\int dxdy\phi_{00}(x,y)V\Phi-\frac{\hbar^2}{2\mu}2ik\delta(z)N_{00}^2f_{00}e^{ik|z|}=0 \\ &\Rightarrow\phi_{00}(0,0)\frac{2\pi\hbar^2a_{sc}}{\mu}\delta(z)\left.\frac{\partial}{\partial r}(r\Phi)\right|_{x=0,y=0}-\frac{\hbar^2}{2\mu}2ik\delta(z)N_{00}^2f_{00}e^{ik|z|}=0 \\ &\Rightarrow f_{00}=\frac{1}{2ikN_{00}^2}\phi_{00}(0,0)4\pi a_{sc}\eta;\eta=\left.\frac{\partial}{\partial r}(r\Phi)\right|_{x=0,y=0,z=0}\end{aligned} \tag{3.38}$$

For the closed channels:

$$\int dxdy\phi_i(x,y)V\Phi + \frac{\hbar^2}{2\mu}2k_i\delta(z)f_iN_i^2e^{-k_i|z|} = 0$$

$$\Rightarrow \phi_i(0,0)\frac{2\pi\hbar^2a_{sc}}{\mu}\delta(z)\ \frac{\partial}{\partial r}(r\Phi)\bigg|_{x=0,y=0} + \frac{\hbar^2}{2\mu}2k_i\delta(z)f_iN_i^2e^{-k_i|z|} = 0 \tag{3.39}$$

$$\Rightarrow f_i = -\frac{1}{2k_iN_i^2}\phi_i(0,0)4\pi a_{sc}\eta$$

The wave function is thus determined:

$$\Phi(x=0,y=0,z) = \phi_{00}(0,0)(e^{ikz} + \frac{1}{2ikN_{00}^2}\phi_{00}(0,0)4\pi a_{sc}\eta e^{ik|z|}) - \sum_i \frac{1}{2k_iN_i^2}\phi_i^2(0,0)4\pi a_{sc}\eta e^{-k_i|z|} \tag{3.40}$$

The value of η is determined self-consistently from the wave function:

$$\eta = \frac{\partial}{\partial z}(z\Phi(0,0,z)) = \phi_{00}(0,0)(1 + \frac{1}{2ikN_{00}^2}\phi_{00}(0,0)4\pi a_{sc}\eta) - \textstyle\sum_i \frac{1}{2k_iN_i^2}\phi_i^2(0,0)4\pi a_{sc}\eta$$

$$\eta(1 - \frac{\phi_{00}(0,0)^2 4\pi a_{sc}}{2ikN_{00}^2} + 4\pi a_{sc}\textstyle\sum_i \frac{1}{2k_iN_i^2}\phi_i^2(0,0)) = \phi_{00}(0,0)$$

$$\Rightarrow \eta = \frac{\phi_{00}(0,0)}{(1 - \frac{\phi_{00}(0,0)^2 4\pi a_{sc}}{2ikN_{00}^2} + 4\pi a_{sc}\sum_i \frac{1}{2k_iN_i^2}\phi_i^2(0,0))}$$

$$\Rightarrow f_{00} = \frac{\phi_{00}(0,0)4\pi a_{sc}}{2ikN_{00}^2}\frac{\phi_{00}(0,0)}{(1 - \frac{\phi_{00}(0,0)^2 4\pi a_{sc}}{2ikN_{00}^2} + 4\pi a_{sc}\sum_i \frac{1}{2k_iN_i^2}\phi_i^2(0,0))} \tag{3.41}$$

$$\Rightarrow t_{00} = 1 + f_{00} = \frac{1 + 4\pi a_{sc}\sum_i \frac{1}{2k_iN_i^2}\phi_i^2(0,0)}{(1 - \frac{\phi_{00}(0,0)^2 4\pi a_{sc}}{2ikN_{00}^2} + 4\pi a_{sc}\sum_i \frac{1}{2k_iN_i^2}\phi_i^2(0,0))}$$

$$\Rightarrow g_{1D} = \frac{f_{00}}{f_{00}+1}\frac{2\hbar^2ik}{2\mu}, \tan\phi_{00} = -\frac{g_{1D}}{k}\frac{\mu}{\hbar^2}$$

After simplifying the normalization coefficients N_i and transverse wave functions $\phi_i(0,0)$, a much

simpler form of the transmission t_{00} can be derived as a dimensionless function of $\frac{a_{sc}}{a_\perp}$ and $ka_\perp$:

$$1 + f_{00} = \frac{1 + \frac{a_{sc}}{a_\perp}\tilde{\Lambda}(\epsilon)}{1 - \frac{a_{sc}}{a_\perp}\frac{1}{a_\perp ik} + \frac{a_{sc}}{a_\perp}\tilde{\Lambda}(\epsilon)}. \tag{3.42}$$

Poles of denominator of t_{00} corresponds to $1 + \frac{a_{sc}}{a_\perp}\tilde{\Lambda} = 0$. The function $\tilde{\Lambda}$ refer to summation over all the closed channel (i) contribution to η, weighted by the momentum above threshold k_i. In the formula of g_{1D} we have to emphasis that g_{1D} can be only described using a single number when there is only one open channel. In cases where more than one channels are open, g_{1D} is in general an interaction matrix. In the perturbative limit, g_{1D} is proportional to the K-matrix.

For completeness, the eigenfunction method can also be used to solve for the bound state energies and the multi-open-channel scattering amplitudes or S-matrices.

For the bound state problem:

$$1 = -\frac{\partial}{\partial z}\left(z 2\pi a_{sc} \textstyle\sum_i \phi_i^2(x=0,y=0)\frac{1}{N_i^2}\frac{e^{-k_i|z|}}{k_i}\right)\Big|_{z\to 0^+}. \tag{3.43}$$

For multi-open-channel scattering problem, if the incoming wave has only $(0,0)$ component, but the outgoing waves have all the energetically allowed components:

$$f_i = s_{0,0}\frac{\frac{2\pi}{a_\perp iq_i}\frac{a_{sc}}{a_\perp}}{1 + \frac{a_{sc}}{a_\perp}\Lambda(\epsilon) - \frac{a_{sc}}{a_\perp}\sum_{i'}\frac{2\pi}{a_\perp iq_{i'}}}, \tag{3.44}$$

in which i denotes the two-dimensional quantum number that labels the scattering channel (i_x, i_y), q_i refers to the magnitude of momentum above each threshold E_i, $q_i = \sqrt{2\mu(E - E_i)}$, i' in the summation denotes the open channel indices.

3.3.1.2 Frame Transformation Method

Unlike the eigenfunction expansion method for computing the asymptotic eigenstates for the quasi-1D Hamiltonian, the frame transformation method directly calculates poles of the quasi-1D reaction matrix $K^{1D,Phys}$ from the 3D reaction matrix K^{3D}, as discussed in the first section of this chapter. We will first present how the transformation from K^{3D} to K^{1D} comes up in matching

the wave functions in the "local" region, where the full solutions of the scattering problem can be expanded in both Hamiltonians approximately in the context of quasi-1D scattering in a waveguide. Subsequently, we will show how the closed channel elimination poses a constraint on the quasi-1D reaction matrix K^{1D} to give a physically convergent solution in the asymptotic regime $z \to \pm\infty$.

The eigenfunctions at short distance $r_c \ll r \ll a_\perp$ can be represented as linear combinations of non-interacting channel functions:

$$\Psi_{lm\epsilon}(\mathbf{r}) = \sum_{l'm'} F_{l'm'\epsilon}\delta_{l,l'}\delta_{m,m'} - G_{l'm'\epsilon}K^{3D}_{l'm',lm}(\epsilon), \tag{3.45}$$

where the reaction matrix K^{3D} encapsulates all the information about the short-range scattering caused by the potential, l is the orbital angular momentum quantum number, m is the orbital magnetic quantum number. F and G are the energy-normalized regular and irregular solutions in spherical coordinates for a given scattering energy ϵ:

$$\begin{cases} F_{lm\epsilon}(\mathbf{r}) = Y_{lm}(\hat{\mathbf{r}})f_{l\epsilon}(r) \quad f = \sqrt{\dfrac{2k}{\pi}}j_l(kr) \\ G_{lm\epsilon}(\mathbf{r}) = Y_{lm}(\hat{\mathbf{r}})g_{l\epsilon}(r) \quad g = \sqrt{\dfrac{2k}{\pi}}n_l(kr), \end{cases} \tag{3.46}$$

f and g are the energy-normalized spherical Bessel functions, f is regular at $r \to 0$, g is irregular at $r \to 0$, and they oscillate as $r \to \infty$ with a $\pi/2$ difference in phase. The z-parity quantum number of the solutions is $(-1)^{l-m}$, which is important to keep in mind, since later the 3D solutions will be projected onto outgoing waves in the z-direction.

The 2D isotropic harmonic confinement is a special case, in which the m quantum number is conserved in both the spherical and cylindrical symmetries, so there is no need to explicitly specify m [GB04]. However, for a 2D transverse trap in general, all $l-$ and $m-$values might be coupled. In the unitary limit, of course, with short-range interactions, the lowest one or two partial waves for each symmetry are expected to dominate the scattering observables.

The regular ψ and irregular χ eigenfunctions at large distances $a_\perp \ll |z|$ are:

$$\begin{cases} \psi_{n_x,n_y,q}(\mathbf{r}) = \phi_{n_x,n_y}(x,y)(\pi q)^{-\frac{1}{2}} \begin{cases} \cos(qz), & \pi_z = +1 \\ \sin(qz), & \pi_z = -1 \end{cases} \\ \chi_{n_x,n_y,q}(\mathbf{r}) = \phi_{n_x,n_y}(x,y)(\pi q)^{-\frac{1}{2}} \begin{cases} \sin(q|z|), & \pi_z = +1 \\ -sign(z)\cos(qz), & \pi_z = -1 \end{cases} \end{cases} \tag{3.47}$$

where n_x, n_y are quantum numbers in the transverse plane. For example, in the square well cross section case, the eigenstates in the transverse plane for the even parity, of immediate interest here, are $\frac{2}{L}\cos(\frac{(2n_x+1)\pi}{L}x)\cos(\frac{(2n_y+1)\pi}{L}y)$. The confinement in the $x-y$ plane forces the scattered waves to be asymptotically directed along either the positive or negative z-axis.

The evolution of the spherical wave function near the scattering center ($r_c \leq r \ll a_\perp$) into an asymptotic wave function at $|z| \gg a_\perp$ on the fixed energy shell ϵ can be accomplished by projecting the eigenfunctions near the scattering center onto the eigenfunctions relevant in the asymptotic region:

$$\begin{aligned} \psi_{n_x,n_y,q_{n_x,n_y}}(\mathbf{r}) &= \textstyle\sum_{l,m} U_{n_x,n_y,q_{n_x,n_y};l,m,\epsilon} F_{lm\epsilon}(\mathbf{r}), \\ \chi_{n_x,n_y,q_{n_x,n_y}}(\mathbf{r}) &= \textstyle\sum_{l,m} (U^{-1})^T{}_{n_x,n_y,q_{n_x,n_y};l,m,\epsilon} G_{lm\epsilon}(\mathbf{r}), \end{aligned} \tag{3.48}$$

U is the transformation matrix between the two sets of eigenstates, and the U matrix is energy dependent, since the expansion is performed on an energy shell. The value of U-matrix elements, as discussed in the last section, can be obtained by expanding the solution as a function of r. In the following, we refer U as the first term in the expansion defined by Fano in his 1981 paper [Fan81]. The summation includes only solutions of the same z-parity. Two examples of U are shown in the following section.

In the transformation of the "irregular" solution sets, the inverse of U-matrix is needed. However, since the transformation is not unitary and have infinite dimension in principle, the inverse of U-matrix may not have a legitimate definition by itself. Nevertheless, as will show below, only the transformation of the regular solution sets is needed.

The closed channel elimination can give a physical quasi-1D solution after eliminating the divergent terms from closed channels. In the following, the closed channel elimination is demonstrated in a quasi-1D scattering context.

The asymptotic wave function can be represented as a matrix notation:

$$\begin{aligned}&\underline{\Psi} = \underline{F} - \underline{GK^{3D}} \\ &= \left(\Psi_{lm,l'm'}\right) = \left(F_{lm}\delta_{lm,l'm'}\right) + \left(F_{lm}\sum_{l^a,m^a}\delta_{lm,l^am^a}K_{l^am^a,l'm'}\right).\end{aligned} \tag{3.49}$$

Assume we have N channels, N_c of them are closed and N_o of them are open. The closed channels needs to be fixed by closed channel elimination, otherwise there would be exponential divergence in $|z| \to \infty$. A wave function which respects the boundary conditions can be written as:

$$\Psi_i = \sum_{j\in o}\psi_j(x,y)[f_j(z)\delta_{ij} - g_j(z)K_{ij}^{1D}] + \sum_{j\in c}\psi_j(x,y)[f_j(z)\delta_{ij} - g_j(z)K_{ij}^{1D}]$$

$$\Psi = \underline{f} - \underline{g}\underline{K} = \begin{pmatrix} f_o & 0 \\ 0 & f_c \end{pmatrix} - \begin{pmatrix} g_o & 0 \\ 0 & g_c \end{pmatrix}\begin{pmatrix} K_{oo} & K_{oc} \\ K_{co} & K_{cc} \end{pmatrix} = \begin{pmatrix} f_o - g_oK_{oo} & -g_oK_{oc} \\ -g_cK_{co} & f_c - g_cK_{cc} \end{pmatrix} \tag{3.50}$$

The physical solutions are pulled out from the full set of linear independent solutions of the system:

$$\Psi^{phys} = \Psi\begin{pmatrix} A_{oo} \\ A_{co} \end{pmatrix} = \begin{pmatrix} (f_o - g_oK_{oo})A_{oo} - g_oK_{oc}A_{co} \\ -g_cK_{co}A_{oo} + (f_c - g_cK_{cc})A_{co} \end{pmatrix}. \tag{3.51}$$

The part corresponds to closed channels is $-g_cK_{co}A_{oo} + (f_c - g_cK_{cc})A_{co}$. In this part, we need to eliminate those having $\exp(k|z|)$ divergence. f and g rely on the definition of regular and irregular functions and parities. So we follow the definition in the last page, and we give a general derivation in the following. For regular closed channel functions, the $\exp(k|z|)$'s coefficient is w_+^c, and for irregular closed channel function, the $\exp(k|z|)$'s coefficient is v_+^c, + refers to $\exp(k|z|)$ divergence, c refers to closed channels.

Closed channel elimination requires:

$$-v_+K_{co}A_{oo} + (w_+^c - v_+^cK_{cc})A_{co} = 0 \Rightarrow A_{co} = (w_+^c - v_+^cK_{cc})^{-1}v_+^cK_{co}A_{oo}. \tag{3.52}$$

For $\Pi_z = 1$, $w_+^c = 1$, $v_+^c = i$; for $\Pi_z = -1$, $w_+^c = i$, $v_+^c = -1$. This imposes even more restriction

on the open part of the physical wave function, resulting in:

$$\Phi \quad \sim \quad f_o - g_o(K_{oo} + iK_{oc}(1 - iK_{cc})^{-1}K_{co}). \tag{3.53}$$

Thus the relation between $K^{1D,Phys}$ and the bare reaction matrix K^{1D} is:

$$K^{1D,Phys} = K^{1D}_{oo} + iK^{1D}_{oc}(1 - iK^{1D}_{cc})^{-1}K^{1D}_{co} \tag{3.54}$$

The pole of the physical quasi-1D reaction matrix $K^{1D,Phys}$ predicts the positions of the so called confinement induced resonance (CIR). Since K^{1D}_{oc}, K^{1D}_{co}, K^{1D}_{oo} are all non diverging functions of energy, the only poles of the physical reaction matrix come from the zeros of $1 - iK^{1D}_{cc}$. Hence, comes the mathematical requirement for CIR:

$$\mathrm{Det}[1 - iK_{cc}(\epsilon)] = 0. \tag{3.55}$$

K_{cc} is a function of both the energy and the scattering information from the short-range scattering center (a_{sc} for zero-range s-wave scattering *e.g.*).

In addition to all the general properties mentioned above concerning quasi-1D scattering, the properties of the short-range potential can in some cases allow a further simplification of the problem. If K^{3D} is block-diagonal and only one angular momentum partial wave dominates the 3D scattering phase shift, a good approximation to the K matrix is $K^{3D}_{lm,l'm'} = \delta_{l,l'}\delta_{m,m'}\tan\delta_l$, $K^{1D,Phys}_{oo}(E) = K^{1D}_{oo}[1-i\lambda_c(E)]^{-1}$, where $\lambda_c = TrK^{1D}_{cc} = \tan\delta_l \sum_{\text{closed channels}}(U_{n_x,n_y,q_{n_x,n_y};l,m,\epsilon})^2$ [GB04]. Under this single partial wave approximation, each pole of the physical $K^{1D,Phys}$ is determined by the vanishing of $1 - i\lambda_c(E)$.

In general, the summation of squared transformation matrix elements can be expressed as a summation over all closed channel quantum numbers (n_x, n_y as mentioned above) in the 2D confinement portion of Hilbert space. Under the single partial wave approximation,

$$\begin{aligned}\lambda_c &= \tan\delta_l \sum{}'(U_{n_x,n_y,q;l,m,\epsilon})^2 \\ &= \tan\delta_l \sum{}' \frac{1}{ka_\perp}(\epsilon_{n_x,n_y} - \epsilon)^{\frac{1}{2}},\end{aligned} \tag{3.56}$$

in which $a_\perp$ is one characteristic length of the transverse confinement, ϵ_{n_x,n_y} is the threshold energy divided by the characteristic energy in the system (usually associtated with the characteristic length), ϵ is the total energy divided the same characteristic energy, $\sum'$ indicates the summation over all $(n_x, n_y) \in$ closed channels.

3.3.2 Confinement Induced Resonances in Cylindrical Harmonic Confinement

The purpose of this subsection is to demonstrate the frame transformation theory in the simplest case, and to compare the outcome of this general formalism to existing results. Another important purpose is to demonstrate how the divergence in the summation of closed channels U-matrix elements come up, and how the regularization in this case is handled by the well known Hurwitz zeta function. The next two chapters following the general formalism, but the regularizations of the divergence are handled differently.

Fig. 3.1 is a sketch of a quasi-1D system with azimuthal symmetry. As is discussed in the general formalism of the local frame transformation theory, the region where the local FT is applied is $r_c \ll r \ll a_\perp$. In this case, at the radius r we do the frame transformation, the energy normalized even parity channel function in 2D geometry is:

$$\psi^H_{n,m,q}(\mathbf{r}) = (2\pi)^{-\frac{1}{2}} e^{im\phi} J_m(\sqrt{k^2 - q^2}\rho)(\pi q)^{-\frac{1}{2}} \cos(qz), \tag{3.57}$$

Eigenfunction in Eqn. 3.57 is not solution of a harmonically confined 2D particle. However, in the region where local FT is applied, the transformation does not care about this issue at least in the first order of r. The method to approximate Hermite polynomial solution by a Bessel J function is already used in the context of Stark effect in magnetic field [Gre87]. The essence of the local FT is to find the appropriate region within which two solution sets can expand the same function. Thus within this region, the expansion and the reaction matrix should be insensitive to the boundary conditions in either xy-plane or r. The harmonic trap term will matter in a higher order expansion of the transformation as a function of r.

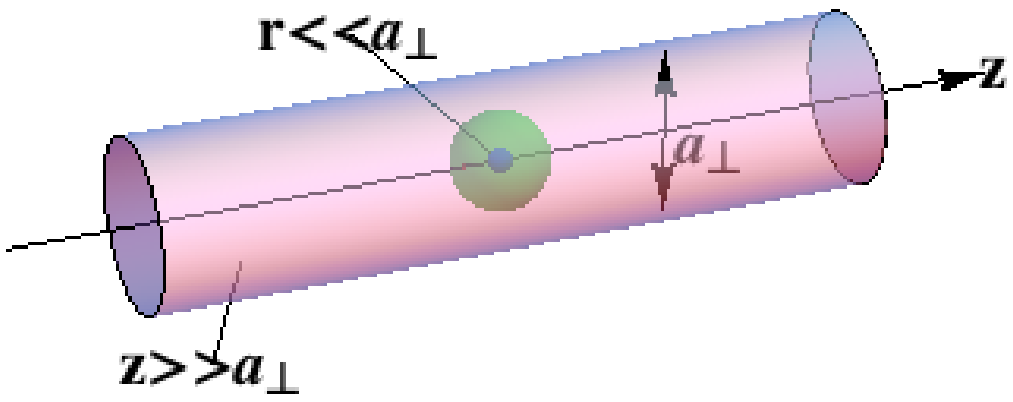

Figure 3.1: A sketch of a quasi-1D system with azimuthal symmetry. In addition, the separation of length scales in the system is also demonstrated.

The energy normalized spherical wave function is:

$$F_{lm,k}(\mathbf{r}) = Y_{lm}(\theta,\phi)\sqrt{\frac{2k}{\pi}}j_l(kr) \tag{3.58}$$

The U-matrix elements we use are the special case for $m = 0$, $l = 0$. For the angle part of the integration, formula 7.333 in [GR94] is applied.

$$U_{n,m=0,q;l=0,m=0,\epsilon} = \frac{\int d\Omega Y_{00}(\hat{\mathbf{r}})\psi^H_{n,m,q}(\mathbf{r})}{j_0(kr)\sqrt{2k/\pi}} = \sqrt{\frac{1}{ka_\perp}}\left(\frac{k^2}{2\hbar\omega_\perp} - (2n+1)\right)^{-\frac{1}{4}}. \tag{3.59}$$

Interestingly, this expansion can also be understood as the transformation between the spherical and cylindrical expansion of a plane wave $e^{i\mathbf{k}\cdot\mathbf{r}}$.

In the treatments of this quantity $\lambda_c(E)$ in 2D isotropic harmonic confinement [GB04, GDS12], its expression takes one of the following forms as an infinite summation:

$$\begin{aligned}\lambda_c^{l=1} &= \frac{V_p}{a_\perp^3}\sum_{n=1}^{\infty}\sqrt{n+\frac{3}{2}-\epsilon}\ (p\text{-wave})\\ \lambda_c^{l=0} &= \frac{a_s}{a_\perp}\sum_{n=1}^{\infty}\frac{1}{\sqrt{n+\frac{3}{2}-\epsilon}}\ (s\text{-wave}),\end{aligned} \tag{3.60}$$

in which a_s is the energy dependent s-wave scattering length, V_p is the energy dependent p-wave scattering volume, $a_\perp$ is the characteristic length of the transverse trap, in the case of 2D isotropic harmonic trap, $a_\perp = a_{ho} = \sqrt{\hbar/\mu\omega}$. Moreover, in the s-wave case, Olshanii [Ols98] encountered this same summation of squared transformation matrix elements, which is clearly divergent. A regularization method is developed in the following paragraphs, motivated by other analyses that have regularized different types of zeta functions in various contexts.

The relevant special function for the 2D isotropic harmonic oscillator confinement is the Hurwitz zeta function. Observe that in the definition of the Hurwitz zeta function:

$$\zeta_H(s,q) = \sum_{n=0}^{\infty}\frac{1}{(q+n)^s}, (s>1) \tag{3.61}$$

the same functional form is present in the region $s \in (1,\infty)$ where the series is convergent. So the analytical continuation of the Hurwitz zeta function from $s \in (1,\infty)$ to $s \in (-\infty,1]$ can potentially

regularize the divergent summation and yield a physically relevant value. A similar spirit has been implemented in the calculation of the Casmir force between two infinitely large planes and between other shapes of conductors [PMG86, MSSvS03]. The extensive work on the Hurwitz zeta function in the mathematics community suggests a way to develop the regularization in general. For the present quasi-1D scattering system, we implement a regularization procedure that has been utilized in the mathematics community. The summation can be viewed as the following limit process:

$$\Lambda_H(\xi,\epsilon) = \frac{\partial}{\partial\xi}\left(\xi\sum_{n=0}^{\infty}\frac{\exp(-\xi\sqrt{n+1+\epsilon})}{\sqrt{n+1+\epsilon}}\right)\Bigg|_{\xi\to 0}. \tag{3.62}$$

This summation is not uniformly convergent, which means that interchanging the order of taking the limit $\xi \to 0$ and summing over all terms might not be justified. For any finite ξ, the convergence of the summation is guaranteed by the exponential suppression at large n. For $\xi = 0$, however, the summation assumes the same form encountered in the $l = 0$ case. The divergence in the local frame transformation approach can be viewed as having originated in an unjustifiable interchange of the order of these two operations.

Olshanii *et.al* [Ols98, DMBO11] encountered the same divergence problem while solving for the scattering amplitude in the open channel. They treated the divergence as follows. The summation in Eq. 3.62 can be expanded as a power series in ξ (where $\xi = \frac{z}{L_\perp}$) near the energy of the lowest threshold, giving:

$$\Lambda_H(\xi,\epsilon) = F(\xi) + \tilde{\Lambda}_H(\xi,\epsilon). \tag{3.63}$$

Here F is the integral approximation of the summation right at threshold, $F(\xi) = \int_0^\infty d\nu \frac{\exp(-\xi\sqrt{\nu})}{\sqrt{\nu}} = \frac{2}{\xi} = \sum_{s=1}^{\infty}\int_{s-1}^{s} d\nu \frac{\exp(-x\sqrt{\nu})}{\sqrt{\nu}}$, which exhibits the divergence with respect to ξ. $\tilde{\Lambda}_H$ is the regular, physically relevant part of Λ_H. At an arbitrary scattering energy, the integration approximation becomes $\int_1^N d\nu \frac{\exp(-\xi\sqrt{\nu+\epsilon})}{\sqrt{\nu+\epsilon}} = \frac{2}{\xi}(\exp(-\xi\sqrt{1+\epsilon}) - \exp(-\xi\sqrt{N+\epsilon}))$. Thus the summation in Eq.3.62

can be cast as:

$$\Lambda_H(\xi,\epsilon) = \frac{2}{\xi} + \tilde{\Lambda}_H(\xi,\epsilon)$$

$$= \frac{2}{\xi} - \frac{2}{\xi} + 2\frac{\exp(-\xi\sqrt{1+\epsilon})}{\xi} + \lim_{N\to\infty}(-\frac{2}{\xi}(\exp(-\xi\sqrt{1+\epsilon}) - \exp(-\xi\sqrt{N+\epsilon})) + \sum_{n=1}^{N}\frac{\exp(-\xi\sqrt{n+\epsilon})}{\sqrt{n+\epsilon}})$$

$$= \frac{L_{-1}(\epsilon)}{\xi} + \tilde{\Lambda}_H(\xi\to 0^+,\epsilon) + \text{terms that vanish at } \xi = 0, \tag{3.64}$$

in which:

$$\tilde{\Lambda}_H(\xi\to 0^+,\epsilon) = \lim_{N\to\infty}\sum_{n=1}^{N}\frac{1}{\sqrt{n+\epsilon}} - 2\sqrt{N+\epsilon}. \tag{3.65}$$

The present study applies a more general concept to the divergent summation that has been developed in the mathematics community. Our treatment does not rely on the s-wave nature of the scattering, and can be directly deduced from the frame transformation result. The following illustration of our method is developed specifically for the square transverse trap geometry with hard walls, because there are two quantum numbers in a general separable 2D confinement, and the 2D square well trap is a more general example with quite different characteristics than geometries for which this type of analysis has previously been worked out. In addition, we show that the isotropic 2D harmonic oscillator geometry ($\omega_x = \omega_y = \omega_\rho$) is a special case in our treatment.

We benchmark the regularization method in two different ways:

(1) Compare with the mathematical definition of the Hurwitz zeta function, as is shown in the regularization formula Eqn. 3.65.

(2) Compare with the scattering calculations and bound state calculations as have been done in much previous work [GB04, DLO01].

To test our proposed regularization method, we have first applied it to the Hurwitz zeta function summation. This test has verified that it gives the same numerical value for every tested value of q and s in agreement with other definitions [AS64, GR94] of the Hurwitz zeta function, analytically continued into the region $s \in (-\infty, 1]$.

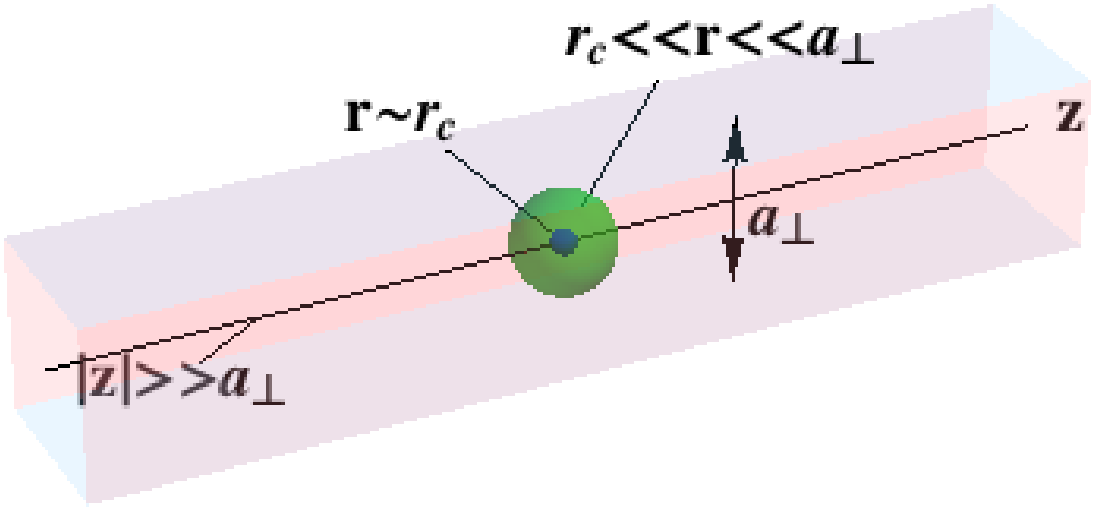

Figure 3.2: A sketch of a quasi-1D system with a square well transverse confinement. In addition, the separation of length scales in the system is also demonstrated.

Both of the comparisons show that our general regularization formalism is working for cylindrically symmetric confinement, which encourages us to apply it to more general confinements.

3.3.3 Confinement Induced Resonances in Square Well Transverse Confinement

In this subsection, we apply the local frame transformation theory to a quasi-1D system with a square well transverse confinement. The focus of this subsection is to demonstrate the regularization of closed channel contributions from a general 2D transverse confinement. The regularization result is then compared to a numerical study of quasi-1D scattering in the single-open-channel scenario.

Fig. 3.2 is a sketch of a quasi-1D system with a square well transverse confinement. In this case, at radius r where the frame transformation is performed, the energy normalized even parity channel function is:

$$\psi_{n_x,n_y,q} = \frac{2}{L_\perp}\cos(\frac{(2n_x+1)\pi x}{L_\perp})\cos(\frac{(2n_y+1)\pi y}{L_\perp})(\pi q)^{-\frac{1}{2}}\cos(qz) \tag{3.66}$$

We use the spherical expansion of a plane wave to get the U-matrix elements:

$$\exp(i\mathbf{k}\cdot\mathbf{r}) = \textstyle\sum_{lm} i^l 4\pi Y^*_{lm}(\hat{\mathbf{k}}) Y_{lm}(\hat{\mathbf{r}}) j_l(kr),$$

$$\begin{aligned}
&\cos(k_x x)\cos(k_y y)\cos(qz) \\
&= \frac{1}{8}(e^{ik_x x + ik_y y + iqz} + e^{ik_x x - ik_y y + iqz} + e^{ik_x x + ik_y y - iqz} + e^{ik_x x - ik_y y - iqz} \\
&+ e^{-ik_x x + ik_y y + iqz} + e^{-ik_x x - ik_y y + iqz} + e^{-ik_x x - ik_y y - iqz} + e^{-ik_x x + ik_y y - iqz}) \\
&= \frac{1}{8}\textstyle\sum_j e^{i\mathbf{k}_j\cdot\mathbf{r}}
\end{aligned} \tag{3.67}$$

The energy normalization delta function $\delta(E - E')$ comes into the following integration as well, so the on-shell U-matrix elements can be obtained by dividing out the delta function.

$$\begin{aligned}
U_{n_x,n_y,q;l=0,m=0,\epsilon} &= \frac{\int d\Omega Y_{00}(\hat{\mathbf{r}})\psi_{n_x,n_y,q}(\mathbf{r})}{j_0(kr)\sqrt{2k/\pi}} = \frac{1}{4L_\perp}\frac{\sum_j \int d\Omega Y_{00}(\hat{\mathbf{r}})(\mathbf{r}) e^{i\mathbf{k}_j\cdot\mathbf{r}}}{j_0(kr)\sqrt{2k/\pi}} \\
&= \frac{2}{L_\perp}\sqrt{\frac{1}{2\pi k q_{n_x,n_y}}} = \sqrt{\frac{4}{kL_\perp}}\left(\frac{k^2 L_\perp^2}{4\pi^2} - (n_x+\frac{1}{2})^2 - (n_y+\frac{1}{2})^2\right)^{-\frac{1}{4}}
\end{aligned} \tag{3.68}$$

The summation of squared $\underline{U}$-matrix elements for the 2D square confinement geometry is:

$$\sum_{n_x,n_y\geq 0}^{(n_x,n_y)\neq(0,0)} \frac{1}{\sqrt{(n_x+\frac{1}{2})^2 + (n_y+\frac{1}{2})^2 - \epsilon}}. \tag{3.69}$$

This sum, which must be evaluated before differentiation, takes the following form:

$$\begin{aligned}
\Lambda_E(\xi,\epsilon) &= \frac{\partial}{\partial\xi}\left(\xi {\sum}' \frac{\exp(-\xi\sqrt{(n_x+\frac{1}{2})^2 + (n_y+\frac{1}{2})^2 - \epsilon})}{\sqrt{(n_x+\frac{1}{2})^2 + (n_y+\frac{1}{2})^2 - \epsilon}}\right)\Bigg|_{\xi\to 0^+} \\
&= \frac{1}{4}\frac{\partial}{\partial\xi}\left(\xi \sum_{n_x,n_y} \frac{\exp(-\xi\sqrt{(n_x+\frac{1}{2})^2 + (n_y+\frac{1}{2})^2 + \epsilon})}{\sqrt{(n_x+\frac{1}{2})^2 + (n_y+\frac{1}{2})^2 + \epsilon}}\right)\Bigg|_{\xi\to 0^+} - \frac{\exp(-\xi\sqrt{\frac{1}{2}-\epsilon})}{\sqrt{\frac{1}{2}-\epsilon}}.
\end{aligned} \tag{3.70}$$

The summation ${\sum}'$ is over all closed-channel quantum numbers in one quarter of the 2D (n_x, n_y) plane.

The number of points in one ring $\frac{1}{2}(2n-1)^2 < |\mathbf{n}+(\frac{1}{2},\frac{1}{2})|^2 \leq \frac{1}{2}(2n+1)^2$ can be understood as the density of states in the quantum number space, $\mathbf{n} = (n_x, n_y)$. The summation over all the quantum numbers can be approximated by an integral over the density of states in the 2D quantum number space, and this approximation can be used to separate out the nature of the infinite sum singularity. The integral can be evaluated by changing to the polar plane:

$$\int_{-\infty}^{\infty}\int_{-\infty}^{\infty} dn_x dn_y \frac{\exp(-\xi\sqrt{(n_x+\frac{1}{2})^2+(n_y+\frac{1}{2})^2-\epsilon})}{\sqrt{(n_x+\frac{1}{2})^2+(n_y+\frac{1}{2})^2-\epsilon}}$$

$$= \lim_{N\to\infty}\int_{\frac{\sqrt{2}}{2}}^{\frac{(2N+1)\sqrt{2}}{2}} 2\pi r dr \frac{\exp(-\xi\sqrt{r^2-\epsilon})}{\sqrt{r^2-\epsilon}} = \lim_{N\to\infty}\sum_{n=1}^{N}\int_{(2n-1)\sqrt{2}/2}^{(2n+1)\sqrt{2}/2} 2\pi r dr \frac{\exp(-\xi\sqrt{r^2-\epsilon})}{\sqrt{r^2-\epsilon}} \tag{3.71}$$

$$= \lim_{N\to\infty}\frac{2\pi}{\xi}(\exp(-\xi\sqrt{\frac{1}{2}-\epsilon}) - \exp(-\xi\sqrt{\frac{(2N+1)^2}{2}-\epsilon}))$$

By using the series expansion of Λ_E in terms of ξ, which has the same spirit of Eq. 3.64, we have:

$$4\Lambda_E(\xi,\epsilon) = \frac{2\pi}{\xi} + (-\frac{2\pi}{\xi} + \frac{2\pi}{\xi}\exp(-\xi\sqrt{\tfrac{1}{2}-\epsilon})) + \lim_{N\to\infty}\left[(-\frac{2\pi}{\xi}(e^{-\xi\sqrt{\frac{1}{2}-\epsilon}} - e^{\xi\sqrt{\frac{(2N+1)^2}{2}-\epsilon}})).\right.$$

$$\left. + \sum_{n=1}^{N}\sum_{\frac{1}{2}<|\mathbf{n}+(\frac{1}{2},\frac{1}{2})|^2\leq\frac{(2n+1)^2}{2}} \frac{\exp(-\xi\sqrt{(n_x+\frac{1}{2})^2+(n_y+\frac{1}{2})^2-\epsilon})}{\sqrt{(n_x+\frac{1}{2})^2+(n_y+\frac{1}{2})^2-\epsilon}})\right] \tag{3.72}$$

The terms inside the limiting process $\lim_{N\to\infty}$ can be rearranged as two parts, one of which is constant as $\xi \to 0$, while the other vanishes as $\xi \to 0$.

$$4\Lambda_E(\xi,\epsilon) = \frac{2\pi}{\xi} + 4\tilde{\Lambda}_E(\xi\to 0^+,\epsilon) + \text{terms vanish at } \xi\to 0^+ \tag{3.73}$$

At this point, the form of the Λ_E function resembles that of the Λ_H function which arises for the harmonic oscillator trap. The corresponding residual part is the regularized summation:

$$4\tilde{\Lambda}_E(\xi\to 0^+,\epsilon) = \sum_{n=1}^{N}\sum_{\frac{1}{2}<|\mathbf{n}+(\frac{1}{2},\frac{1}{2})|^2\leq\frac{(2n+1)^2}{2}} \frac{1}{\sqrt{(n_x+\frac{1}{2})^2+(n_y+\frac{1}{2})^2-\epsilon}} - 2\pi\sqrt{\frac{(2N+1)^2}{2}-\epsilon}. \tag{3.74}$$

The ring region in $\{n_x, n_y\}$ is demonstrated in Fig. 3.3. The definition of the term $\tilde{\Lambda}_E(\xi \to 0^+, \epsilon = 0)$ is unique, because if one adds a term proportional to ξ, it will vanish as $\xi \to 0^+$, while the other term $2\pi/\xi$ is the integral approximation to the summation at the threshold energy ($\epsilon = \frac{1}{2}$ in this case), which also has a unique definition. For 2D harmonic confinement, by the way of contrast, the summation over magnetic quantum numbers is trivially carried out due to the symmetry of that problem. This analysis calculates the position of the CIR in this geometry to be:

$$\frac{a_s(\epsilon)}{L_\perp} = \frac{1}{4\Lambda_E(\xi \to 0, \epsilon)}. \tag{3.75}$$

$\Lambda_E(\xi \to 0, \epsilon)$ turns out to be a special case of the Epstein zeta function [Eli94] (chapter 1, section 2.2, also briefly discussed below in the Appendix), $a_s(\epsilon)$ is the energy dependent 3D scattering length. Many applications of the Epstein zeta function in physics are summarized in [KW10], including its application in the zeta regularization method of high energy physics [Eli12, Haw77].

The generalized form of the Epstein zeta function [Eli94] in the first chapter is:

$$Z\begin{bmatrix}\overrightarrow{g}\\ \overrightarrow{h}\end{bmatrix}^{\epsilon}(s)_\phi = Z\begin{bmatrix}g_1 & \cdots & g_p\\ h_1 & \cdots & h_p\end{bmatrix}^{\epsilon}(s)_\phi = {\sum_{m_1,\cdots,m_p=-\infty}^{\infty}}'[\psi(\overrightarrow{m}+\overrightarrow{g})+\epsilon]^{-s/2}e^{2\pi i(\overrightarrow{m},\overrightarrow{h})}, \tag{3.76}$$

in which p is a positive integer, $\overrightarrow{g}$ and $\overrightarrow{h}$ are p-dimensional real vectors, $g_i, h_i \in R$, $\overrightarrow{m}$ is a p-dimensional integer vector, $m_i \in Z$. $\phi(x)$ is quadratic form of vector x, $\phi(x) = \sum_{\mu,\nu}^{p} c_{\mu\nu}x_\mu x_\nu$, in which c is $p \times p$ non-singlular symmetric matrix associated with ψ. The salar product of p-dimensional vectors $(\overrightarrow{g}, \overrightarrow{h}) = \sum_{\nu=1}^{p} g_\nu h_\nu$. ϵ is the "inhomogeneity" of the generalized Epstein zeta function. The type of inhomogenous Epstein zeta function we use in this paper is the special case when $s = 1$, $p = 2$, $\overrightarrow{g} = (-\frac{1}{2}, -\frac{1}{2})$, $\overrightarrow{h} = 0$, namely:

$$Z\begin{bmatrix}-\frac{1}{2} & -\frac{1}{2}\\ 0 & 0\end{bmatrix}^{\epsilon}(\tfrac{1}{2})_\phi = {\sum_{m_1,m_2=-\infty}^{\infty}}'((m_1+\tfrac{1}{2})^2+(m_2+\tfrac{1}{2})^2+\epsilon)^{-\frac{1}{2}}, \tag{3.77}$$

in which $\phi(x) = \sum_{\mu=1}^{2} x_\mu^2$ in our case.

Our predicted position of the CIR can be tested further by performing a variational R-matrix scattering calculation for the square well 2D trap system using a set of B-spline basis functions.

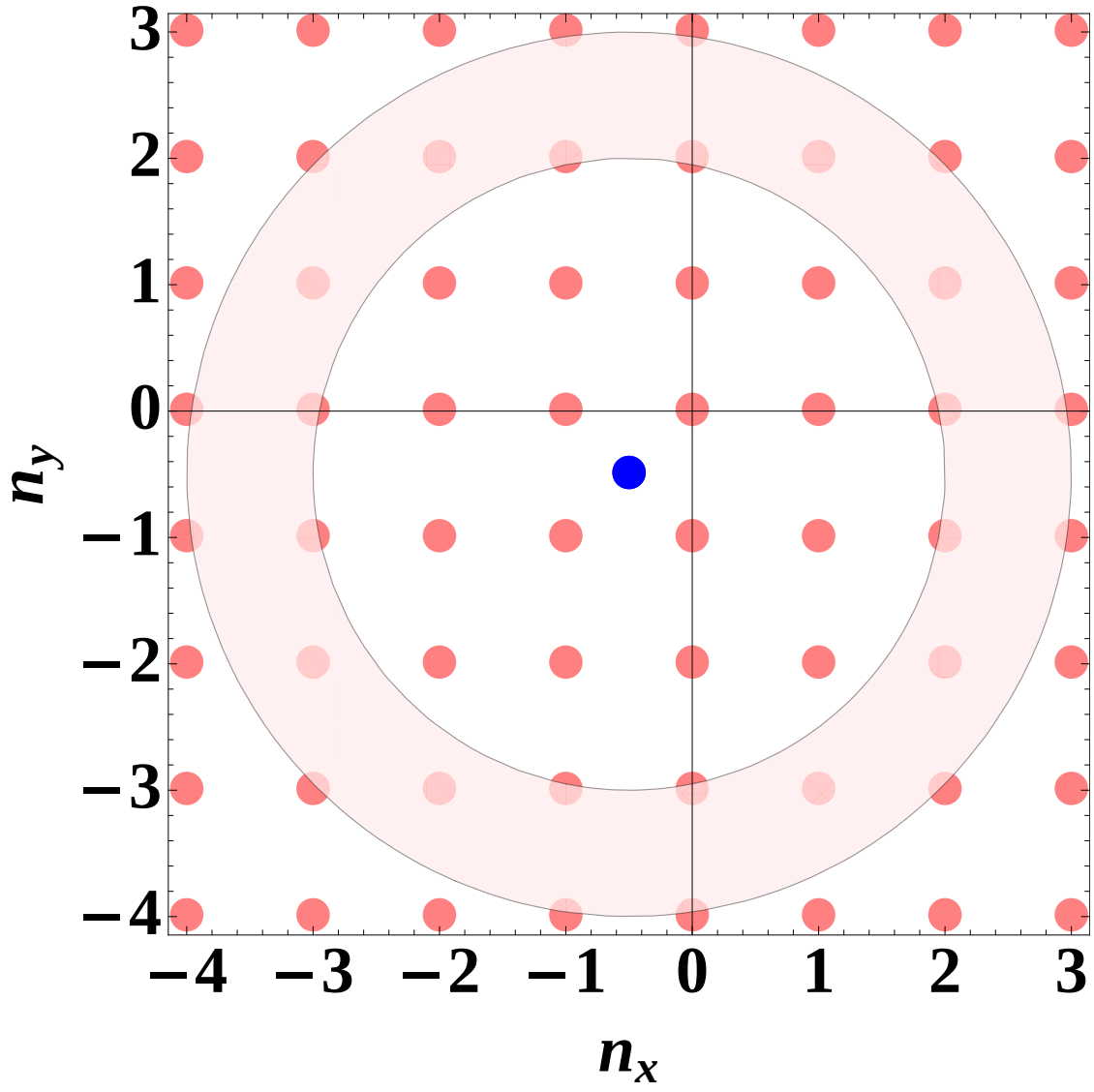

Figure 3.3: Plot of quantum numbers $\mathbf{n} = (n_x, n_y)$ that are summed over in the 2D integer plane, shown as smaller circles (pink online). The ring region is defined by the range $(2n-1)^2/2 \leq |\mathbf{n} + (\frac{1}{2}, \frac{1}{2})|^2 \leq \frac{(2n+1)^2}{2}$, with $n = 3$. The large point (blue online) is at $(-\frac{1}{2}, -\frac{1}{2})$.

The CIR position for a zero-range 3D interaction is extracted by taking its limiting value from finite range model potential calculations. Moreover, the leading finite range correction to the CIR position is also extrapolated and compared with the prediction of effective range theory, in which the scattering length and the effective range of a finite range model potential is defined in terms of small energy expansion of the s-wave scattering phase shift $-\frac{1}{a_s(E)} = -\frac{1}{a_s(0)} + \frac{k^2}{2} r_{eff}$.

For short-range interactions $d_0 \ll a_s(\text{CIR})$, the numerical model calculations agree accurately with the analytical prediction, as is shown in Fig. 3.4. The correction plotted versus the effective range of the potential exhibits a linear behavior, and the slope agrees with the prediction from a finite range expansion of the energy dependent scattering length. Some points deviate from the linear relation, as in Fig. 3.4. The reason for this is that the width d_0 of the interaction is comparable to or larger than the CIR scattering length, which sets a new characteristic length scale that limits the applicability of the "short" range model potential approximation: $\frac{d_0}{a_s(CIR)} \ll 1$.

The dot plotted at $r_{eff} = 0$ in Fig. 3.4 is the prediction from the present regularized frame transformation method, and it agrees with an extrapolation of the numerical calculation to a zero-range potential. The intercept, which corresponds to the resonance position at zero energy, occur in Fig. 3.4 occurs at $\frac{a_\perp}{a_s(0)} = 5.850(\pm 0.005)$ from extrapolation of the numerical results, and at $5.864(\pm 0.008)$ from the present regularized analytical summation. The slope of the extrapolation line can be deduced from the low-energy effective range expansion of the s-wave scattering length: $-\frac{a_\perp}{a_s(E)} = -\frac{a_\perp}{a_s(0)} + a_\perp^2 \frac{k^2}{2} \frac{r_{eff}}{a_\perp}$, in which $a_\perp$ is the width of the square well, and $\frac{k^2}{2} = E$ is the first threshold energy of the 2D confinement, $a_s(E)$ is the energy dependent scattering length, r_{eff} is the effective range of the potential, which usually changes very slowly with $a_s(0)$.

In addition, the quasi-1D scattering phase shift recovers the behavior of the pure-1D scattering phase shift at perturbative values of the 3D scattering length. Fig. 3.5 is our numerical calculation for the square well transverse trapped system. The perturbative region $|a_s| \ll L_\perp$ is far away from the CIR region, and thus the closed channels in the transverse degree of freedom becomes effectively "frozen" into the lowest mode.

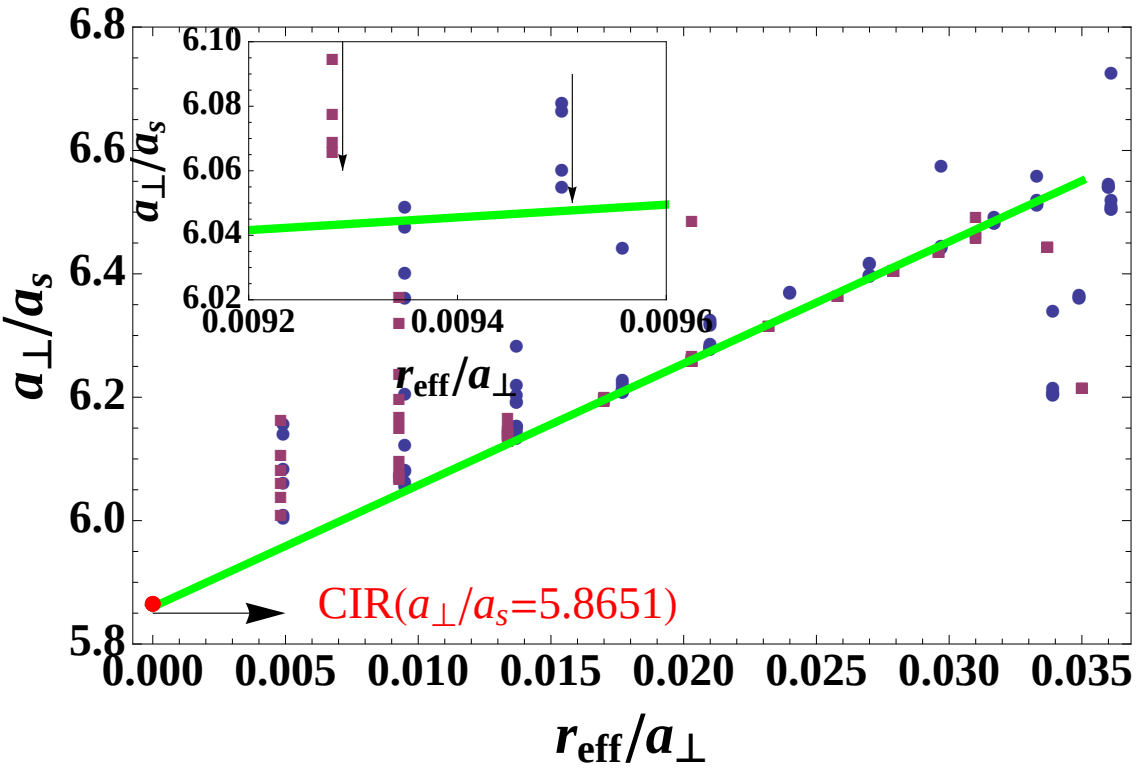

Figure 3.4: The CIR position obtained from finite range interaction model calculations is plotted along with the extrapolation to zero range. The square dots (purple online) are from the potential $V = V_0 \exp(-\frac{r^2}{2d_0^2})$, while the circlar dots (blue online) are from the potential $V = V_0 \frac{1}{\cosh(\frac{r}{d_0})^2}$. The x-axis is the effective range of the potential at the position of the CIR. The solid line (green online) is derived from the effective range expansion of the 3D scattering length $|\frac{a_\perp}{a_s}| = |\frac{a_\perp}{a_s(0)}| + a_\perp^2 E_0 \frac{r_{eff}}{a_\perp}$, E_0 is the lowest threshold energy.The single point at $r_{eff} = 0$ (red online) is the predicted CIR position from our regularized frame transformation method. The inset shows the pattern of convergence to the analytical value, which is seen in the numerical calculation near $\frac{r_{eff}}{a_\perp} \sim 0.010$ (the arrows indicate the better converged numerical values of the CIR position). At larger values of the 3D effective range, the numerical calculation begins to deviate from the analytical prediction. This is because the range of interaction d_0 in those calculations has become comparable to the CIR scattering length, and hence the "short" range approximation of the model potential has become less accurate.

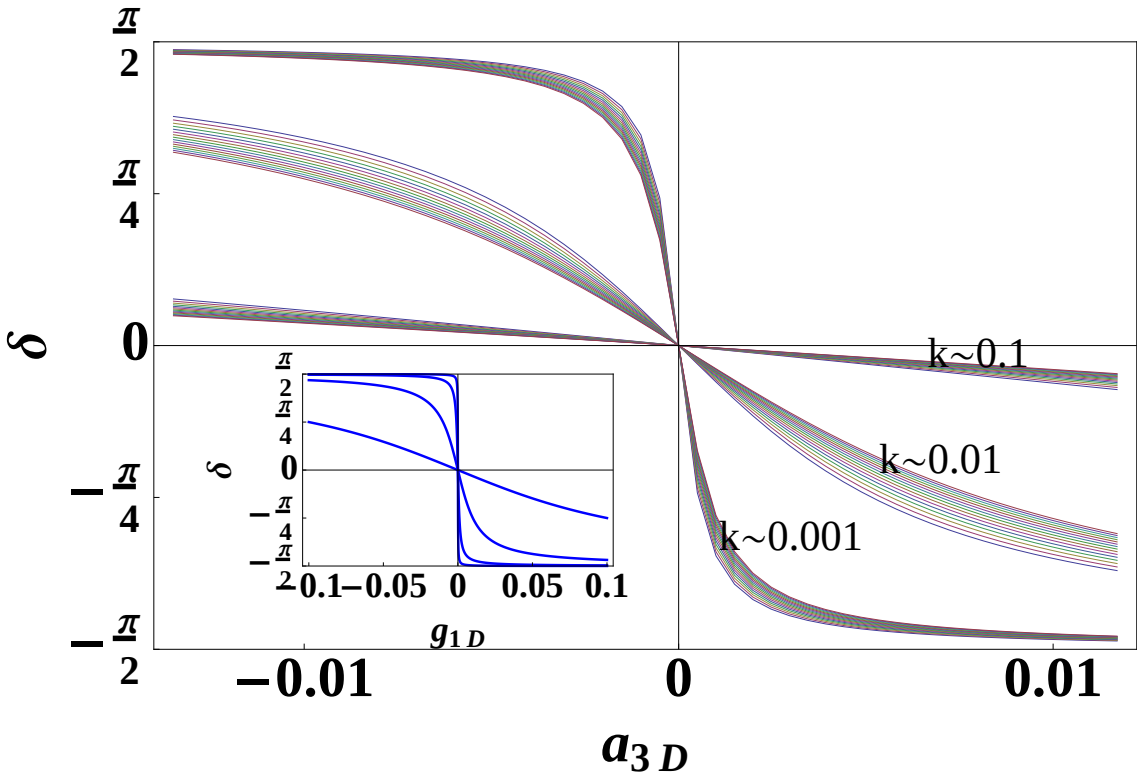

Figure 3.5: Plot of the quasi-1D scattering phase shift in the transverse square well trapped system, as a function of the 3D scattering length a_s. The effective 1D interaction strength in this quasi-1D system is $\frac{g_{1D}}{a_\perp E_0} = \pi \frac{4a_s/a_\perp}{1-\Lambda_E(\frac{1}{2}E_0)4a_s/a_\perp}$. $\Lambda_E(\epsilon)$ is the regularized Epstein zeta function discussed in the last section. $E_0 = \frac{\hbar^2}{2\mu}\frac{4\pi^2}{a_\perp^2}$. The strips of curves clustered together are calculations for a range of energies in different regions of k: $k \sim 0.1, 0.01, 0.001$. k denotes the momentum in z-direction, and the scattering energy $E_z = \frac{k^2}{2\mu}$. The inset is the pure-1D scattering phase shift as a function of g_{1D}, which comes into the effective 1D Hamiltonian as $V_{int} = g_{1D}\delta(z)$.

3.3.4 Lattice Induced Opacity in 2D Lattices

In this subsection, we will discuss a system that has similar mathematical structure to the quasi-1D scattering amplitude in a square well wave guide. We begin with a discussion of an atomic beam that scatters from an infinite 2D atomic lattice, as shown in Fig. 3.6. A quantum matter wave transistor mechanism is proposed that is based on the transmission-reflection property of a coherent matter wave. This mechanism relies on controlling the atom-atom interactions in a reduced dimension scattering process that is shown in Fig. 3.7. In addition, a possible mechanism for coherently controlling the peak scattering intensity into the angles that correspond to different Bravais lattice vectors is discussed, in the framework of a series of Fano-Feshbach resonances. The proposed mechanism could be a promising candidate for an atomtronic transistor using ultracold atoms confined in a 2D optical lattice at an ultracold temperature.

The Hamiltonian that describes the atomic matter wave interacting with a 2D lattice of tightly-trapped scattering centers reduces to:

$$H = -\frac{\hbar^2\nabla^2}{2\mu} + \sum_{(i_x,i_y)} V(\mathbf{r} - \mathbf{R}_{i_x,i_y}), \tag{3.78}$$

in which $\mathbf{R}_{i_x,i_y} = a(i_x, j_y, 0), i_x, j_y \in Z$ represent the positions of the scatterers, and a denotes the square lattice constant. Each scattering potential is approximated by a regularized delta function $V(\mathbf{r}) = \frac{2\pi a_{sc}}{\mu}\delta(\mathbf{r})\frac{\partial}{\partial r}(r\cdot)$, where a_{sc} is the s-wave scattering length between a beam atom and each scatterer.

For a "slow" atomic beam, in which only the lowest transverse channel of the 2D lattice is energetically open, the quasi-1D scattering amplitude $f_{0,0}$ in the lowest channel $(0, 0)$ is calculated analytically and regularized using the zeta-function regularization method developed in our preceding work [ZG13a]. (We denote the reflection amplitude as $f_{0,0}$, while the transmission amplitude

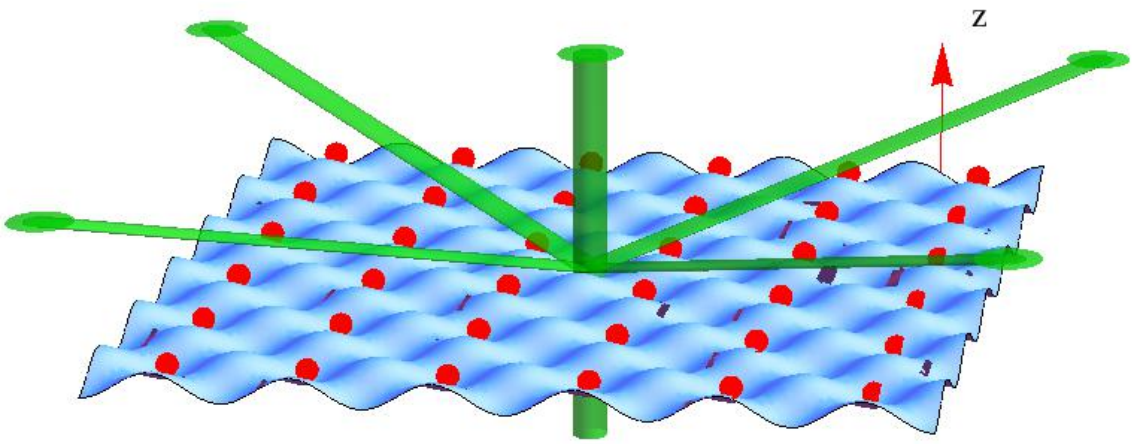

Figure 3.6: Sketch of a beam of an atomic matter wave scattering from an infinite 2D square lattice of fixed atoms. For simplicity, the incoming wave is restricted to be normal to the 2D optical lattice.

is $1 + f_{0,0}$.) The asymptotic wave function for the scattered atomic matter wave is:

$$\Psi = e^{ikz} + f_{0,0}e^{ik|z|} + \sum_{(n_x,n_y)\neq(0,0)} \exp(-\frac{2\pi}{a}\sqrt{n_x^2+n_y^2-\epsilon})e^{in_x x+in_y y}C_{n_x,n_y}, \tag{3.79}$$

where k is the momentum of the incoming matter wave in the z direction, the corresponding kinetic energy in the lattice recoil energy unit is $\epsilon = \frac{1}{E_0}\frac{\hbar^2k^2}{2\mu}$, $E_0 = \frac{\hbar^2}{2\mu}(\frac{2\pi}{a})^2$. A Green's function calculation for a 3D optical lattice was carried out in [FBZ04]. Because we consider only a normal incoming matter wave to the lattice plane, the Green's function formulation is simplified to a coupled-channel formulation. The scattering amplitude encapsulates contributions from all the closed channels, turning out to be an Epstein zeta function [Eli94]:

$$f_{0,0} = \frac{2\pi a_{sc}}{a^2 ik}\frac{1}{1-\frac{2\pi a_{sc}}{a^2 ik}+\frac{a_{sc}}{a}\Lambda_E(\epsilon)}, \tag{3.80}$$

where

$$\Lambda_E(\epsilon) = \frac{\partial}{\partial z}\left(z\sum_{(n_x,n_y)\neq(0,0)}\frac{\exp(-\frac{2\pi|z|}{a}\sqrt{n_x^2+n_y^2-\epsilon})}{\sqrt{n_x^2+n_y^2-\epsilon}}\right)\Bigg|_{z\to 0}. \tag{3.81}$$

The positions of resonances correspond to zeros of the transmission amplitude $(1 + f_{0,0})$, which gives $\frac{a_{sc}}{a} = -\frac{1}{\Lambda_E(\epsilon)}$ at resonance. At such a resonance there is vanishing transmission probability, or in other words, "opacity'' of the 2D lattice to the matter wave.

The mapping from the reduced dimensional system to a transistor works as follows. In a transistor, the crux of the idea is to use a small tunable voltage to control a comparatively large current. The atomic matter wave, of course, serves as the current from the emitter that is experimentally implemented using two atomic reservoirs with different chemical potentials. The tunable scattering length a_{sc} plays the role of the "control voltage''. It is not literally a voltage, but it exhibits every aspect that a "control voltage'' element in an atomtronic circuit needs to have. This inter-species scattering length can be tuned either very adiabatically or else quite diabatically by controlling the ramping speed of the external magnetic field, which makes this reduced dimensional system a candidate for gate operations. The energies where a resonance occurs lie between the

lowest and the first-excited transverse mode(s) of the 2D lattice plane. This resonance happens at a nondiverging value of the 3D inter-species scattering length a_{sc}, keeping the system from having strong three-body losses.

The fact that the numerator of $1 + f_{0,0}$ is purely real makes it possible to find a complete "shut down'' of the transmitted matter wave. The $f_{0,0} = -1$ line is the white line in Fig. 3.7. This corresponds to one case of the Fano-Feshbach theory, namely, the case in which a single bound state is embedded in a single continuum. However if there are more than one continuum channels present, the transmitted wave intensity can no longer be fully turned off, but only tuned to a local minimum. Consequently, the signal-to-noise ratio of the transparency and opacity of the lowest open channel deteriorates in the presence of multiple open channels.

Besides proposing the matter wave transistor scheme, we also estimate the temperature range in which this matter wave transistor can work perfectly, meaning that the velocity spread in both the transverse direction and the longitudinal direction is comparatively small to the recoil velocity of the optical lattice $v = \frac{2\pi\hbar}{mL}$. Continuous atomic current from a BEC was demonstrated in the output coupler [MAK$^+$97]. A typical optical lattice constant ranges from 1.3μm to 9.1μm [BBS$^+$13], and an even smaller value has recently been achieved using a magnetic field and a type II superconductor [RINS$^+$13]. And the finite temperature will result in velocity spread in the atomic beam $\Delta v \sim \sqrt{2k_BT/m}$ [RWMC90, MAK$^+$97], m is the atomic mass. The spread of the velocity and the characteristic lattice velocity scale different with atomic mass. To achieve small relative spread, lighter atomic spices are favored. For example, in the recent sub wavelength optical lattice [RINS$^+$13], $\Delta v/v$ can be as small as 3% for lithium BEC. However, the atomic velocity spread $\Delta v = \sqrt{2k_BT/m}$ is an estimation of the upper bound. The noise in the longitudinal velocity spread was reduced to 1/10 of this upper bound in by Bloch *et.al* in [MAK$^+$97]. So the lattice indued opacity can also be achieved in a traditional optical lattice with smaller recoil energy than a sub wavelength optical lattice.

The discussion above implies that, for the quantum transistor proposed here, the temperature criterion is determined by the kinetic energy of the incoming matter wave and its spread, such that

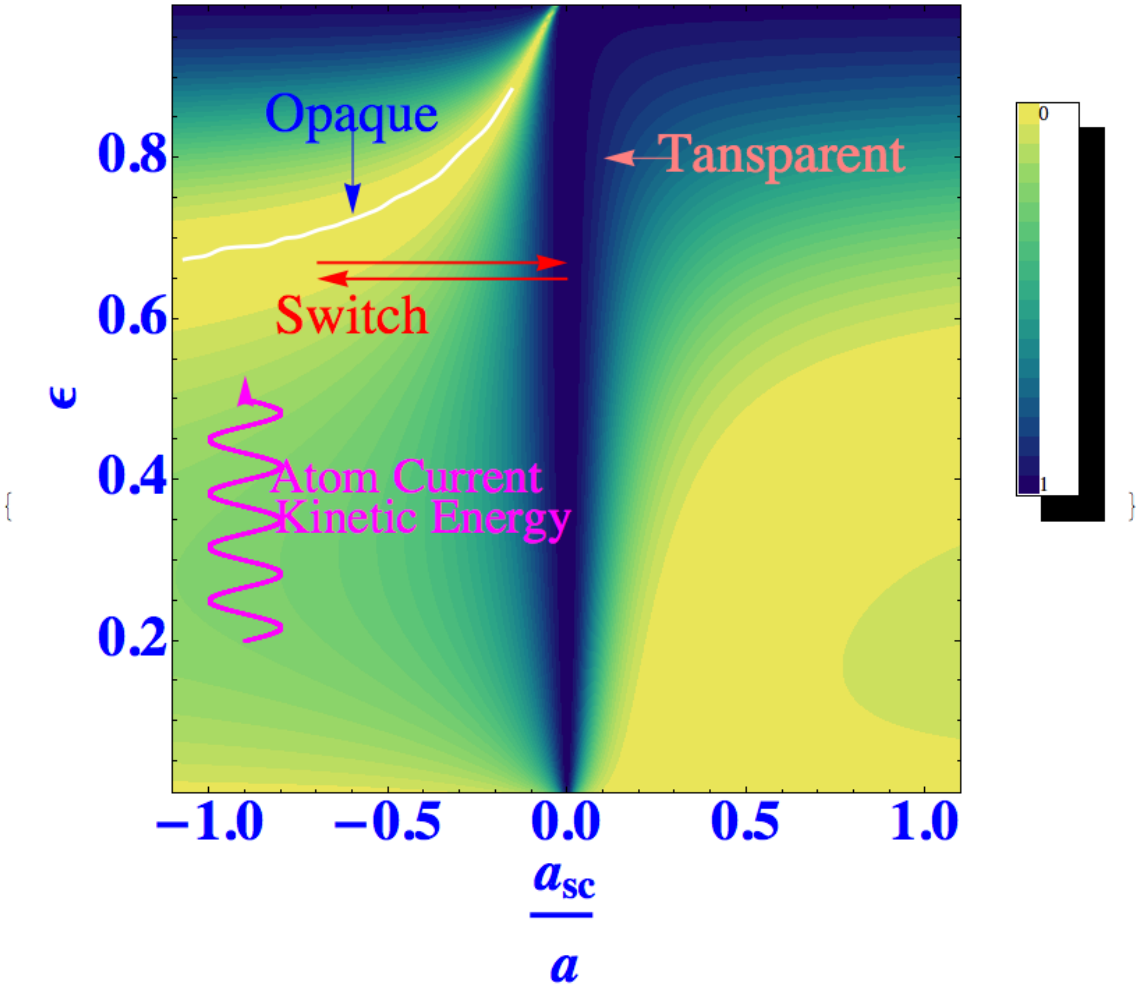

Figure 3.7: This graph plots the quasi-1D transmission probability, $|1 + f_{0,0}|^2$, as a function of the 3D scattering length a_{sc} and the kinetic energy ϵ of the incoming atom for scattering in the case of a single open channel. The energy unit in this figure is $\frac{\hbar^2\pi^2}{2ma^2}$. There are two regions in this parameter space where the scattering amplitude is close to zero. However, only the one that is associated with a negative 3D scattering length a_{sc} provides a usable lattice-size-induced opacity. At positive values of a_{sc}, although there exists a region where a_{sc} and ϵ cooperatively result in a small transmission amplitude, the tunability there is poorer than the negative a_{sc} region. This is because in the region $a_{sc} > 0$, even tuning ϵ and a_{sc} over a large range does not significantly change the transmission amplitude. $f_{0,0} = -1$ corresponds to the white line, and the $f_{0,0}$ corresponds to the deepest navy colored line.

only the lowest channel in the 2D periodic lattice plane is energetically open. In multi-open-channel quasi-1D scattering, no zero point of transmission in any single channel occurs, meaning no complete opacity of any channel can be achieved. However, in the multi-open-channel scenario, a similar confinement-induced opacity can be observed while the imaginary part of the complex transmission amplitude hits zero. The scattering amplitude in a system having multiple open channels was explained and classified by Fano [Fan61] as an example of multi-continuum resonances, nowadays termed a Fano lineshape.

After discussing the single-open-channel case, a higher energy incoming atomic beam is considered. The discussion below assumes that the incident channel is the lowest transverse mode of the 2D lattice plane $\psi(z \to -\infty) = \psi_{0,0}(x,y)e^{ikz}$. The reason this case is singled out is that this matter wave in the lowest mode is the easiest to implement experimentally. By increasing the k_z in the incoming wave, it is possible to excite higher modes in the xy-direction as outgoing waves. We now demonstrate the inelastic scattering in a problem involving two open channels of the 2D square lattice. Under the assumption that no modes in the excited channels exist in the incoming beam, the general expression of the outgoing matter wave to a higher transverse mode is:

$$f_{0,\pm1} = f_{\pm1,0} = s_{0,0}\frac{\frac{2\pi}{aiq}\frac{a_{sc}}{a}}{1+\frac{a_{sc}}{a}\Lambda_E - \frac{2\pi}{aik}\frac{a_{sc}}{a} - 4\frac{2\pi}{aiq}\frac{a_{sc}}{a}}. \tag{3.82}$$

In multi-open-channel scattering, as an analogue to the confinement-induced resonance in the single-open-channel case, the zero point of $1+\frac{a_{sc}}{a}\Lambda_E$ causes a π phase jump of the outgoing wave into $(0,\pm1)$ and $(\pm1,0)$ with respect to the incoming wave, in which Λ_E is the Epstein zeta function. Moreover, the zero point of $1+\frac{a_{sc}}{a}\Lambda_E$ gives rise to a maximum inelastic scattering amplitude. Thus for a given incoming wave vector perpendicular to the 2D lattice plane, a similar resonance can also emerge in the inelastic scattering process by tuning the 3D scattering length. This process can be viewed as a coherent matter wave beam splitter, in the sense that it creates phase-coherent waves that propagate in different spatial directions. Therefore, this process is a class of the Kapitza-Dirac type thin-grating diffraction, which was first realized in BEC scattering from a 2D optical lattice [GLDE01], in which BEC atoms directly gain momentum from the counter-propagating laser that

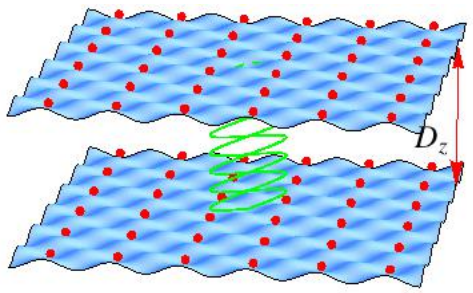

Figure 3.8: Sketch of a matter wave cavity utilizing two parallel 2D optical lattices where the effective 1D interaction strength g_{1D} for each of them is infinite.

forms the optical lattice. However, the configuration in this letter is different from that in the approach of Gupta *et.al* [GLDE01]. In the present reduced-dimensional system, the number of interference peaks is controlled by the incoming matter wave kinetic energy and the short range interaction between atoms in the matter wave and atoms trapped in the 2D optical lattice. As a result, it is possible to completely turn off the intensity of the perpendicular wave which cannot occur in a traditional Kapiza-Dirac thin grating.

Since the s-wave interaction between atoms in the matter wave and those in the 2D lattice of atoms can be described using a single effective 1D delta function in z: $g_{1D}\delta(z)$, it is possible to make a matter wave cavity by placing two optical lattices separated by a certain distance D_z, sketched in Fig. 3.8. The quasi-1D matter wave cavity can be simply described by two delta function potentials in 1D:

$$H_{1D} = -\frac{\hbar^2}{2\mu}\frac{\partial^2}{\partial z^2} + g_{1D}\delta(z - \frac{D_z}{2}) + g_{1D}\delta(z + \frac{D_z}{2}). \tag{3.83}$$

The cavity is realized by tuning the transmission coefficients of the 2D optical lattices outside the region $(-\frac{D_z}{2}, \frac{D_z}{2})$ to zero. By adjusting the distance between the two lattice planes, the standing matter wave $(k_z D_z = n\pi, n = 1, 2, \cdots)$ can be created inside this cavity configuration. This matter wave resonant cavity scheme can potentially be applied in matter wave interferometry experiments. The high precision and controllability of atoms in matter wave interferometry should enable the combination of matter waves and optical lattices to be implemented as an important precision measurements platform [PWT$^+$11, CCZ$^+$12].

The quasi-1D scattering process with a transverse confinement does, in principle, apply to Fano-Feshbach resonance theory, but the resonance width is quite significant compared to the assumption of an isolated resonance that was made in [Fan61]. This large width means each individual resonance profile may deviate from the exact analytical expression derived by Fano because of an influence from a series of cuts by transverse thresholds. However, the analytical expression still preserves the asymmetric feature compared to a symmetric Lorentz line shape. Quantitatively, this asymmetric feature is embedded in the piecewise Epstein zeta function for different energy regions $E \in (E_0, E_1), E \in (E_1, E_2) \cdots$.

In the expression of the Epstein zeta function, when the energy reaches each channel threshold E_n, the divergent scattering cross section behaves like $\sim \frac{1}{\sqrt{E-E_n}}$, while other terms vary much more slowly. This diverging behavior reflects the fundamental origin of Fano-Feshbach resonance, namely, the embedded bound state in a continuum. But the actual lineshape of observables is changed because the near-threshold density of states is not flat as was assumed in the Fano formulation. Quasi-1D systems with different transverse confinement spectra, exhibit qualitative similarity in their resonance profiles, as is shown in Table. 3.1. This similarity comes from the mathematical structure of the transmission probability. All of them have the general form of the zeta function, namely

$$\xi_H(q, s) = \sum_{n=0}^{\infty} \frac{1}{(n+q)^s} \tag{3.84}$$

is the Hurwitz zeta function that describes confinement-induced resonances in an isotropic transverse harmonic trap. The quantity

$$\xi_E(q, s) = \sum_{n_x, n_y}^{\infty} \frac{1}{((n_x - q_x)^2 + (n_y - q_y)^2 + \epsilon)^s}, \tag{3.85}$$

is the Epstein zeta function, describing both the square well waveguide [ZG13a] and the infinite 2D square lattice, in which $q = (q_x, q_y, \epsilon)$ denotes the "shift'' coming from the ground state mode of system, the power s is determined by the partial wave expansion of the interaction potential that is dominant in the relevant energy and symmetry of the system. For an s wave, the zeta function parameter is $s = \frac{1}{2}$ [Ols98] and for a p wave [GB04], $s = -\frac{1}{2}$.

The regularization method developed here works for both short range s and p wave scattering, and in principle for higher partial waves as well. The d-wave, *e.g.*, is essential in describing the dipole-dipole interaction in a quasi-1D confinement geometry[GDS12, GCQZ13]. Mathematically, the Epstein zeta function and the Hurwitz zeta function have very different origins in analytic number theory. However, in describing the class of confinement-induced resonance phenomena, their emergence is quite intuitive and naturally generalized from one to another.

3.4 Summary and Outlook

3.4.1 Summary

In this chapter, we present the development of the regularization technique for the effective quasi-1D coupling constant and the quasi-1D scattering amplitude. The regularization technique is developed in the framework of the local frame transformation, and generalize previous results to general transverse confinements.

Subsequently, we apply this technique to systems with various transverse trapping potential. The analytical regularization result agree perfectly with numerical calculation using variational eigenchannel R-matrix approach. All of the three example systems we have calculated exhibit clear structure of Fano-Feshbach resonance, although the width of the resonance is always larger than the energy spacing in the transverse plane.

Up to now, the regularization technique we have developed has only been applied to s-wave scattering processes. However, this method can be applied to p-wave scattering processes and more exotic transverse traps without additional difficulty.

In the summation of formula of the effective 1D coupling constant, we can infer that the asymptotic behavior of the transverse spectrum controls the diverging series. Thus, the essence of this regularization technique is that we subtract the contribution associated with the deep closed channels from the scattering amplitude or the effective 1D coupling constant.

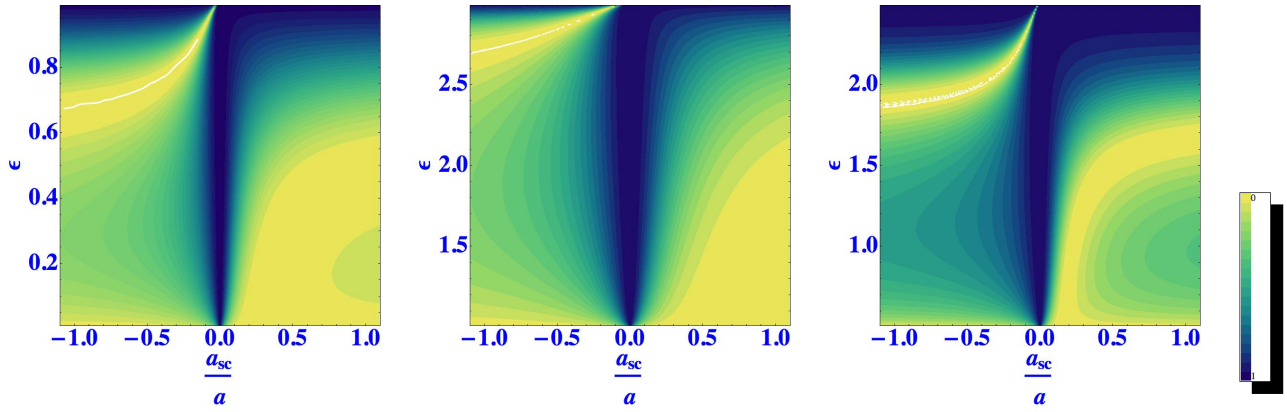

Table 3.1: Comparison of confinement-induced resonances in different systems. The transmission probability for one open channel, in (from left to right) (i) two dimensional lattice (ii) square well waveguide (iii) two dimensional isotropic harmonic trap. The transmission probabilities for the case of one open channel are plotted. The units in each plot are the relevant system-characteristic energy scale, namely $\frac{\hbar^2}{2\mu}(\frac{2\pi}{a})^2$, $\frac{\hbar^2}{2\mu}(\frac{2\pi}{L})^2$, $\hbar\omega_\perp$. a is the lattice constant, L is the size of the square waveguide, and $\omega_\perp$ is the transverse trap frequency. Lighter colors correspond to less transmission, and the thin white line locates the positions of confinement-induced opacities.

3.4.2 Outlook

The regularization technique can be immediately applied to p-wave scattering in square well wave guide or square lattices. In these systems, the group elements of the rotational symmetry group of the p-wave state do not commute with the symmetry group of the lattice. This will result in interesting nontrivial irreducible representations of the reaction matrix K, with implications for the quasi-1D scattering amplitude.

Another direction of generalization is to include spin degree of freedom (spin-exchange scattering, spin-orbit coupling) in the short-range interaction center. The spin-spin interaction in this reduced dimensional system may introduce spin-momentum locking, just like what happens in the spintronics devices.

Chapter 4

Summary and Outlook

In this thesis, we have covered two topics. One is the few-body ultracold Bose-Fermi mixture, and the other is the quasi-1D scattering in elongated traps.

The quantum statistics of particles in a Bose-Fermi mixture enrich the spectrum and dynamics of ultracold quantum gases, compared to their counterparts in identical bosons or two-component fermions. In the study of ultracold Bose-Fermi mixtures, we have calculated the three-body and four-body spectrum of KRb and the three-body spectrum of LiCs.

Based on the spectrum and the adiabatic eigenstates of the few-body systems, we have calculated the time evolution of the KRb system across a broad Fano-Feshbach resonance. Although the spectrum shows complicated structures of avoided crossings that correspond to the Efimov trimer formation and the Feshbach molecule formation, the time evolution of the few-body Bose-Fermi mixtures can be parameterized as an incoherent sequence of two-level Landau-Zener transitions between configurations. This leads to a simple description of the dynamics of quantum gases in the magneto association processes.

Morever, we explore the Efimov trimer's scattering properties at unitarity. The Efimov trimer states can be viewed as bound states that break the continuous scaling symmetry of a unitary Bose gas. A direct consequence is that the scattering properties of an Efimov trimer with the remaining atoms in the quantum gas are solely determined by its own three-body parameter. We have discovered a universal relation between the effective fermion-trimer (BBF-F) scattering length and the three-body parameter of the Efimov trimer at unitarity.

We also propose a quantum beat experiment that could be used to measure the binding energy of Efimov trimer states at unitary, by applying a sequence of quenches of the interparticle interaction strength. From the simulated quantum beat data, we identify the correspondence between the oscillation periods and the trimer's binding energy. This suggests an accessible way of measuring the absolute binding energies of the Efimov series, thus yielding a more direct proof the descrete scaling symmetry exhibited by a three-body system.

However, there are open questions with respect to the few-body theoretical description of the ultracold Bose-Fermi mixture. We have studied the adiabatic time evolution of the four-body BBFF system. By identifying the important Landau-Zener couplings between configurations, we have a simplified model for describing the formation efficiency of the heteronuclear dipolar molecule. How to generalize this scheme to a many-body system? At what range of ramping speed of the adiabatic parameter, can we ramp the mixture of an BEC and an atomic Fermi sea to a molecular Fermi sea? From the BBFF spectra that are presented in this thesis, we can already see a competition between the cluster states (trimer, tetramer and so on) with the formation of a molecular Fermi sea. Generalization of the correlated Gaussian method into larger number of particles in Bose-Fermi mixtures will suddenly involve calculation of series of cluster states, so it is more challenging than the two component Fermi gas and more rewarding for understanding the ground-to-ground state transition between atomic states and molecular states.

Another class of open questions are raised immediately after the realization of ultracold Bose-Fermi mixtures. Namely, the systematics of heteronuclear cluster bound states, $BBBF$, $FFFB$ and so on. In these systems, both the quantum statistics and the mass ratio poses challenges to existing theories. However, the experimental advances in the heteronuclear Bose-Fermi mixtures are pushing forward the frontier of studies into these questions. Precise control of the magnetic field in traps offers more observables to study in these novel cluster states. What is their role in the non equilibrium dynamics of a degenerate quantum gas? This question arises at the same time as the development of quenching the interparticle interactions inside a BEC. Table 4.1 summarizes the current stages of experimental realizations of few-body clusters.

	homonuclear	heteronuclear		
Efimov States(Three-Body)	BBB	BBB′	BBF	BFF
	✓	✓	✓	x
Four-Body and beyond	BBBB	any heteronuclear combination		
	✓	x		

Table 4.1: Stages of few-body clusters.

In the study of the quasi-1D scattering, we have developed a regularization method of quasi-1D scattering amplitude for generic transverse traps. We have applied the local frame transformation theory to derive the quasi-1D reaction matrix. From the local frame transformation theory, we immediately see that the reason why this method and the previous zero-range model potential work well. The reason behind the theories is that these quasi-1D system possesses clearly distinct length scales. Although the local frame transformation is not unitary, the next order corrections are small in these cases.

The regularization technique we developed relies only on the asymptotic behavior of the functional form of the transverse energy spectrum in the quantum number plane. As a starting point, we have tested our technique for the 2D isotropic harmonic confinement. We have reached excellent agreement with existing theoretical works. Subsequently, we applied our technique to a square well wave guide. Extrapolations of our numerical model potential R-matrix calculation exhibits good agreement with the theoretical prediction of our proposed regularization technique.

We find that the transmission coefficient of a matter wave through a 2D atomic lattice have a mathematical structure quite similar to that in the quasi-1D scattering process in a wave guide. We propose a matter wave transistor mechanism based on this finding. A matter wave cavity is also proposed that would use two parallel atomic lattice planes.

An immediate generalization of the regularization technique suggested by this work would be to treat the p-wave reaction matrix inside a square well wave guide. In this system, the rotational symmetry group of the p-wave scattering center does not commute with the symmetry group of the wave guide. The resulting scattering matrix is reduced to a 2D irreducible representation rather than a single effective 1D coupling constant. Thus the quasi-1D scattering phenomena in this

system are expected to be much richer that their s-wave counter part.

Another immediate generalization of the application would be to apply the regularization technique to a short-range spin-dependent scattering center confined in a quasi-1D trap. Reduced dimensional systems often break the rotational symmetry of the angular momentum, and thus the spin rotational symmetry could be easily broken. This generic feature makes quasi-1D systems promising candidates for realizing spin-momentum locked currents, which are the essence of spintronics.

Another class of prospective research directions for a quasi-1D scattering problem is the implementation this two-body scattering information into a many-body quasi-1D system. As is introduced in the beginning of the quasi-1D scattering chapter, many exactly solvable 1D models have been predicted in the past century. So observing the evolution of the 1D quantum gases from one phase to anther by adjusting the transverse confinement and the short-range interaction is promising from both experimental and theoretical perspectives.

In quasi-1D systems, the fermionization of strongly interacting bosons has already been observed, which leads to active discussions of gauge theories in 1D. For a pure 1D system, identical particles exhibit strikingly different behaviors in quantum statistics from their 3D counter parts. Interacting quasi-1D systems have the flexibility to be engineered into regimes that exhibit exotic particle statistics.

Bibliography

[AAK+88] A. Aspect, E. Arimondo, R. Kaiser, N. Vansteenkiste, and C. Cohen-Tannoudji. Laser cooling below the one-photon recoil energy by velocity-selective coherent population trapping. Phys. Rev. Lett., 61:826–829, Aug 1988.

[ABT13] Y. Avishai, Y. B. Band, and M. Trippenbach. Feshbach resonance without a closed-channel bound state. Phys. Rev. Lett., 111:155301, Oct 2013.

[Ada71] I. Adawi. Scattering of waves in many dimensions. J. Math. Phys., 12(3):358–359, 1971.

[AEM+95] M. H. Anderson, J. R. Ensher, M. R. Matthews, C. E. Wieman, and E. A. Cornell. Observation of bose-einstein condensation in a dilute atomic vapor. Science, 269(5221):198–201, 1995.

[AGR04] A. V. Andreev, V. Gurarie, and L. Radzihovsky. Nonequilibrium dynamics and thermodynamics of a degenerate fermi gas across a feshbach resonance. Phys. Rev. Lett., 93(13):130402, Sep 2004.

[AIE03] Alexander Albus, Fabrizio Illuminati, and Jens Eisert. Mixtures of bosonic and fermionic atoms in optical lattices. Phys. Rev. A, 68:023606, Aug 2003.

[AJN+13] Manuel Andia, Raphael Jannin, Francois Nez, Francois Biraben, Saida Guellati-Khelifa, and Pierre Clade. Compact atomic gravimeter based on a pulsed and accelerated optical lattice. arxiv, 1309.1713, 2013.

[AS64] M. Abramowitz and I.A. Stegun. Handbook of Mathematical Functions. Dover, New York, fifth edition, 1964.

[Ash70] A. Ashkin. Acceleration and trapping of particles by radiation pressure. Phys. Rev. Lett., 24:156–159, Jan 1970.

[AWT+12] Peter Anders, Philipp Werner, Matthias Troyer, Manfred Sigrist, and Lode Pollet. From the cooper problem to canted supersolids in bose-fermi mixtures. Phys. Rev. Lett., 109:206401, Nov 2012.

[BAR+04] M. Bartenstein, A. Altmeyer, S. Riedl, S. Jochim, C. Chin, J. Hecker Denschlag, and R. Grimm. Crossover from a molecular bose-einstein condensate to a degenerate fermi gas. Phys. Rev. Lett., 92:120401, Mar 2004.

[BB36] H. A. Bethe and R. F. Bacher. Nuclear physics a. stationary states of nuclei. Rev. Mod. Phys., 8:82–229, Apr 1936.

[BB97] Matthias Brackm and Rajat K. Bhaduri. Semiclassical Physics. Addison-Welsley publishing company, inc., 1997.

[BBG03] Bogdan Borca, D Blume, and Chris H Greene. A two-atom picture of coherent atom–molecule quantum beats. New J. Phy., 5(1):111, 2003.

[BBH00] P. F. Bedaque, Eric Braaten, and H.-W. Hammer. Three-body recombination in bose gases with large scattering length. Phys. Rev. Lett., 85:908–911, Jul 2000.

[BBS+13] Thierry Botter, Daniel W. C. Brooks, Sydney Schreppler, Nathan Brahms, and Dan M. Stamper-Kurn. Optical readout of the quantum collective motion of an array of atomic ensembles. Phys. Rev. Lett., 110:153001, Apr 2013.

[BD09] D. Blume and K. M. Daily. Universal relations for a trapped four-fermion system with arbitrary s-wave scattering length. Phys. Rev. A, 80:053626, Nov 2009.

[BD10a] D. Blume and K. M. Daily. Breakdown of universality for unequal-mass fermi gases with infinite scattering length. Phys. Rev. Lett., 105:170403, Oct 2010.

[BD10b] D. Blume and K. M. Daily. Few-body resonances of unequal-mass systems with infinite interspecies two-body s-wave scattering length. Phys. Rev. A, 82:063612, Dec 2010.

[BDNnt] Immanuel Bloch, Jean Dalibard, and Sylvain Nascimbene. Quantum simulations with ultracold quantum gases. Nat Phys, 8:267–276, 2012/04//print.

[BDZ08] Immanuel Bloch, Jean Dalibard, and Wilhelm Zwerger. Many-body physics with ultracold gases. Rev. Mod. Phys., 80:885–964, Jul 2008.

[BEKW98] Thomas Busch, Berthold-Georg Englert, Rzazewski Kazimierz, and Martin Wilkens. Two cold atoms in a harmonic trap. Foundation of Physics, 28(4):549–559, 1998.

[Bet31] H. Bethe. Zur theorie der metalle. Zeitschrift fuer Physik, 71(3-4):205–226, 1931.

[BFAP78] J. E. Bjorkholm, R. R. Freeman, A. Ashkin, and D. B. Pearson. Observation of focusing of neutral atoms by the dipole forces of resonance-radiation pressure. Phys. Rev. Lett., 41:1361–1364, Nov 1978.

[BH06] Eric Braaten and H.-W. Hammer. Universality in few-body systems with large scattering length. Physics Reports, 428(56):259 – 390, 2006.

[BHE99] Immanuel Bloch, Theodor W. Hänsch, and Tilman Esslinger. Atom laser with a cw output coupler. Phys. Rev. Lett., 82:3008–3011, Apr 1999.

[BHvK00] P.F. Bedaque, H.-W. Hammer, and U. van Kolck. Effective theory of the triton. Nuclear Physics A, 676(14):357 – 370, 2000.

[BKC+04] T. Bourdel, L. Khaykovich, J. Cubizolles, J. Zhang, F. Chevy, M. Teichmann, L. Tarruell, S. J. J. M. F. Kokkelmans, and C. Salomon. Experimental study of the bec-bcs crossover region in lithium 6. Phys. Rev. Lett., 93:050401, Jul 2004.

[Blo08] Immanuel Bloch. Quantum coherence and entanglement with ultracold atoms in optical lattices. Nature, 453:1016–1022, 2008.

[Blu08] D. Blume. Small mass- and trap-imbalanced two-component fermi systems. Phys. Rev. A, 78:013613, Jul 2008.

[Blu12] D. Blume. Universal four-body states in heavy-light mixtures with a positive scattering length. Phys. Rev. Lett., 109:230404, Dec 2012.

[BM13] Bertrand Berche and Ernesto Medina. Classical yangmills theory in condensed matter physics. European Journal of Physics, 34(1):161, 2013.

[BP35] H. Bethe and R. Peierls. Quantum theory of the diplon. Proc. Roy. Soc., Series A - Mathematical and Physical Sciences, 148(863):146–156, 1935.

[BPT+10] W. S. Bakr, A. Peng, M. E. Tai, R. Ma, J. Simon, J. I. Gillen, S. Flling, L. Pollet, and M. Greiner. Probing the superfluidtomott insulator transition at the single-atom level. Science, 329(5991):547–550, 2010.

[BR96] Silvio J. Benetton Rabello. 1d generalized statistics gas: A gauge theory approach. Phys. Rev. Lett., 76:4007–4009, May 1996.

[BR09] D. Blume and D. Rakshit. Excitation spectrum and effective interactions of a highly elongated fermi gas. Phys. Rev. A, 80:013601, Jul 2009.

[BSM+07] Micah Boyd, Erik W. Streed, Patrick Medley, Gretchen K. Campbell, Jongchul Mun, Wolfgang Ketterle, and David E. Pritchard. Atom trapping with a thin magnetic film. Phys. Rev. A, 76:043624, Oct 2007.

[BSTH95] C. C. Bradley, C. A. Sackett, J. J. Tollett, and R. G. Hulet. Evidence of bose-einstein condensation in an atomic gas with attractive interactions. Phys. Rev. Lett., 75:1687–1690, Aug 1995.

[BTJ03] E. L. Bolda, E. Tiesinga, and P. S. Julienne. Pseudopotential model of ultracold atomic collisions in quasi-one- and two-dimensional traps. Phys. Rev. A, 68:032702, Sep 2003.

[BvSG07] D. Blume, J. von Stecher, and Chris H. Greene. Universal properties of a trapped two-component fermi gas at unitarity. Phys. Rev. Lett., 99(23):233201, Dec 2007.

[BWS+09] Th. Best, S. Will, U. Schneider, L. Hackermüller, D. van Oosten, I. Bloch, and D.-S. Lühmann. Role of interactions in $rb87 - k40$ bose-fermi mixtures in a 3d optical lattice. Phys. Rev. Lett., 102(3):030408, Jan 2009.

[Cal71] F. Calogero. Solution of the onedimensional nbody problems with quadratic and/or inversely quadratic pair potentials. Journal of Mathematical Physics, 12(3):419–436, 1971.

[CBB+13] Wenlan Chen, Kristin M. Beck, Robert Bcker, Michael Gullans, Mikhail D. Lukin, Haruka Tanji-Suzuki, and Vladan Vuletic. All-optical switch and transistor gated by one stored photon. Science, 341(6147):768–770, 2013.

[CCG+11] M. A. Cazalilla, R. Citro, T. Giamarchi, E. Orignac, and M. Rigol. One dimensional bosons: From condensed matter systems to ultracold gases. Rev. Mod. Phys., 83:1405–1466, Dec 2011.

[CCZ+12] Renée Charrière, Malo Cadoret, Nassim Zahzam, Yannick Bidel, and Alexandre Bresson. Local gravity measurement with the combination of atom interferometry and bloch oscillations. Phys. Rev. A, 85:013639, Jan 2012.

[CEI04] M. Cramer, J. Eisert, and F. Illuminati. Inhomogeneous atomic bose-fermi mixtures in cubic lattices. Phys. Rev. Lett., 93:190405, Nov 2004.

[CFV+13] P. Cheiney, C. M. Fabre, F. Vermersch, G. L. Gattobigio, R. Mathevet, T. Lahaye, and D. Guéry-Odelin. Matter-wave scattering on an amplitude-modulated optical lattice. Phys. Rev. A, 87:013623, Jan 2013.

[CG86] Th. Cornelius and W. Glckle. Efimov states for three 4he atoms? The Journal of Chemical Physics, 85(7):3906–3912, 1986.

[CGJT10] Cheng Chin, Rudolf Grimm, Paul Julienne, and Eite Tiesinga. Feshbach resonances in ultracold gases. Rev. Mod. Phys., 82:1225–1286, Apr 2010.

[CHB+85] Steven Chu, L. Hollberg, J. E. Bjorkholm, Alex Cable, and A. Ashkin. Three-dimensional viscous confinement and cooling of atoms by resonance radiation pressure. Phys. Rev. Lett., 55:48–51, Jul 1985.

[Chi12] Cheng Chin. Universal scaling of efimov resonance positions in cold atom systems. arxiv, 1111.1484, 2012.

[CHT+11] Yu-Ao Chen, Sebastian D. Huber, Stefan Trotzky, Immanuel Bloch, and Ehud Altman. Many-body landau-zener dynamics in coupled one-dimensional bose liquids. Nature Phys., 7(1):61–67, 01 2011.

[Cla79] Charles W. Clark. The calculation of non-adiabatic transition probabilities. Phy. Lett. A, 70(4):295 – 296, 1979.

[Cla83] Charles W. Clark. Low-energy electron-atom scattering in a magnetic field. Phys. Rev. A, 28:83–90, Jul 1983.

[CMP10] Yvan Castin, Christophe Mora, and Ludovic Pricoupenko. Four-body efimov effect for three fermions and a lighter particle. Phys. Rev. Lett., 105:223201, Nov 2010.

[Cra11] M. Cramer. Interaction-dependent temperature effects in bose-fermi mixtures in optical lattices. Phys. Rev. Lett., 106:215302, May 2011.

[CSZA12] Seth C Caliga, Cameron J. E. Straatrma, Alex A. Zozulya, and Dana Z. Anderson. A matterwave transistor oscillator. arXiv, 1208.3109, 2012.

[CWZ10] Xiaoling Cui, Yupeng Wang, and Fei Zhou. Resonance scattering in optical lattices and molecules: Interband versus intraband effects. Phys. Rev. Lett., 104:153201, Apr 2010.

[CZ95] J. I. Cirac and P. Zoller. Quantum computations with cold trapped ions. Phys. Rev. Lett., 74:4091–4094, May 1995.

[DB78] Carl De Boor. A Practical Guide to Splines. Springer-Verlag, first edition, 1978.

[DB10] K. M. Daily and D. Blume. Energy spectrum of harmonically trapped two-component fermi gases: Three- and four-particle problem. Phys. Rev. A, 81:053615, May 2010.

[DB12] K. M. Daily and D. Blume. Thermodynamics of the two-component fermi gas with unequal masses at unitarity. Phys. Rev. A, 85:013609, Jan 2012.

[dCDGC+06] A. del Campo, F. Delgado, G. García-Calderón, J. G. Muga, and M. G. Raizen. Decay by tunneling of bosonic and fermionic tonks-girardeau gases. Phys. Rev. A, 74:013605, Jul 2006.

[dCP62] Jacques des Cloizeaux and J. J. Pearson. Spin-wave spectrum of the antiferromagnetic linear chain. Phys. Rev., 128:2131–2135, Dec 1962.

[DE06a] J. P. D'Incao and B. D. Esry. Enhancing the observability of the efimov effect in ultracold atomic gas mixtures. Phys. Rev. A, 73:030703, Mar 2006.

[DE06b] J. P. D'Incao and B. D. Esry. Mass dependence of ultracold three-body collision rates. Phys. Rev. A, 73:030702, Mar 2006.

[DEHnt] HANS G DEHMELT. Entropy reduction by motional sideband excitation. Nature, 262:777, 1976/08/26/print.

[Del11] A. Deltuva. Shallow efimov tetramer as inelastic virtual state and resonant enhancement of the atom-trimer relaxation. EPL (Europhysics Letters), 95(4):43002, 2011.

[Der05] Andrei Derevianko. Revised huang-yang multipolar pseudopotential. Phys. Rev. A, 72:044701, Oct 2005.

[DG14] K. M. Daily and Chris H. Greene. Extension of the correlated gaussian hyperspherical method to more particles and dimensions. Phys. Rev. A, 89:012503, Jan 2014.

[DGJbuO11] Jean Dalibard, Fabrice Gerbier, Gediminas Juzeliūnas, and Patrik Öhberg. ¡i¿colloquium¡/i¿: Artificial gauge potentials for neutral atoms. Rev. Mod. Phys., 83:1523–1543, Nov 2011.

[DHR+01] S. Dettmer, D. Hellweg, P. Ryytty, J. J. Arlt, W. Ertmer, K. Sengstock, D. S. Petrov, G. V. Shlyapnikov, H. Kreutzmann, L. Santos, and M. Lewenstein. Observation of phase fluctuations in elongated bose-einstein condensates. Phys. Rev. Lett., 87:160406, Oct 2001.

[DJ99] B. DeMarco and D. S. Jin. Onset of fermi degeneracy in a trapped atomic gas. Science, 285(5434):1703–1706, 1999.

[DLO01] V. Dunjko, V. Lorent, and M. Olshanii. Bosons in cigar-shaped traps: Thomas-fermi regime, tonks-girardeau regime, and in between. Phys. Rev. Lett., 86:5413–5416, Jun 2001.

[DMA+95] K. B. Davis, M. O. Mewes, M. R. Andrews, N. J. van Druten, D. S. Durfee, D. M. Kurn, and W. Ketterle. Bose-einstein condensation in a gas of sodium atoms. Phys. Rev. Lett., 75:3969–3973, Nov 1995.

[DMBO11] Vanja Dunjko, Michael G. Moore, Thomas Bergeman, and Maxim Olshanii. Chapter 10 - confinement-induced resonances. Adv. At. Mol. Opt. Phys., 60:461 – 510, 2011.

[Dod70] L. R. Dodd. Exact solution of the faddeev equations for a one-dimensional system. J. Math. Phys., 11(1):207–213, 1970.

[DRB+07] T. Donner, S. Ritter, T. Bourdel, A. Ottl, M. Kohl, and T. Esslinger. Critical behavior of a trapped interacting bose gas. Science, 315(5818):1556–1558, 2007.

[DRB12] K. M. Daily, D. Rakshit, and D. Blume. Degeneracies in trapped two-component fermi gases. Phys. Rev. Lett., 109:030401, Jul 2012.

[DvSG09a] J. P. D'Incao, J. von Stecher, and Chris H. Greene. Universal four-boson states in ultracold molecular gases: Resonant effects in dimer-dimer collisions. Phys. Rev. Lett., 103:033004, Jul 2009.

[DvSG09b] J. P. D'Incao, J. von Stecher, and Chris H. Greene. Universal four-boson states in ultracold molecular gases: Resonant effects in dimer-dimer collisions. Phys. Rev. Lett., 103:033004, Jul 2009.

[Dyk62] A. M. Dykhne. Adiabatic perturbation of discrete spectrum states. Soviet Physics JETP-USSR, 14(4):941–943, 1962.

[DZS+03] B. Damski, J. Zakrzewski, L. Santos, P. Zoller, and M. Lewenstein. Atomic bose and anderson glasses in optical lattices. Phys. Rev. Lett., 91:080403, Aug 2003.

[Efi70a] V. Efimov. Energy levels arising from resonant two-body forces in a three-body system. Physics Letters B, 33(8):563 – 564, 1970.

[Efi70b] V. Efimov. Weakly-bound states of three resonantly-interacting particles. Sov. J. Nucl. Phys., 12, 1970.

[Efi73] V. Efimov. Energy levels of three resonantly interacting particles. Nuclear Physics A, 210(1):157 – 188, 1973.

[EGS01] B. D. Esry, Chris H. Greene, and H. Suno. Threshold laws for three-body recombination. Phys. Rev. A, 65:010705, Dec 2001.

[Ein17] A. Einstein. On the quantum theory of radiation. Phys. Z., 18, 1917.

[ELG96] B. D. Esry, C. D. Lin, and Chris H. Greene. Adiabatic hyperspherical study of the helium trimer. Phys. Rev. A, 54:394–401, Jul 1996.

[Eli94] E. Elizalde. Zeta Regularization Techniques With Applications. World Scientific Publishing Company, Incorporated, 1994.

[Eli12] E. Elizalde. Ten physical applications of spectral zeta functions. Lect.Notes Phys., 855:1–225, 2012.

[EM04] J. P. Eisenstein and A. H. MacDonald. Bose-einstein condensation of excitons in bilayer electron systems. Nature, 432:691, 2004.

[ETS+06] J. Esteve, J.-B. Trebbia, T. Schumm, A. Aspect, C. I. Westbrook, and I. Bouchoule. Observations of density fluctuations in an elongated bose gas: Ideal gas and quasi-condensate regimes. Phys. Rev. Lett., 96:130403, Apr 2006.

[Fan61] U. Fano. Effects of configuration interaction on intensities and phase shifts. Phys. Rev., 124:1866–1878, Dec 1961.

[Fan81] U. Fano. Stark effect of nonhydrogenic rydberg spectra. Phys. Rev. A, 24:619–622, Jul 1981.

[FBZ04] P. O. Fedichev, M. J. Bijlsma, and P. Zoller. Extended molecules and geometric scattering resonances in optical lattices. Phys. Rev. Lett., 92:080401, Feb 2004.

[FDH+13] T. Frederico, A. Delfino, M.R. Hadizadeh, Lauro Tomio, and M.T. Yamashita. Universality in four-boson systems. Few-Body Systems, 54(5-6):559–568, 2013.

[Fey57] R. P. Feynman. Superfluidity and superconductivity. Rev. Mod. Phys., 29:205–212, Apr 1957.

[FFV+11] Bernd Fröhlich, Michael Feld, Enrico Vogt, Marco Koschorreck, Wilhelm Zwerger, and Michael Köhl. Radio-frequency spectroscopy of a strongly interacting two-dimensional fermi gas. Phys. Rev. Lett., 106:105301, Mar 2011.

[FHY+13] T. Frederico, M.R. Hadizadeh, M.T. Yamashita, Lauro Tomio, and A. Delfino. Range corrections to universal tetramer properties. Few-Body Systems, 54(7-10):1537–1542, 2013.

[FJ93] D. V. Fedorov and A. S. Jensen. Efimov effect in coordinate space faddeev equations. Phys. Rev. Lett., 71:4103–4106, Dec 1993.

[FOH+05] C. D. Fertig, K. M. O'Hara, J. H. Huckans, S. L. Rolston, W. D. Phillips, and J. V. Porto. Strongly inhibited transport of a degenerate 1d bose gas in a lattice. Phys. Rev. Lett., 94:120403, Apr 2005.

[FRS96] P. O. Fedichev, M. W. Reynolds, and G. V. Shlyapnikov. Three-body recombination of ultracold atoms to a weakly bound ¡span class="aps-inline-formula"¿¡math¿¡mi mathvariant="italic"¿s¡/mi¿¡/math¿¡/span¿ level. Phys. Rev. Lett., 77:2921–2924, Sep 1996.

[FTD+11] T. Frederico, Lauro Tomio, A. Delfino, M.R. Hadizadeh, and M.T. Yamashita. Scales and universality in few-body systems. Few-Body Systems, 51(2-4):87–112, 2011.

[Gau67] M. Gaudin. Un systeme a une dimension de fermions en interaction. Physics Letters A, 24(1):55 – 56, 1967.

[GB04] Brian E. Granger and D. Blume. Tuning the interactions of spin-polarized fermions using quasi-one-dimensional confinement. Phys. Rev. Lett., 92:133202, Apr 2004.

[GBL13] Xi-Wen Guan, Murray T. Batchelor, and Chaohong Lee. Fermi gases in one dimension: From bethe ansatz to experiments. Rev. Mod. Phys., 85:1633–1691, Nov 2013.

[GBM+01] Markus Greiner, Immanuel Bloch, Olaf Mandel, Theodor W. Hänsch, and Tilman Esslinger. Exploring phase coherence in a 2d lattice of bose-einstein condensates. Phys. Rev. Lett., 87:160405, Oct 2001.

[GCQZ13] Liming Guan, Xiaoling Cui, Ran Qi, and Hui Zhai. Quasi-one-dimensioanl dipolar quantum gases. arxiv, 1307.0899, 2013.

[GDB12a] Seyed Ebrahim Gharashi, K. M. Daily, and D. Blume. Three s-wave-interacting fermions under anisotropic harmonic confinement: Dimensional crossover of energetics and virial coefficients. Phys. Rev. A, 86:042702, Oct 2012.

[GDB12b] Seyed Ebrahim Gharashi, K. M. Daily, and D. Blume. Three s-wave-interacting fermions under anisotropic harmonic confinement: Dimensional crossover of energetics and virial coefficients. Phys. Rev. A, 86:042702, Oct 2012.

[GDS12] P. Giannakeas, F. K. Diakonos, and P. Schmelcher. Coupled l-wave confinement-induced resonances in cylindrically symmetric waveguides. Phys. Rev. A, 86:042703, Oct 2012.

[Gia04] Thierry Giamarchi. Quantum Physics in One Dimension. Oxford, 2004.

[GIO+04] J. Goldwin, S. Inouye, M. L. Olsen, B. Newman, B. D. DePaola, and D. S. Jin. Measurement of the interaction strength in a bose-fermi mixture with $rb87$ and $k40$. Phys. Rev. A, 70(2):021601, Aug 2004.

[Gir60] M. Girardeau. Relationship between systems of impenetrable bosons and fermions in one dimension. J. Math. Phys., 1(6):516–523, 1960.

[Gir65] M. D. Girardeau. Permutation symmetry of many-particle wave functions. Phys. Rev., 139:B500–B508, Jul 1965.

[GJ85] Chris H. Greene and Ch. Jungen. Vibrational frame transformation for electron-molecule scattering. Phys. Rev. Lett., 55:1066–1069, Sep 1985.

[GLDE01] S. Gupta, A. E. Leanhardt, Cronin A. D., and Pritchard D. E. Coherent manipulation of atoms with standing light waves. C. R. Acac. Sci. Ser IV: Phys., Astrophys., 2:479, 2001.

[GMS11] P. Giannakeas, V. S. Melezhik, and P. Schmelcher. Resonant d-wave scattering in harmonic waveguides. Phys. Rev. A, 84:023618, Aug 2011.

[GMS12] P. Giannakeas, V. S. Melezhik, and P. Schmelcher. Analytical treatment of bosonic d-wave scattering in isotropic harmonic waveguides. Phys. Rev. A, 85:042703, Apr 2012.

[GPR+11] Bryce Gadway, Daniel Pertot, Jeremy Reeves, Matthias Vogt, and Dominik Schneble. Glassy behavior in a binary atomic mixture. Phys. Rev. Lett., 107:145306, Sep 2011.

[GPRS12] Bryce Gadway, Daniel Pertot, Jeremy Reeves, and Dominik Schneble. Probing an ultracold-atom crystal with matter waves. Nature Phys., 8:544–549, July 2012.

[GR94] I. S. Gradshteyn and I. M. Ryzhik. Table of Integrals, Series, and Products, Fifth Edition. Academic Press, 5th edition, January 1994.

[Gre80] Chris H. Greene. Dependence of photoabsorption spectra on long-range fields. Phys. Rev. A, 22:149–157, Jul 1980.

[Gre83] Chris H. Greene. Atomic photoionization in a strong magnetic field. Phys. Rev. A, 28:2209–2216, Oct 1983.

[Gre87] Chris H. Greene. Negative-ion photodetachment in a weak magnetic field. Phys. Rev. A, 36:4236–4244, Nov 1987.

[Gri64] Robert B. Griffiths. Magnetization curve at zero temperature for the antiferromagnetic heisenberg linear chain. Phys. Rev., 133:A768–A775, Feb 1964.

[GRJ03] Markus Greiner, Cindy A. Regal, and Deborah S. Jin. Emergence of a molecular bose-einstein condensate from a fermi gas. Nature, 426(6966):537–540, 2003.

[Gro63] Eugene P. Gross. Hydrodynamics of a superfluid condensate. J. Math. Phys., 4(2):195–207, 1963.

[Gro92] David J. Gross. Gauge theory–past, present and future. Chinese Journal of Physics, 30(7):955, 1992.

[GSG+13] Alexander L. Gaunt, Tobias F. Schmidutz, Igor Gotlibovych, Robert P. Smith, and Zoran Hadzibabic. Bose-einstein condensation of atoms in a uniform potential. Phys. Rev. Lett., 110:200406, May 2013.

[GSM+05a] Kenneth Günter, Thilo Stöferle, Henning Moritz, Michael Köhl, and Tilman Esslinger. p-wave interactions in low-dimensional fermionic gases. Phys. Rev. Lett., 95:230401, Nov 2005.

[GSM+05b] Kenneth Günter, Thilo Stöferle, Henning Moritz, Michael Köhl, and Tilman Esslinger. p-wave interactions in low-dimensional fermionic gases. Phys. Rev. Lett., 95:230401, Nov 2005.

[GSM+06] Kenneth Günter, Thilo Stöferle, Henning Moritz, Michael Köhl, and Tilman Esslinger. Bose-fermi mixtures in a three-dimensional optical lattice. Phys. Rev. Lett., 96(18):180402, May 2006.

[GVL+01] A. Görlitz, J. M. Vogels, A. E. Leanhardt, C. Raman, T. L. Gustavson, J. R. Abo-Shaeer, A. P. Chikkatur, S. Gupta, S. Inouye, T. Rosenband, and W. Ketterle. Realization of bose-einstein condensates in lower dimensions. Phys. Rev. Lett., 87:130402, Sep 2001.

[GWO00] Rudolf Grimm, Matthias Weidemuller, and Yurii B. Ovchinnikov. Optical dipole traps for neutral atoms. Adv. At. Mol. Opt. Phys., 42:95 – 170, 2000.

[GZHCnt] Nathan Gemelke, Xibo Zhang, Chen-Lung Hung, and Cheng Chin. In situ observation of incompressible mott-insulating domains in ultracold atomic gases. Nature, 460:995–998, 2009/08/20/print.

[Hal81] F. D. M. Haldane. Effective harmonic-fluid approach to low-energy properties of one-dimensional quantum fluids. Phys. Rev. Lett., 47:1840–1843, Dec 1981.

[Hal88] F. D. M. Haldane. Exact jastrow-gutzwiller resonating-valence-bond ground state of the spin-1/2 antiferromagnetic heisenberg chain with $1/r^2$ exchange. Phys. Rev. Lett., 60:635–638, Feb 1988.

[Hal06] Karen A. Hallberg. New trends in density matrix renormalization. Advances in Physics, 55(5-6):477–526, 2006.

[Har81] David A. Harmin. Hydrogenic stark effect: Properties of the wave functions. Phys. Rev. A, 24:2491–2512, Nov 1981.

[Har82a] David A. Harmin. Theory of the nonhydrogenic stark effect. Phys. Rev. Lett., 49:128–131, Jul 1982.

[Har82b] David A. Harmin. Theory of the nonhydrogenic stark effect. Phys. Rev. Lett., 49:128–131, Jul 1982.

[Har82c] David A. Harmin. Theory of the stark effect. Phys. Rev. A, 26:2656–2681, Nov 1982.

[Har84] David A. Harmin. Analytical study of quasidiscrete stark levels in rydberg atoms. Phys. Rev. A, 30:2413–2428, Nov 1984.

[Har86] David A. Harmin. Precise theory of field enhancement of dielectronic recombination. Phys. Rev. Lett., 57:1570–1573, Sep 1986.

[Haw77] S.W. Hawking. Zeta function regularization of path integrals in curved spacetime. Comm. Math. Phys., 55:133–148, 1977.

[HCK+03] D. Hellweg, L. Cacciapuoti, M. Kottke, T. Schulte, K. Sengstock, W. Ertmer, and J. J. Arlt. Measurement of the spatial correlation function of phase fluctuating bose-einstein condensates. Phys. Rev. Lett., 91:010406, Jul 2003.

[HGK+11] J. Heinze, S. Götze, J. S. Krauser, B. Hundt, N. Fläschner, D.-S. Lühmann, C. Becker, and K. Sengstock. Multiband spectroscopy of ultracold fermions: Observation of reduced tunneling in attractive bose-fermi mixtures. Phys. Rev. Lett., 107:135303, Sep 2011.

[HGM+09] Elmar Haller, Mattias Gustavsson, Manfred J. Mark, Johann G. Danzl, Russell Hart, Guido Pupillo, and Hanns-Christoph Ngerl. Realization of an excited, strongly correlated quantum gas phase. Science, 325(5945):1224–1227, 2009.

[HGS02] E. L. Hamilton, C. H. Greene, and H. R. Sadeghpour. Shape-resonance-induced long-range molecular rydberg states. J. Phys. B, 35:L199, May 2002.

[HMH+10] Elmar Haller, Manfred J. Mark, Russell Hart, Johann G. Danzl, Lukas Reichsöllner, Vladimir Melezhik, Peter Schmelcher, and Hanns-Christoph Nägerl. Confinement-induced resonances in low-dimensional quantum systems. Phys. Rev. Lett., 104:153203, Apr 2010.

[Ho83] Y.K. Ho. The method of complex coordinate rotation and its applications to atomic collision processes. Physics Reports, 99(1):1 – 68, 1983.

[HP07] H.-W. Hammer and L. Platter. Universal properties of the four-body system with large scattering length. The European Physical Journal A, 32(1):113–120, 2007.

[HS75] T.W. Hnsch and A.L. Schawlow. Cooling of gases by laser radiation. Optics Communications, 13(1):68 – 69, 1975.

[HS06] Wenfang Hu and George C. Schatz. Theories of reactive scattering. The Journal of Chemical Physics, 125(13):–, 2006.

[HSD+02] Z. Hadzibabic, C. A. Stan, K. Dieckmann, S. Gupta, M. W. Zwierlein, A. Görlitz, and W. Ketterle. Two-species mixture of quantum degenerate bose and fermi gases. Phys. Rev. Lett., 88:160401, Apr 2002.

[HSGH14] Bo Huang, Leonid A. Sidorenkov, Rudolf Grimm, and Jeremy M. Hutson. Observation of the second triatomic resonance in efimov's scenario. arxiv, 1402.6161, 2014.

[HTR+05] E. Hodby, S. T. Thompson, C. A. Regal, M. Greiner, A. C. Wilson, D. S. Jin, E. A. Cornell, and C. E. Wieman. Production efficiency of ultracold feshbach molecules in bosonic and fermionic systems. Phys. Rev. Lett., 94:120402, Mar 2005.

[HWC+12] Myoung-Sun Heo, Tout T. Wang, Caleb A. Christensen, Timur M. Rvachov, Dylan A. Cotta, Jae-Hoon Choi, Ye-Ryoung Lee, and Wolfgang Ketterle. Formation of ultracold fermionic nali feshbach molecules. Phys. Rev. A, 86:021602, Aug 2012.

[HYT+11] M. R. Hadizadeh, M. T. Yamashita, Lauro Tomio, A. Delfino, and T. Frederico. Scaling properties of universal tetramers. Phys. Rev. Lett., 107:135304, Sep 2011.

[HYT+12] M. R. Hadizadeh, M. T. Yamashita, Lauro Tomio, A. Delfino, and T. Frederico. Binding and structure of tetramers in the scaling limit. Phys. Rev. A, 85:023610, Feb 2012.

[IC06] Zbigniew Idziaszek and Tommaso Calarco. Pseudopotential method for higher partial wave scattering. Phys. Rev. Lett., 96:013201, Jan 2006.

[IGO+04] S. Inouye, J. Goldwin, M. L. Olsen, C. Ticknor, J. L. Bohn, and D. S. Jin. Observation of heteronuclear feshbach resonances in a mixture of bosons and fermions. Phys. Rev. Lett., 93:183201, Oct 2004.

[JAB13] Benjamin Jaramillo Avila and Michael C. Birse. Universal behavior of four-boson systems from a functional-renormalization-group analysis. Phys. Rev. A, 88:043613, Oct 2013.

[Jac02] J. D. Jackson. From lorenz to coulomb and other explicit gauge transformations. American Journal of Physics, 70(9):917–928, 2002.

[JBA+03] S. Jochim, M. Bartenstein, A. Altmeyer, G. Hendl, S. Riedl, C. Chin, J. Hecker Denschlag, and R. Grimm. Bose-einstein condensation of molecules. Science, 302(5653):2101–2103, 2003.

[JBC+98] D. Jaksch, C. Bruder, J. I. Cirac, C. W. Gardiner, and P. Zoller. Cold bosonic atoms in optical lattices. Phys. Rev. Lett., 81:3108–3111, Oct 1998.

[JCF+99] A.S. Jensen, A. Cobis, D.V. Fedorov, E. Garrido, and E. Nielsen. Adiabatic hyperspherical expansion and three-body halos. In Bertrand Desplanques, Konstantin Protasov, Bernard Silvestre-Brac, and Jaume Carbonell, editors, Few-Body Problems in Physics 98, volume 10 of Few-Body Systems, pages 19–26. Springer Vienna, 1999.

[JR98] Ch. Jungen and G. Raseev. Spin-electronic-rotational frame transformation for photoionization and rydberg spectra of diatomic molecules. Phys. Rev. A, 57:2407–2419, Apr 1998.

[JR03] Juha Javanainen and Janne Ruostekoski. Optical detection of fractional particle number in an atomic fermi-dirac gas. Phys. Rev. Lett., 91:150404, Oct 2003.

[JRFG04] A. S. Jensen, K. Riisager, D. V. Fedorov, and E. Garrido. Structure and reactions of quantum halos. Rev. Mod. Phys., 76:215–261, Feb 2004.

[JZC+13] Michael Jag, Matteo Zaccanti, Marko Cetina, Rianne S. Lous, Florian Schreck, and Rudolf Grimm. Observation of a strong atom-dimer attraction in a mass-imbalanced fermi-fermi mixture. arxiv, 1311.5146, 2013.

[KB04] K. Kanjilal and D. Blume. Nondivergent pseudopotential treatment of spin-polarized fermions under one- and three-dimensional harmonic confinement. Phys. Rev. A, 70:042709, Oct 2004.

[KFM+nt] S. Knoop, F. Ferlaino, M. Mark, M. Berninger, H. Schobel, H.-C. Nagerl, and R. Grimm. Observation of an efimov-like trimer resonance in ultracold atom-dimer scattering. Nat Phys, 5:227–230, 2009/03//print.

[Kle89] Hagen Kleinert. Gauge Fields in Condensed Matter. World Scientific, first edition, 1989.

[KMS06] J. I. Kim, V. S. Melezhik, and P. Schmelcher. Suppression of quantum scattering in strongly confined systems. Phys. Rev. Lett., 97:193203, Nov 2006.

[KMW+06] T. Kraemer, M. Mark, P. Waldburger, J. G. Danzl, C. Chin, B. Engeser, A. D. Lange, K. Pilch, A. Jaakkola, H.-C. NAgerl, and R. Grimm. Evidence for efimov quantum states in an ultracold gas of caesium atoms. Nature, 440:315–318, 2006.

[KS96] Eugene B. Kolomeisky and Joseph P. Straley. Phase diagram and correlation exponents for interacting fermions in one dimension. Rev. Mod. Phys., 68:175–214, Jan 1996.

[KS99] A. B. Kuklov and B. V. Svistunov. Testing quantum correlations in a confined atomic cloud by the scattering of fast atoms. Phys. Rev. A, 60:R769–R772, Aug 1999.

[KS03] A. B. Kuklov and B. V. Svistunov. Counterflow superfluidity of two-species ultracold atoms in a commensurate optical lattice. Phys. Rev. Lett., 90:100401, Mar 2003.

[KSS05] J. I. Kim, J. Schmiedmayer, and P. Schmelcher. Quantum scattering in quasi-one-dimensional cylindrical confinement. Phys. Rev. A, 72:042711, Oct 2005.

[Kup97] Aron Kuppermann. Reactive scattering with row-orthonormal hyperspherical coordinates. 2. transformation properties and hamiltonian for tetraatomic systems. The Journal of Physical Chemistry A, 101(36):6368–6383, 1997.

[KW10] Klaus Kirsten and Floyd L. Williams. A window into zeta and modular physics. Cambridge: Cambridge University Press, 2010.

[KWW04] Toshiya Kinoshita, Trevor Wenger, and David S. Weiss. Observation of a one-dimensional tonks-girardeau gas. Science, 305(5687):1125–1128, 2004.

[KWW05] Toshiya Kinoshita, Trevor Wenger, and David S. Weiss. Local pair correlations in one-dimensional bose gases. Phys. Rev. Lett., 95:190406, Nov 2005.

[LCB+10] G. Lamporesi, J. Catani, G. Barontini, Y. Nishida, M. Inguscio, and F. Minardi. Scattering in mixed dimensions with ultracold gases. Phys. Rev. Lett., 104:153202, Apr 2010.

[LCJG+nt] Y.-J. Lin, R. L. Compton, K. Jimenez-Garcia, J. V. Porto, and I. B. Spielman. Synthetic magnetic fields for ultracold neutral atoms. Nature, 462:628–632, 2009/12/03/print.

[LD98] Daniel Loss and David P. DiVincenzo. Quantum computation with quantum dots. Phys. Rev. A, 57:120–126, Jan 1998.

[LDacZ+00] Å. Larson, N. Djurić, W. Zong, C. H. Greene, A. E. Orel, A. Al-Khalili, A. M. Derkatch, A. Le Padellec, A. Neau, S. Rosén, W. Shi, L. Vikor, H. Danared, M. af Ugglas, M. Larsson, and G. H. Dunn. Resonant ion-pair formation in electron collisions with hd^+ and oh^+. Phys. Rev. A, 62:042707, Sep 2000.

[Leb01] P. N. Lebedev. Experimental examination of light pressure. Ann. der Physik, 6, 1901.

[Leg01] Anthony J. Leggett. Bose-einstein condensation in the alkali gases: Some fundamental concepts. Rev. Mod. Phys., 73:307–356, Apr 2001.

[LH12] Weiran Li and Tin-Lun Ho. Bose gases near unitarity. Phys. Rev. Lett., 108:195301, May 2012.

[LL63] Elliott H. Lieb and Werner Liniger. Exact analysis of an interacting bose gas. i. the general solution and the ground state. Phys. Rev., 130:1605–1616, May 1963.

[LR83] K. T. Lu and A. R. P. Rau. Multichannel quantum-defect theory of perturbed rydberg atoms in external fields. Phys. Rev. A, 28:2623–2633, Nov 1983.

[LSA+07] Maciej Lewenstein, Anna Sanpera, Veronica Ahufinger, Bogdan Damski, Aditi Sen(De), and Ujjwal Sen. Ultracold atomic gases in optical lattices: mimicking condensed matter physics and beyond. Advances in Physics, 56(2):243–379, 2007.

[LSBF04] M. Lewenstein, L. Santos, M. A. Baranov, and H. Fehrmann. Atomic bose-fermi mixtures in an optical lattice. Phys. Rev. Lett., 92:050401, Feb 2004.

[LSY03] Elliott H. Lieb, Robert Seiringer, and Jakob Yngvason. One-dimensional bosons in three-dimensional traps. Phys. Rev. Lett., 91:150401, Oct 2003.

[LSY04] Elliott H. Lieb, Robert Seiringer, and Jakob Yngvason. One-dimensional behavior of dilute, trapped bose gases. Communications in Mathematical Physics, 244(2):347–393, 2004.

[LWW+88] Paul D. Lett, Richard N. Watts, Christoph I. Westbrook, William D. Phillips, Phillip L. Gould, and Harold J. Metcalf. Observation of atoms laser cooled below the doppler limit. Phys. Rev. Lett., 61:169–172, Jul 1988.

[Mac68] J Macek. Properties of autoionizing states of helium. Journal of Physics B: Atomic and Molecular Physics, 1(5):831, 1968.

[Maint] T. H. Maiman. Stimulated optical radiation in ruby. Nature, 187:493–494, 1960/08/06/print.

[MAJ88] leuthre lie Nicolas Mascart, Edmund Atkinson, and Jules Franois Joubert. A treatise on electricity and magnetism by Mascart, E. [E.N.] and Joubert, J.; translated by Atkinson, E., volume 1. London :Thos. De La Rue and Co.,, 1883-1888. http://www.biodiversitylibrary.org/bibliography/26619.

[MAK+97] M.-O. Mewes, M. R. Andrews, D. M. Kurn, D. S. Durfee, C. G. Townsend, and W. Ketterle. Output coupler for bose-einstein condensed atoms. Phys. Rev. Lett., 78:582–585, Jan 1997.

[MBH+13] Jim Mitroy, Sergiy Bubin, Wataru Horiuchi, Yasuyuki Suzuki, Ludwik Adamowicz, Wojciech Cencek, Krzysztof Szalewicz, Jacek Komasa, D. Blume, and Kálmán Varga. Theory and application of explicitly correlated gaussians. Rev. Mod. Phys., 85:693–749, May 2013.

[MC06] Pietro Massignan and Yvan Castin. Three-dimensional strong localization of matter waves by scattering from atoms in a lattice with a confinement-induced resonance. Phys. Rev. A, 74:013616, Jul 2006.

[McG64] J. B. McGuire. Study of exactly soluble one-dimensional n-body problems. J. Math. Phys., 5(5):622–636, 1964.

[MD11] D C McKay and B DeMarco. Cooling in strongly correlated optical lattices: prospects and challenges. Reports on Progress in Physics, 74(5):054401, 2011.

[MDJZ04] A. Micheli, A. J. Daley, D. Jaksch, and P. Zoller. Single atom transistor in a 1d optical lattice. Phys. Rev. Lett., 93:140408, Oct 2004.

[MEG05] C. Mora, R. Egger, and A. O. Gogolin. Three-body problem for ultracold atoms in quasi-one-dimensional traps. Phys. Rev. A, 71:052705, May 2005.

[MEGK04] C. Mora, R. Egger, A. O. Gogolin, and A. Komnik. Atom-dimer scattering for confined ultracold fermion gases. Phys. Rev. Lett., 93:170403, Oct 2004.

[MJP09] Francesca M. Marchetti, Th. Jolicoeur, and Meera M. Parish. Stability and pairing in quasi-one-dimensional bose-fermi mixtures. Phys. Rev. Lett., 103:105304, Sep 2009.

[MKG+13] Philip Makotyn, Catherine E. Klauss, David L. Goldberger, Eric A. Cornell, and Deborah S. Jin. Universal dynamics of a degenerate unitary bose gas. arxiv, 1308.3696, 2013.

[MKS+02] M. Mudrich, S. Kraft, K. Singer, R. Grimm, A. Mosk, and M. Weidemüller. Sympathetic cooling with two atomic species in an optical trap. Phys. Rev. Lett., 88:253001, Jun 2002.

[MKV07] J. Zs. Mezei, A. T. Kruppa, and K. Varga. Charged exciton resonances in two and three dimensions. Few-Body Systems, 41(3-4):233–244, 2007.

[MO96] J. H. Macek and S. Yu. Ovchinnikov. Hyperspherical theory of three-particle fragmentation and wanniers threshold law. Phys. Rev. A, 54:544–560, Jul 1996.

[MRR+02] Giovanni Modugno, Giacomo Roati, Francesco Riboli, Francesca Ferlaino, Robert J. Brecha, and Massimo Inguscio. Collapse of a degenerate fermi gas. Science, 297(5590):2240–2243, 2002.

[MS09] V S Melezhik and P Schmelcher. Quantum dynamics of resonant molecule formation in waveguides. New Journal of Physics, 11(7):073031, 2009.

[MSG+05a] Henning Moritz, Thilo Stöferle, Kenneth Günter, Michael Köhl, and Tilman Esslinger. Confinement induced molecules in a 1d fermi gas. Phys. Rev. Lett., 94:210401, Jun 2005.

[MSG+05b] Henning Moritz, Thilo Stöferle, Kenneth Günter, Michael Köhl, and Tilman Esslinger. Confinement induced molecules in a 1d fermi gas. Phys. Rev. Lett., 94:210401, Jun 2005.

[MSKE03] Henning Moritz, Thilo Stöferle, Michael Köhl, and Tilman Esslinger. Exciting collective oscillations in a trapped 1d gas. Phys. Rev. Lett., 91:250402, Dec 2003.

[MSRW90] C. Monroe, W. Swann, H. Robinson, and C. Wieman. Very cold trapped atoms in a vapor cell. Phys. Rev. Lett., 65:1571–1574, Sep 1990.

[MSSvS03] Francisco D. Mazzitelli, Maria J. Sánchez, Norberto N. Scoccola, and Javier von Stecher. Casimir interaction between two concentric cylinders: Exact versus semiclassical results. Phys. Rev. A, 67:013807, Jan 2003.

[MVR12] M. Manninen, S. Viefers, and S.M. Reimann. Quantum rings for beginners ii: Bosons versus fermions. Physica E: Low-dimensional Systems and Nanostructures, 46(0):119 – 132, 2012.

[MWH+04] L. Mathey, D.-W. Wang, W. Hofstetter, M. D. Lukin, and Eugene Demler. Luttinger liquid of polarons in one-dimensional boson-fermion mixtures. Phys. Rev. Lett., 93:120404, Sep 2004.

[NFJ98] E Nielsen, D V Fedorov, and A S Jensen. The structure of the atomic helium trimers: halos and efimov states. Journal of Physics B: Atomic, Molecular and Optical Physics, 31(18):4085, 1998.

[NFJG01] E. Nielsen, D.V. Fedorov, A.S. Jensen, and E. Garrido. The three-body problem with short-range interactions. Physics Reports, 347(5):373 – 459, 2001.

[NH01] E. F. Nichols and G. F. Hull. A preliminary communication on the pressure of heat and light radiation. Phys. Rev. (Series I), 13:307–320, Nov 1901.

[NHTD78] W. Neuhauser, M. Hohenstatt, P. Toschek, and H. Dehmelt. Optical-sideband cooling of visible atom cloud confined in parabolic well. Phys. Rev. Lett., 41:233–236, Jul 1978.

[Nic12] Amy N. Nicholson. N-body efimov states from two-particle noise. Phys. Rev. Lett., 109:073003, Aug 2012.

[Nis10] Yusuke Nishida. Phases of a bilayer fermi gas. Phys. Rev. A, 82:011605, Jul 2010.

[NM99] Esben Nielsen and J. H. Macek. Low-energy recombination of identical bosons by three-body collisions. Phys. Rev. Lett., 83:1566–1569, Aug 1999.

[NOdM+08] K.-K. Ni, S. Ospelkaus, M. H. G. de Miranda, A. Pe'er, B. Neyenhuis, J. J. Zirbel, S. Kotochigova, P. S. Julienne, D. S. Jin, and J. Ye. A high phase-space-density gas of polar molecules. Science, 322(5899):231–235, 2008.

[NOW+nt] K.-K. Ni, S. Ospelkaus, D. Wang, G. Quemener, B. Neyenhuis, M. H. G. de Miranda, J. L. Bohn, J. Ye, and D. S. Jin. Dipolar collisions of polar molecules in the quantum regime. Nature, 464:1324–1328, 2010/04/29/print.

[NSS+08] Chetan Nayak, Steven H. Simon, Ady Stern, Michael Freedman, and Sankar Das Sarma. Non-abelian anyons and topological quantum computation. Rev. Mod. Phys., 80:1083–1159, Sep 2008.

[NT10] Yusuke Nishida and Shina Tan. Confinement-induced p-wave resonances from s-wave interactions. Phys. Rev. A, 82:062713, Dec 2010.

[NTMJ07] Pascal Naidon, Eite Tiesinga, William F Mitchell, and Paul S Julienne. Effective-range description of a bose gas under strong one- or two-dimensional confinement. New Journal of Physics, 9(1):19, 2007.

[OdMF+04] H. Ott, E. de Mirandes, F. Ferlaino, G. Roati, G. Modugno, and M. Inguscio. Collisionally induced transport in periodic potentials. Phys. Rev. Lett., 92:160601, Apr 2004.

[Ols98] M. Olshanii. Atomic scattering in the presence of an external confinement and a gas of impenetrable bosons. Phys. Rev. Lett., 81:938–941, Aug 1998.

[Ols09] M. L. Olsen. Experiments with Feshbach molecules in a Bose-Fermi mixture. PhD thesis, University of Colorado, Boulder and JILA, 2009.

[OMD+99] Yu. B. Ovchinnikov, J. H. Müller, M. R. Doery, E. J. D. Vredenbregt, K. Helmerson, S. L. Rolston, and W. D. Phillips. Diffraction of a released bose-einstein condensate by a pulsed standing light wave. Phys. Rev. Lett., 83:284–287, Jul 1999.

[OOH+06] C. Ospelkaus, S. Ospelkaus, L. Humbert, P. Ernst, K. Sengstock, and K. Bongs. Ultracold heteronuclear molecules in a 3d optical lattice. Phys. Rev. Lett., 97(12):120402, Sep 2006.

[OOW+06] S. Ospelkaus, C. Ospelkaus, O. Wille, M. Succo, P. Ernst, K. Sengstock, and K. Bongs. Localization of bosonic atoms by fermionic impurities in a three-dimensional optical lattice. Phys. Rev. Lett., 96(18):180403, May 2006.

[OP01] Maxim Olshanii and Ludovic Pricoupenko. Rigorous approach to the problem of ultraviolet divergencies in dilute bose gases. Phys. Rev. Lett., 88:010402, Dec 2001.

[OPCJ09] M. L. Olsen, J. D. Perreault, T. D. Cumby, and D. S. Jin. Coherent atom-molecule oscillations in a bose-fermi mixture. Phys. Rev. A, 80(3):030701, Sep 2009.

[Orb59] R. Orbach. Antiferromagnetic magnon dispersion law and bloch wall energies in ferromagnets and antiferromagnets. Phys. Rev., 115:1181–1184, Sep 1959.

[PAEC95] Wolfgang Petrich, Michael H. Anderson, Jason R. Ensher, and Eric A. Cornell. Stable, tightly confining magnetic trap for evaporative cooling of neutral atoms. Phys. Rev. Lett., 74:3352–3355, Apr 1995.

[PCAH09] R. A. Pepino, J. Cooper, D. Z. Anderson, and M. J. Holland. Atomtronic circuits of diodes and transistors. Phys. Rev. Lett., 103:140405, Sep 2009.

[PDH09] Scott E. Pollack, Daniel Dries, and Randall G. Hulet. Universality in three- and four-body bound states of ultracold atoms. Science, 326(5960):1683–1685, 2009.

[PHLD11] Shi-Guo Peng, Hui Hu, Xia-Ji Liu, and Peter D. Drummond. Confinement-induced resonances in anharmonic waveguides. Phys. Rev. A, 84:043619, Oct 2011.

[PHM04] L. Platter, H.-W. Hammer, and Ulf-G. Meißner. Four-boson system with short-range interactions. Phys. Rev. A, 70:052101, Nov 2004.

[PK11] Jacobus Portegies and Servaas Kokkelmans. Efimov trimers in a harmonic potential. Few-Body Systems, 51(2-4):219–234, 2011.

[Pla09] Lucas Platter. Low-energy universality in atomic and nuclear physics. Few-Body Systems, 46(3):139–171, 2009.

[PMC$^+$nt] Guido Pagano, Marco Mancini, Giacomo Cappellini, Pietro Lombardi, Florian Schafer, Hui Hu, Xia-Ji Liu, Jacopo Catani, Carlo Sias, Massimo Inguscio, and Leonardo Fallani. A one-dimensional liquid of fermions with tunable spin. Nat Phys, 10:198–201, 2014/03//print.

[PMG86] Gnter Plunien, Berndt Mller, and Walter Greiner. The casimir effect. Physics Reports, 134(23):87 – 193, 1986.

[Pos06] Anna Posazhennikova. Colloquium: Weakly interacting, dilute bose gases in 2d. Rev. Mod. Phys., 78:1111–1134, Oct 2006.

[PPND12] Ville Pietilä, David Pekker, Yusuke Nishida, and Eugene Demler. Pairing instabilities in quasi-two-dimensional fermi gases. Phys. Rev. A, 85:023621, Feb 2012.

[PRB$^+$86] D. E. Pritchard, E. L. Raab, V. Bagnato, C. E. Wieman, and R. N. Watts. Light traps using spontaneous forces. Phys. Rev. Lett., 57:310–313, Jul 1986.

[PS01] D. S. Petrov and G. V. Shlyapnikov. Interatomic collisions in a tightly confined bose gas. Phys. Rev. A, 64:012706, Jun 2001.

[PS04] C. J. Pethick and H. Smith. Bose-Einstein Condendation in Dilute Gases. Cambridge University Press, Cambridge, first edition, 2004.

[PSB05] Stephen Powell, Subir Sachdev, and Hans Peter Büchler. Depletion of the bose-einstein condensate in bose-fermi mixtures. Phys. Rev. B, 72:024534, Jul 2005.

[PTB+05] E. Pazy, I. Tikhonenkov, Y. B. Band, M. Fleischhauer, and A. Vardi. Nonlinear adiabatic passage from fermion atoms to boson molecules. Phys. Rev. Lett., 95(17):170403, Oct 2005.

[PTME05] V Peano, M Thorwart, C Mora, and R Egger. Confinement-induced resonances for a two-component ultracold atom gas in arbitrary quasi-one-dimensional traps. New Journal of Physics, 7(1):192, 2005.

[PTVHR06] Lode Pollet, Matthias Troyer, Kris Van Houcke, and Stefan M. A. Rombouts. Phase diagram of bose-fermi mixtures in one-dimensional optical lattices. Phys. Rev. Lett., 96:190402, May 2006.

[PW06] S. B. Papp and C. E. Wieman. Observation of heteronuclear feshbach molecules from a rubidium 85–87 gas. Phys. Rev. Lett., 97(18):180404, Oct 2006.

[PWM+nt] Belen Paredes, Artur Widera, Valentin Murg, Olaf Mandel, Simon Folling, Ignacio Cirac, Gora V. Shlyapnikov, Theodor W. Hansch, and Immanuel Bloch. Tonks-girardeau gas of ultracold atoms in an optical lattice. Nature, 429:277–281, 2004/05/20/print.

[PWS+12] Jee Woo Park, Cheng-Hsun Wu, Ibon Santiago, Tobias G. Tiecke, Sebastian Will, Peyman Ahmadi, and Martin W. Zwierlein. Quantum degenerate bose-fermi mixture of chemically different atomic species with widely tunable interactions. Phys. Rev. A, 85:051602, May 2012.

[PWT+11] N. Poli, F.-Y. Wang, M. G. Tarallo, A. Alberti, M. Prevedelli, and G. M. Tino. Precision measurement of gravity with cold atoms in an optical lattice and comparison with a classical gravimeter. Phys. Rev. Lett., 106:038501, Jan 2011.

[QGZ11] Yinyin Qian, Ming Gong, and Chuanwei Zhang. Quantum transport of bosonic cold atoms in double-well optical lattices. Phys. Rev. A, 84:013608, Jul 2011.

[Rau79] A R P Rau. Rydberg states in electric and magnetic fields: near-zero-energy resonances. Journal of Physics B: Atomic and Molecular Physics, 12(6):L193, 1979.

[RGC+06] J.-F. Riou, W. Guerin, Y. Le Coq, M. Fauquembergue, V. Josse, P. Bouyer, and A. Aspect. Beam quality of a nonideal atom laser. Phys. Rev. Lett., 96:070404, Feb 2006.

[RGJ04] C. A. Regal, M. Greiner, and D. S. Jin. Observation of resonance condensation of fermionic atom pairs. Phys. Rev. Lett., 92:040403, Jan 2004.

[RINS+13] O. Romero-Isart, C. Navau, A. Sanchez, P. Zoller, and J. I. Cirac. Superconducting vortex lattices for ultracold atoms. Phys. Rev. Lett., 111:145304, Oct 2013.

[Rit09] Seth T. Rittenhouse. Control and Dynamics of Few-Body Systems at Ultracold Temperatures. PhD thesis, University of Colorado at Boulder, 2009.

[RJ06] C.A. Regal and D.S. Jin. Experimental realization of the bcs-bec crossover with a fermi gas of atoms. In C.C. Lin P.R. Berman and E. Arimondo, editors, elseiver, volume 54 of Advances In Atomic, Molecular, and Optical Physics, pages 1 – 79. Academic Press, 2006.

[RM04] A. Ruschhaupt and J. G. Muga. Atom diode: A laser device for a unidirectional transmission of ground-state atoms. Phys. Rev. A, 70:061604, Dec 2004.

[RMG10] Seth T. Rittenhouse, N. P. Mehta, and Chris H. Greene. Greens functions and the adiabatic hyperspherical method. Phys. Rev. A, 82:022706, Aug 2010.

[RPC+87] E. L. Raab, M. Prentiss, Alex Cable, Steven Chu, and D. E. Pritchard. Trapping of neutral sodium atoms with radiation pressure. Phys. Rev. Lett., 59:2631–2634, Dec 1987.

[RRMI02a] G. Roati, F. Riboli, G. Modugno, and M. Inguscio. Fermi-bose quantum degenerate ^{40}K ^{87}Rb mixture with attractive interaction. Phys. Rev. Lett., 89:150403, Sep 2002.

[RRMI02b] G. Roati, F. Riboli, G. Modugno, and M. Inguscio. Fermi-bose quantum degenerate ^{40}K-^{87}Rb mixture with attractive interaction. Phys. Rev. Lett., 89:150403, Sep 2002.

[RTBJ03] Cindy A. Regal, Christopher Ticknor, John L. Bohn, and Deborah S. Jin. Creation of ultracold molecules from a fermi gas of atoms. Nature, 424:47–50, Jul 2003.

[RTF85] A Rabinovitch, R Thieberger, and M Friedmann. Effective phaseshifts in the presence of electric fields. Journal of Physics B: Atomic and Molecular Physics, 18(3):393, 1985.

[RvSD+11] S T Rittenhouse, J von Stecher, J P DIncao, N P Mehta, and C H Greene. The hyperspherical four-fermion problem. Journal of Physics B: Atomic, Molecular and Optical Physics, 44(17):172001, 2011.

[RWMC90] Erling Riis, David S. Weiss, Kathryn A. Moler, and Steven Chu. Atom funnel for the production of a slow, high-density atomic beam. Phys. Rev. Lett., 64:1658–1661, Apr 1990.

[Sak86] K Sakimoto. Multichannel quantum-defect theory of the stark effect. Journal of Physics B: Atomic and Molecular Physics, 19(19):3011, 1986.

[SCE+12] Peter Schausz, Marc Cheneau, Manuel Endres, Takeshi Fukuhara, Sebastian Hild, Ahmed Omran, Thomas Pohl, Christian Gross, Stefan Kuhr, and Immanuel Bloch. Observation of spatially ordered structures in a two-dimensional rydberg gas. Nature, 491:87, 2012.

[Sch05] U. Schollwöck. The density-matrix renormalization group. Rev. Mod. Phys., 77:259–315, Apr 2005.

[Sch11] Ulrich Schollwck. The density-matrix renormalization group in the age of matrix product states. Annals of Physics, 326(1):96 – 192, 2011. January 2011 Special Issue.

[SFR+03] A. Simoni, F. Ferlaino, G. Roati, G. Modugno, and M. Inguscio. Magnetic control of the interaction in ultracold K − Rb mixtures. Phys. Rev. Lett., 90:163202, Apr 2003.

[SIC+99] J. Stenger, S. Inouye, A. P. Chikkatur, D. M. Stamper-Kurn, D. E. Pritchard, and W. Ketterle. Bragg spectroscopy of a bose-einstein condensate. Phys. Rev. Lett., 82:4569–4573, Jun 1999.

[SIT+nt] Seiji Sugawa, Kensuke Inaba, Shintaro Taie, Rekishu Yamazaki, Makoto Yamashita, and Yoshiro Takahashi. Interaction and filling-induced quantum phases of dual mott insulators of bosons and fermions. Nat Phys, 7:642–648, 2011/08//print.

[SKC+01] F. Schreck, L. Khaykovich, K. L. Corwin, G. Ferrari, T. Bourdel, J. Cubizolles, and C. Salomon. Quasipure bose-einstein condensate immersed in a fermi sea. Phys. Rev. Lett., 87:080403, Aug 2001.

[SM10] Schmidt, R. and Moroz, S. Functional renormalization group approach to the four-body problem. EPJ Web of Conferences, 3:02006, 2010.

[SMH10] Scott N. Sanders, Florian Mintert, and Eric J. Heller. Matter-wave scattering from ultracold atoms in an optical lattice. Phys. Rev. Lett., 105:035301, Jul 2010.

[Smi60] Felix T. Smith. Generalized angular momentum in many-body collisions. Phys. Rev., 120:1058–1069, Nov 1960.

[SPLnt] Laurent Sanchez-Palencia and Maciej Lewenstein. Disordered quantum gases under control. Nat Phys, 6:87–95, 2010/02//print.

[SS07] S. Sinha and L. Santos. Cold dipolar gases in quasi-one-dimensional geometries. Phys. Rev. Lett., 99:140406, Oct 2007.

[SSSK08] Yong-il Shin, André Schirotzek, Christian H. Schunck, and Wolfgang Ketterle. Realization of a strongly interacting bose-fermi mixture from a two-component fermi gas. Phys. Rev. Lett., 101(7):070404, Aug 2008.

[STBH11a] Michiel Snoek, Irakli Titvinidze, Immanuel Bloch, and Walter Hofstetter. Effect of interactions on harmonically confined bose-fermi mixtures in optical lattices. Phys. Rev. Lett., 106:155301, Apr 2011.

[STBH11b] Michiel Snoek, Irakli Titvinidze, Immanuel Bloch, and Walter Hofstetter. Effect of interactions on harmonically confined bose-fermi mixtures in optical lattices. Phys. Rev. Lett., 106(15):155301, Apr 2011.

[SV98] Y. Suzuki and K. Varga. Stochastic Variational Approach to Quantum-Mechanical Few-Body Problems. Springer-Verlag, Berlin, 1998.

[SY08] Robert Seiringer and Jun Yin. The lieb-liniger model as a limit of dilute bosons in three dimensions. Communications in Mathematical Physics, 284(2):459–479, 2008.

[SZS+04] C. A. Stan, M. W. Zwierlein, C. H. Schunck, S. M. F. Raupach, and W. Ketterle. Observation of feshbach resonances between two different atomic species. Phys. Rev. Lett., 93:143001, Sep 2004.

[Tho35] L. H. Thomas. The interaction between a neutron and a proton and the structure of H_3. Phys. Rev., 47:903–909, Jun 1935.

[TJGJ+14] Shih-Kuang Tung, Karina Jimemez-Garcia, Jacob Johansen, Colin V. Parker, and Cheng Chin. Observation of geometric scaling of efimov states in a fermi-bose li-cs mixture. arxiv, 1402.5943, 2014.

[TOH+04] B. Laburthe Tolra, K. M. O'Hara, J. H. Huckans, W. D. Phillips, S. L. Rolston, and J. V. Porto. Observation of reduced three-body recombination in a correlated 1d degenerate bose gas. Phys. Rev. Lett., 92:190401, May 2004.

[Ton36] Lewi Tonks. The complete equation of state of one, two and three-dimensional gases of hard elastic spheres. Phys. Rev., 50:955–963, Nov 1936.

[TSH08] I. Titvinidze, M. Snoek, and W. Hofstetter. Supersolid bose-fermi mixtures in optical lattices. Phys. Rev. Lett., 100:100401, Mar 2008.

[TSH09] I. Titvinidze, M. Snoek, and W. Hofstetter. Generalized dynamical mean-field theory for bose-fermi mixtures in optical lattices. Phys. Rev. B, 79:144506, Apr 2009.

[TSM+01] Andrew G. Truscott, Kevin E. Strecker, William I. McAlexander, Guthrie B. Partridge, and Randall G. Hulet. Observation of fermi pressure in a gas of trapped atoms. Science, 291(5513):2570–2572, 2001.

[TSW+11] Jiri Tomkovic, Michael Schreiber, Joachim Welte, Martin Kiffner, Jorg Schmiedmayer, and Markus K. Oberthaler. Single spontaneous photon as a coherent beamsplitter for an atomic matter-wave. Nature Phys., 7:379–382, 2011.

[TW00] Takeya Tsurumi and Miki Wadati. Dynamics of magnetically trapped boson-fermion mixtures. Journal of the Physical Society of Japan, 69(1):97–103, 2000.

[TZ94] I. J. Thompson and M. V. Zhukov. Effects of ^{10}Li virtual states on the structure of ^{11}Li. Phys. Rev. C, 49:1904–1907, Apr 1994.

[US02] J. Usukura and Y. Suzuki. Resonances of positronium complexes. Phys. Rev. A, 66:010502, Jul 2002.

[Viv02] L. Viverit. Boson-induced s-wave pairing in dilute boson-fermion mixtures. Phys. Rev. A, 66:023605, Aug 2002.

[VRCJbu08] J. Y. Vaishnav, Julius Ruseckas, Charles W. Clark, and Gediminas Juzeliūnas. Spin field effect transistors with ultracold atoms. Phys. Rev. Lett., 101:265302, Dec 2008.

[vS08] J. von Stecher. Trapped Ultracold Atoms with Tunable Interactions. PhD thesis, University of Colorado at Boulder, 2008.

[vS10] Javier von Stecher. Weakly bound cluster states of efimov character. Journal of Physics B: Atomic, Molecular and Optical Physics, 43(10):101002, 2010.

[vS11] Javier von Stecher. Five- and six-body resonances tied to an efimov trimer. Phys. Rev. Lett., 107:200402, Nov 2011.

[vSDGnt] J. von Stecher, J. P. D'Incao, and Chris H. Greene. Signatures of universal four-body phenomena and their relation to the efimov effect. Nat Phys, 5:417–421, 2009/06//print.

[vSG07] Javier von Stecher and Chris H. Greene. Spectrum and dynamics of the bcs-bec crossover from a few-body perspective. Phys. Rev. Lett., 99(9):090402, Aug 2007.

[vSG09] Javier von Stecher and Chris H. Greene. Correlated gaussian hyperspherical method for few-body systems. Phys. Rev. A, 80:022504, Aug 2009.

[Wal59] L. R. Walker. Antiferromagnetic linear chain. Phys. Rev., 116:1089–1090, Dec 1959.

[Wan12] Jia Wang. Hyperspherical Approach to Quantal Three-body Theory. PhD thesis, University of Colorado at Boulder, 2012.

[WBB+11] Sebastian Will, Thorsten Best, Simon Braun, Ulrich Schneider, and Immanuel Bloch. Coherent interaction of a single fermion with a small bosonic field. Phys. Rev. Lett., 106:115305, Mar 2011.

[WC06] Félix Werner and Yvan Castin. Unitary quantum three-body problem in a harmonic trap. Phys. Rev. Lett., 97:150401, Oct 2006.

[WDEG12] Jia Wang, J. P. D'Incao, B. D. Esry, and Chris H. Greene. Origin of the three-body parameter universality in efimov physics. Phys. Rev. Lett., 108:263001, Jun 2012.

[WDW78] D. J. Wineland, R. E. Drullinger, and F. L. Walls. Radiation-pressure cooling of bound resonant absorbers. Phys. Rev. Lett., 40:1639–1642, Jun 1978.

[Whi92] Steven R. White. Density matrix formulation for quantum renormalization groups. Phys. Rev. Lett., 69:2863–2866, Nov 1992.

[Wil83] Kenneth G. Wilson. The renormalization group and critical phenomena. Rev. Mod. Phys., 55:583–600, Jul 1983.

[WLvSE12] Yujun Wang, W. Blake Laing, Javier von Stecher, and B. D. Esry. Efimov physics in heteronuclear four-body systems. Phys. Rev. Lett., 108:073201, Feb 2012.

[WPA+12] Cheng-Hsun Wu, Jee Woo Park, Peyman Ahmadi, Sebastian Will, and Martin W. Zwierlein. Ultracold fermionic feshbach molecules of sodium potassium. Phys. Rev. Lett., 109:085301, Aug 2012.

[WRG88] Hin-Yiu Wong, A. R. P. Rau, and Chris H. Greene. Negative-ion photodetachment in an electric field. Phys. Rev. A, 37:2393–2403, Apr 1988.

[WSF+11] Christof Weitenberg, Peter Schauß, Takeshi Fukuhara, Marc Cheneau, Manuel Endres, Immanuel Bloch, and Stefan Kuhr. Coherent light scattering from a two-dimensional mott insulator. Phys. Rev. Lett., 106:215301, May 2011.

[WWDG12] Yujun Wang, Jia Wang, J. P. D'Incao, and Chris H. Greene. Universal three-body parameter in heteronuclear atomic systems. Phys. Rev. Lett., 109:243201, Dec 2012.

[Yan67] C. N. Yang. Some exact results for the many-body problem in one dimension with repulsive delta-function interaction. Phys. Rev. Lett., 19:1312–1315, Dec 1967.

[YMG+nt] Bo Yan, Steven A. Moses, Bryce Gadway, Jacob P. Covey, Kaden R. A. Hazzard, Ana Maria Rey, Deborah S. Jin, and Jun Ye. Observation of dipolar spin-exchange interactions with lattice-confined polar molecules. Nature, 501:521–525, 2013/09/26/print.

[YOW08] Vladimir A. Yurovsky, Maxim Olshanii, and David S. Weiss. Collisions, correlations, and integrability in atom waveguides. Adv. At. Molec. Opt. Phys., 55:61 – 138, 2008.

[YTDF06] M. T. Yamashita, Lauro Tomio, A. Delfino, and T. Frederico. Four-boson scale near a feshbach resonance. EPL (Europhysics Letters), 75(4):555, 2006.

[YY66a] C. N. Yang and C. P. Yang. One-dimensional chain of anisotropic spin-spin interactions. i. proof of bethe's hypothesis for ground state in a finite system. Phys. Rev., 150:321–327, Oct 1966.

[YY66b] C. N. Yang and C. P. Yang. One-dimensional chain of anisotropic spin-spin interactions. ii. properties of the ground-state energy per lattice site for an infinite system. Phys. Rev., 150:327–339, Oct 1966.

[YY66c] C. N. Yang and C. P. Yang. One-dimensional chain of anisotropic spin-spin interactions. iii. applications. Phys. Rev., 151:258–264, Nov 1966.

[ZDD+nt] M. Zaccanti, B. Deissler, C. D/'Errico, M. Fattori, M. Jona-Lasinio, S. Muller, G. Roati, M. Inguscio, and G. Modugno. Observation of an efimov spectrum in an atomic system. Nat Phys, 5:586–591, 2009/08//print.

[ZDF+93] M.V. Zhukov, B.V. Danilin, D.V. Fedorov, J.M. Bang, I.J. Thompson, and J.S. Vaagen. Bound state properties of borromean halo nuclei: 6he and 11li. Physics Reports, 231(4):151 – 199, 1993.

[ZFD+12] L. B. Zhao, I. I. Fabrikant, J. B. Delos, F. Lépine, S. Cohen, and C. Bordas. Coupled-channel theory of photoionization microscopy. Phys. Rev. A, 85:053421, May 2012.

[ZFDB12] L. B. Zhao, I. I. Fabrikant, M. L. Du, and C. Bordas. Test of the stark-effect theory using photoionization microscopy. Phys. Rev. A, 86:053413, Nov 2012.

[ZG13a] Chen Zhang and Chris H. Greene. Quasi-one-dimensional scattering with general transverse two-dimensional confinement. Phys. Rev. A, 88:012715, Jul 2013.

[ZG13b] Chen Zhang and Chris H. Greene. Tunable lattice induced opacity in atom-lattice interaction. arXiv, 1312.6666, 2013.

[Zha09] Hui Zhai. Strongly interacting ultracold quantum gases. Frontiers of Physics in China, 4(1):1–20, 2009.

[ZSS+04] M. W. Zwierlein, C. A. Stan, C. H. Schunck, S. M. F. Raupach, A. J. Kerman, and W. Ketterle. Condensation of pairs of fermionic atoms near a feshbach resonance. Phys. Rev. Lett., 92:120403, Mar 2004.

[ZvSG12] Chen Zhang, Javier von Stecher, and Chris H. Greene. Few-body ultracold reactions in a bose-fermi mixture. Phys. Rev. A, 85:043615, Apr 2012.

[ZZ11] Wei Zhang and Peng Zhang. Confinement-induced resonances in quasi-one-dimensional traps with transverse anisotropy. Phys. Rev. A, 83:053615, May 2011.

Appendix A

Chen Zhang's published work and preprints

(1) Chen Zhang, Javier von Stecher, Chris H. Greene. Few-body ultracold reactions in a Bose-Fermi mixture *Phys. Rev. A* **85**, 043615(2012)

(2) Yuan Sun, Chen Zhang. Stochasticity in narrow transitions induced by laser noise *Phys. Rev. A* **89**, 032516(2014)

(3) Chen Zhang, Chris H. Greene. Quasi-1D scattering with general 2D confinement. *Phys. Rev. A* **88**, 012715(2013)

(4) Tomotake Yamakoshi, Shinichi Watanabe, Chen Zhang, Chris H. Greene. Stochastic and equilibrium pictures of the ultracold Fano-Feshbach resonance molecule conversion rate. *Phys. Rev. A* **87**, 053604 (2013)

(5) Chen Zhang, Chris H. Greene. Tunable lattice induced opacity in atom-lattice interaction arxiv: 1312.6666